Title

Paleoenvironment and Persistent Places Interwoven at Kharaneh IV, Jordan

Author

White, Adam Joshua

Publication Date

2023

Peer reviewed|Thesis/dissertation

Paleoenvironment and Persistent Places Interwoven at Kharaneh IV, Jordan

By

Adam Joshua White

A dissertation submitted in partial satisfaction of the

requirements for the degree of

Doctor of Philosophy

in

Anthropology

in the

Graduate Division

of the

University of California, Berkeley

Committee in charge:

Professor Lisa A. Maher, Chair
Professor Junko Habu
Professor Ronald Amundson

Fall 2023

Abstract

Paleoenvironment and Persistent Places Interwoven at Kharaneh IV, Jordan

by

Adam Joshua White

Doctor of Philosophy in Anthropology

University of California, Berkeley

Professor Lisa Maher, Chair

This dissertation pairs paleoenvironmental analyses with persistent place theory to better understand human-environment relationships at a large Epipaleolithic hunter-gatherer site in eastern Jordan, Kharaneh IV. I use fecal stanol molecules, gazelle tooth enamel stable isotope values, loss-on-ignition, micro- and macrofossils, geoarchaeological excavation and survey, and sedimentological characterization to reconstruct the paleoenvironmental history of the Kharaneh wetland and understand the qualities of the local environment that contributed to the formation of Kharaneh IV as a persistent place on the Epipaleolithic landscape. Although fecal stanols at the site do not appear to reflect ancient conditions, the analysis identified two major limitations of the method in archaeological studies: 1) stanol molecules appear to be mobile through permeable cultural deposits, suggesting that the method is not viable in dryland sites, and 2) non-human producers of fecal stanols may complicate the interpretations of a site's history, as herd animals that pass over the site are a likely source of fecal stanol contamination.

Gazelle tooth enamel isotope values show little variation between the site's older Area B and younger Area A occupations, indicating relatively stable conditions over the course of the site's thousand-year history and supporting notions of Kharaneh IV as a persistent place. However, a -2% excursion in $\delta^{18}O$ values suggests a temporary period of enhanced precipitation during the site's Middle Epipaleolithic occupation. Geoarchaeological excavation and survey identified a permeability gradient between wadi gravels and shallow limestone bedrock surrounding Kharaneh IV that allowed for wetland formation from shallow groundwater flow during the Pleistocene. Loss-on-ignition, micro- and macrofossils, geoarchaeological excavation and survey, and sedimentological characterization data indicate that the wetland fluctuated significantly before and after the site's occupation, but provided a reliable source of water for Epipaleolithic groups, plants, and prey that in turn encouraged place-making activities to occur and develop Kharaneh IV into a persistent place.

Dedication

This work is dedicated to my wife, Amanda Jane Holdsambeck, for her support, love, and encouragement.

Table of Contents

List of Figures

List of Tables

Acknowledgements

I am fortunate to have had the guidance and resources of many people and organizations through the completion of this dissertation. I thank my dissertation committee, Lisa Maher, Junko Habu, and Ron Amundson, for their constructive review and discussions that greatly improved this work. I am particularly grateful to Lisa for serving as my dissertation advisor over six years and for always supporting me in every task large and small.

UC Berkeley, the Department of Anthropology, and the Archaeological Research Facility provided funding through the Dissertation Writing Fellowship, George and Mary LeCrohn Foster Fellowship, Summer Dissertation Writing Grant, Stahl Grant, Lowie Olsen Research Grant, and Graduate Student Instructor positions, and provided material support and laboratory access. The Berkeley Chapter of Sigma Xi and the Geological Society of America provided additional funds and field work associated with this project was made possible by Maher's funding from the National Science Foundation and the National Endowment for the Humanities.

Field work associated with this project was particularly supported by Lisa Maher, Danielle Macdonald, Abdalkareem Al-hebashan, Ahmad Thaher, and my colleagues from Berkeley, Jordan Brown and Felicia De Peña. I thank Felicia for analyzing hundreds of lithic artifacts discussed in Chapter 4 and her permission to include the data in this dissertation. Melanie Miller, Todd Dawson, and Wenbo Yang contributed to isotopic analyses presented in Chapter 3, and Melanie graciously and patiently trained me in tooth sample preparation. Nico Tripcevich provided access and training on laboratory equipment housed in the Archaeological Research Facility. Varenka Lorenzi and the IIRMES laboratory at CSU Long Beach analyzed the fecal stanol samples discussed in Chapter 2.

I had many productive conversations about this project and its themes with my professors and colleagues at Berkeley and elsewhere and thank them for their time, including Wolfgang Alders, Ron Amundson, Theresa Barket, Matt Becker, Jordan Brown, Todd Dawson, Felicia De Peña, Sara Eriksson, Junko Habu, Christine Hastorf, Rosemary Joyce, Kent Lightfoot, Danielle Macdonald, Lisa Maher, Louise Martin, Gabriel Sanchez, Greg Schachner, Ben Siegel, Lora Stevens, and Ahmad Thaher.

Finally, I am forever thankful to my Mom and Dad, Nathan, Oma, Opa, Heidi, Rob, Wes, and Amanda for their love and support.

Chapter 1

Introduction

Archaeologists have an important role to play in contextualizing and understanding the complex effects of climate change on individuals and societies in the past. However, identifying this complexity in the archaeological record is hindered by two main limitations: 1) methodological constraints in the ability to conduct paleoclimatic analyses on archaeological materials and sediments and 2) theoretical problems in understanding the broad range of possibilities for how individuals and groups respond to environmental perturbations. Typically, dense cultural deposits within archaeological sites are not suitable as paleoclimatic archives, which are traditionally found in oceans, lakes, glaciers, and speleothems. These latter archives are frequently found away from archaeological sites and the environmental conditions inferred from these data may not reflect the conditions experienced at a site. Additionally, chronometric error between paleoenvironmental and archaeological datasets is compounded during data correlation.

At a theoretical level, paleoclimatic and archaeological correlations alone are helpful tools to address questions in human-environment dynamics, but they are not answers in their own right. The question of causation between environmental events and cultural changes must be situated within archaeological theories that account for human agency in response to shifts in the local environment. As archaeological thought has progressed from determinist environmental interpretations of the early 20th century (e.g., Childe, 1928; Pumpelly, 1908) to more recent research programs like historical ecology (Balée, 2006) and human ecodynamics (McGlade, 1995), the degree to which human agency in navigating environment perturbations is considered has steadily increased (Figure 1.1). In parallel with this development, researchers have explored the ways in which human impacts, either physically through deforestation, urbanization, and domestication, or phenomenologically through landscapes of memory, tradition, and symbolism, have shaped environments (Cosgrove and Daniels, 1988; Ingold, 1993; Johnson, 2012).

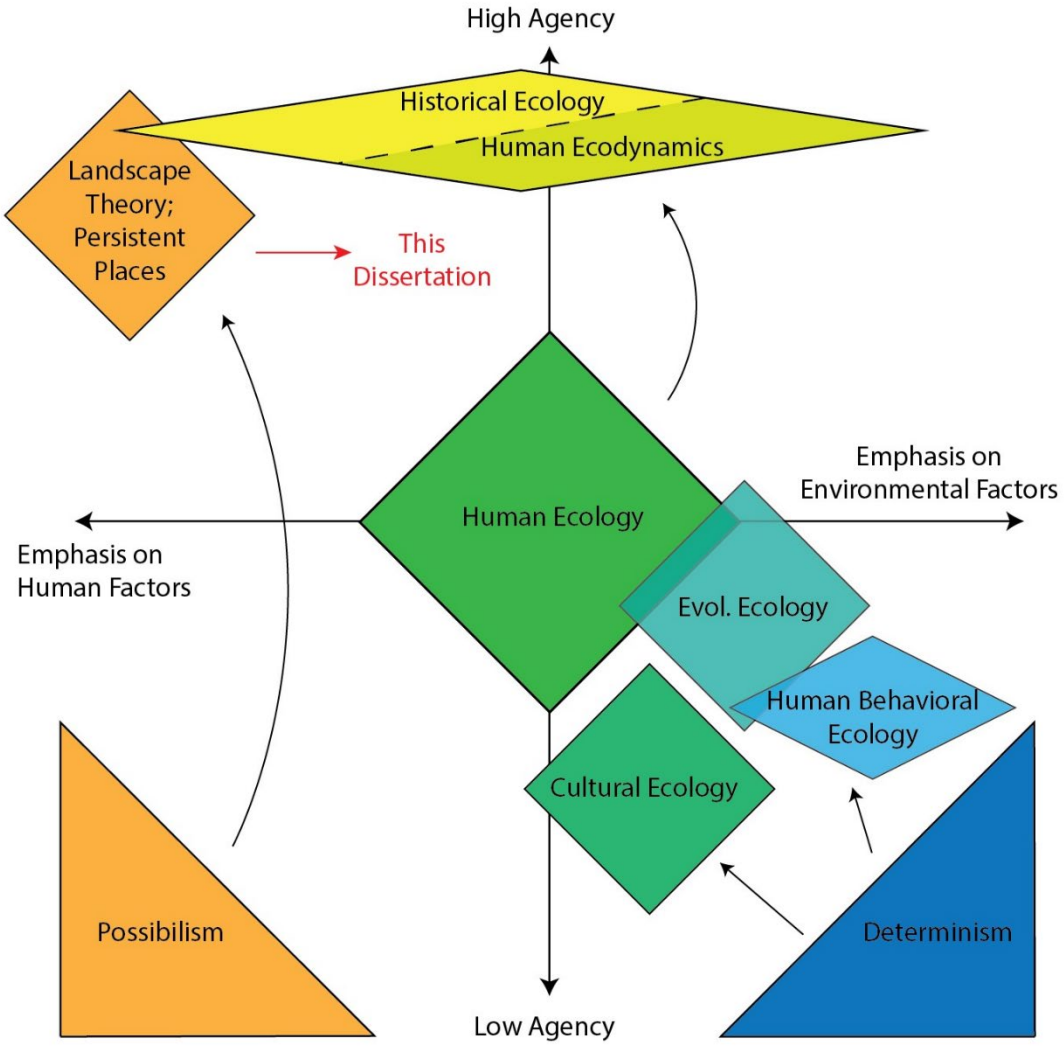

Figure 1.1. A visual comparison of human-environmental theories by emphasis on human or environmental factors and agency. Agency refers to the degree to which a theory allows humans and environmental forces to take active roles in cultural developments. Black unidirectional arrows show the developmental progression of one theory to another. The red arrow shows the goal of this dissertation to expand considerations within persistent place theory.

Archaeological theory in human-environment relations continues to be refined and applied in new ways. Maher (2019) demonstrated the relevancy of geoarchaeology to persistent place theory, a subset of landscape theory that aims to understand the persistence of certain archaeological features on the landscape (Schlanger, 1992). While the concept of persistent places is generally linked to other concepts, like practice theory (Maher, 2019; Moore and Thompson, 2012), this dissertation and others (Buckner, 2020; Parker, 1994; Rodan, 2021) directly associate persistent places with archaeological theory in the sense that "theory is the order we choose to put facts in" (Johnson, 2006:118). This dissertation continues Maher's integration of persistent places and geoarchaeology by showing that paleoclimatic and paleoenvironmental analyses are particularly suited to understanding place-making, that is ways of "inhabiting or dwelling in the world that invest particular locations with personal and

collective significance" (Whitridge, 2004:215). In this way, the theory is expanded to consider how psychical environmental factors intermesh with phenomenological concepts to produce persistent landscapes (Figure 1.1).

Taken together, the purpose of this dissertation is to couple paleoenvironmental analysis and persistent place theory by conducting multiproxy, site-scale geoarchaeological techniques that inform our understanding of a significant persistent place, Kharaneh IV. Kharaneh IV is a large Early to Middle Epipaleolithic site in eastern Jordan that supported multi-seasonal occupations of hunter-gatherer groups over a thousand-year period (Jones, 2012; Maher et al., 2012; Martin et al., 2010). In collaboration with the Epipaleolithic Foragers in Azraq Project (EFAP), I collected data for this project over two field seasons (2018, 2019) and one research season (2022) in order to conduct site-scale paleoenvironmental analyses. This dissertation presents the results of these analyses as individual chapters, beginning with the application of fecal stanol biomarkers in Chapter 2. While the biomarkers did not respond as anticipated, the study presents an opportunity to define the strengths and limitations of fecal stanol molecules in archaeological studies.

Chapter 3 documents oxygen and carbon stable isotope data from gazelle tooth enamel obtained from upper deposits at Kharaneh IV that are so tense in cultural material that it is difficult to gather paleoenvironmental data by traditional means. The isotopic data show little variation across the site's history, suggesting a mostly stable local environment. However, a shift in Middle Epipaleolithic $\delta^{18}O$ values suggests a temporary period of enhanced precipitation that may be related to continuity in the site's archaeological assemblage. Chapter 4 provides a range of physical and chemical geoarchaeological data to reconstruct the Kharaneh IV paleoenvironment and assess how environmental factors contributed to the formation of the site as a persistent place. I find that the site's nearby wetland does not appear to have had a particularly unique hydrological setting that set it apart from the surrounding region, but its reliability over millennia encouraged continued reoccupations of the site and its surrounding landscape before, during, and after Kharaneh IV's Epipaleolithic occupation. Chapter 5 is a brief conclusion to the dissertation that reviews how multiproxy, site-scale paleoenvironmental analyses can be integrated with archaeological theory to produce clearer and more comprehensive evaluations of human-environmental dynamics.

Chapter 2

Sedimentological and zoological limitations of archaeological fecal stanol analysis identified from an application at Kharaneh IV, Jordan

Abstract

Determining population sizes in the past has always been notoriously difficult to do because of the fragile and fragmentary nature of most archaeological residues. Recently, archaeological studies have used changes in the concentration of coprostanol, a recalcitrant human fecal stanol molecule, found in sediments as a proxy for tracking ancient population changes. Despite increased application of this method, its limitations are poorly understood. This study presents sedimentological and molecular data from anthropogenic and non-anthropogenic deposits at Kharaneh IV, an Epipaleolithic archaeological site in eastern Jordan, to suggest that fecal stanol molecules may be more mobile than previously thought in some dryland and desert sediments. Mobility in fecal stanol molecules leads to a loss of temporal context and the possibility of *in situ* mixing of stanol molecules with modern contaminants, rendering archaeological interpretations unreliable. Additionally, we identify contemporary dromedary camel feces, and likely other herd animals in the past, as a likely source of coprostanol at the site and find that camels produce enough coprostanol to complicate the interpretation of a site's fecal stanol record. This study demonstrates that archaeological fecal stanol analysis is best applied to aqueous environmental contexts where the likelihood of stanol migration is low and highlights the need for additional research on potential nonhuman sources of fecal stanol molecules and post-depositional processes that may disturb *in situ* molecules.

Introduction

Fecal stanols are a class of organic molecules that originate in the guts of humans and other animals through the microbial degradation of sterols (Bull et al., 2002). While there are many stanol molecules, the group that is most frequently analyzed in archaeological studies are 5β-stanols and their derivatives, including coprostanol (5β-cholestan-3β-ol), epicoprostanol (5β-cholestan-3α-ol), 5β-stigmastanol (24-ethyl-5β-cholestan-3β-ol), and 5β-epistigmastanol (24-ethyl-5β-cholestan-3α-ol) (Bull et al., 1999). Coprostanol is a derivative form of cholesterol (cholest-5-en-3β-ol) and is the major fecal stanol of humans (Bull et al., 2002). Cholesterol, either ingested through eating meat or secreted or sloughed from cells within the human body, is metabolized by bacteria within the colon, leaving coprostanol as a byproduct (Juste and Gérard, 2021). Coprostanol is introduced into the environment through defecation, and much less frequently through death and decay of the organism's stomach cavity in the open or in graves (Pickering et al., 2018; Queirós et al., 2023; von der Lühe et al., 2020, 2013).

Following defecation, fecal stanols can be either buried in place or transported to a depositional center (Figure 2.1). With time, coprostanol transforms to its derivative form, epicoprostanol, through further microbial degradation in the environment (Bull et al, 1999, 2002), although epicoprostanol has been identified in human stool samples (Phua et al., 2013), suggesting that this process may begin in the gut. Coprostanol and its derivative epicoprostanol are known to persist in sediments for hundreds to thousands of years (Sistiaga et al., 2014; Vachula et al., 2019), likely due to a combination of preferential degradation of organic materials

that are more metabolically efficient and preservation in anaerobic settings. Studies have reported varying concentrations of coprostanol and epicoprostanol through time (Briles et al., 2019; D'Anjou et al., 2012; Keenan et al., 2021; Vachula et al., 2019; White et al., 2018) therefore the transformation of coprostanol to epicoprostanol is not constant and is likely context dependent. Additionally, the longevity reported for coprostanol in sediment or soil (Sistiaga et al., 2014; Vachula et al., 2019) suggests that we should not expect a total replacement of coprostanol by epicoprostanol with time. Due to its abundance in human stools and longevity in soils, researchers have used coprostanol as a human biomarker in archaeological projects (Bethell et al., 1994; Bull et al., 2005; Evershed and Bethell, 1996; Langgut et al., 2016; Prost et al., 2017; Shillito et al., 2011, 2008; Simpson et al., 1999; Sistiaga et al., 2014; Zhang et al., 2020).

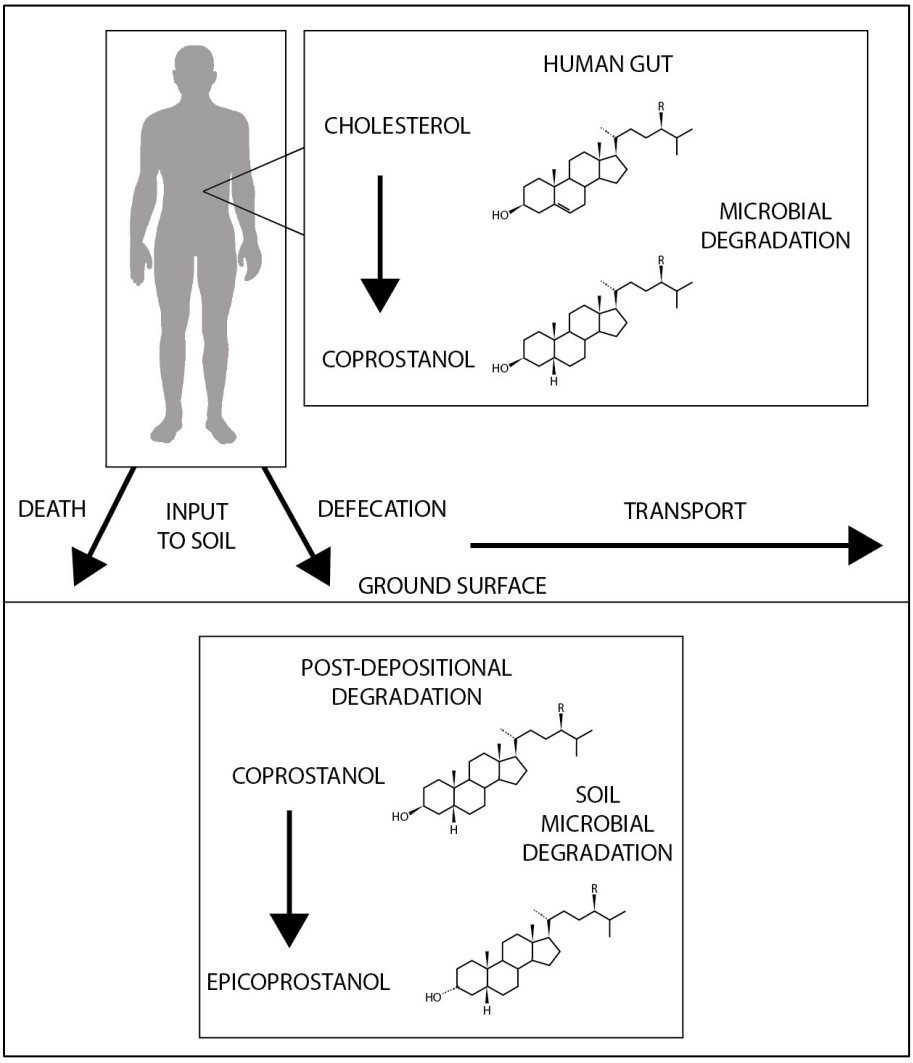

Figure 2.1. Schematic depicting the formation and degradation of major human fecal stanols. Adapted from White et al. (2018); human silhouette from Wikimedia Commons.

A 2012 study by D'Anjou et al. was the first to use fecal stanol molecules as a proxy of human population change. The authors associated changes over time in the concentration of fecal stanols from an arctic lake in Norway with demographic events that may have impacted the

inhabitants of a small archaeological site located within the lake's watershed, including the Black Death and medieval migration episodes (D'Anjou et al., 2012). This study demonstrated the basic premise of fecal stanols as a population proxy: the amount of fecal stanols within a sample can be directly linked to the relative size of a population at that time, as more feces in an environment is representative of more people. Following (D'Anjou et al. (2012), the method has been applied to numerous contexts throughout the world (Arnold et al., 2021; Battistel et al., 2017; Briles et al., 2019; Cheng et al., 2021; Curtin et al., 2021; Keenan et al., 2018; Schroeter et al., 2020; Thienemann et al., 2017; Vachula et al., 2019; White, 2017).

As this approach becomes more prevalent in paleoenvironmental and archaeological research, it is necessary to define its limitations and provide recommendations for the best approaches to using fecal stanols as a proxy of ancient population change. Keenan et al. (2022) identified important limitations in stanol data reporting and interpretation by finding that stanol ratios do not always correlate with human population size and that *in situ* production of stanols is not often considered in fecal stanol analysis. White et al. (2018) suggested that climate does not appear to be a limiting factor in the method's application, and additional studies in Africa (Battistel et al., 2017), Asia (Schroeter et al., 2020), Europe (Thienemann et al., 2017), South America (Arnold et al., 2021), Central America (Keenan et al., 2021), and North America (Vachula et al., 2019) confirm the method's viability in a variety of climatic settings. Additional issues and boundaries of the fecal stanol population method that have not been fully explored include the effect of diet on stanol production, differences in laboratory methods, an unknown number of non-human coprostanol producers, a possible lower limit to population size, the range of sedimentary contexts suitable for the method, the degree to which stanols are mobile before and after deposition, the temporal limit of the method, and the amount of time it takes for stanols to enter the sedimentary record (Table 2.1).

Table 2.1. Limitations of the fecal stanol population proxy method.

Limit	**Problem**	**Status**
Climate	Do differences in climate affect the viability of the method?	Successful applications from around the world (Arnold et al., 2021; Briles et al., 2019; Keenan et al., 2021; Vachula et al., 2019; White et al., 2019) suggest climate is not a limiting methodological factor
Data Reporting	How are stanol data best reported?	Keenan et al. (2022) found issues with reporting stanol ratios and suggested normalizing stanol values to TOC
Human Diet	Do differences in human diet affect the interpretation of fecal stanol data?	Medical studies (Reddy et al., 1998; Walker et al., 1982) show that people who eat a vegetarian diet produce less coprostanol than those who eat meat, but to our knowledge this difference has not been considered in archaeological studies
Laboratory Methods	Do different laboratory methods affect the comparison of stanol datasets?	There is no standard laboratory procedure for the preparation and analysis of fecal stanol samples. It is unclear if the diversity of

		techniques limits our ability to compare fecal stanol datasets
Non-human Producers	How many animals produce levels of coprostanol that could interfere with the human signal?	Numerous studies (Leeming et al., 1996; Prost et al., 2018, 2017; Shah et al., 2007) have reported certain animals, most significantly pigs, cows, and sheep, as considerable coprostanol producers, but only a small number of animals have been tested and the fecal stanol content of most species is unknown
Population Size	Does the method require a minimum population size to exceed background fecal stanol levels?	While many studies have focused on sedentary agricultural societies (Kaiser and Lerch, 2022; Keenan et al., 2021; White et al., 2018), others have employed the method in mobile hunter-gatherer contexts (Vachula et al., 2019; White et al., 2020; 2021), suggesting that the method is viable in small and large-scale societies, but the existence of a lower threshold is unknown
Sedimentary Context	Does the method work in a variety of sedimentary contexts?	Studies have created fecal stanol population reconstructions from lake and wetland sediments, and we are aware of one deep marine application (Kaiser and Lerch, 2022), but to our knowledge the approach has not been attempted in dryland sediments or desiccated water features
Stanol Mobility	How mobile are fecal stanols in sediments and how does this affect data interpretation?	We are aware of one environmental contamination study (Yager et al., 2014) to document vertical stanol mobility, but to our knowledge this has not been considered in archaeological studies nor have researchers measured the rate of lateral stanol mobility
Temporal Extent	How far back in time can the method be applied?	Vachula et al. (2019) present human fecal stanol values from 20,000 BP, which we understand to be the earliest application of the method
Temporal Lag	Is there a meaningful delay between when fecal stanols are produced and when they enter the sedimentary record and does this delay impact data interpretation?	The method is predicated on the transportation of fecal stanols to a depositional center, but we are unaware of research that seeks to understand the rate at which fecal stanol transportation occurs

Archaeological Background

This study was designed to explore the temporal, population size, and sedimentary limits of fecal stanol analysis. We chose to test these limits at the Kharaneh IV archaeological site (Figure 2.2). Kharaneh IV is an early/middle Epipaleolithic aggregation site located in the Azraq Basin in eastern Jordan that was occupied by hunter-gatherer groups from approximately 19,900 to 18,600 BP (Macdonald et al., 2018; Maher et al., 2012; Richter et al., 2013). Its age is near the time depth reached by Vachula et al. (2019) and a successful application of the method at Kharaneh IV would further confirm the method's viability in Pleistocene-aged contexts. Despite the site's many hearths, postholes, pits, flintknapping areas, middens, hut structures, and faunal assemblages that suggest relatively high population densities and multi-seasonal occupation (Jones, 2012; Maher et al., 2012; Martin et al., 2010), Kharaneh IV was nonetheless likely inhabited by small, kin-related groups, perhaps punctuated by aggregations of local and non-local groups, that left the site at times of the year. Kharaneh IV tests the ability of the method to document population changes in small communities. Finally, although Kharaneh IV was once located in a wetland environment (Jones et al., 2016; Maher et al., 2021), today the site and surrounding lands are at the fringes of the Syrian and Arabian Deserts and the Azraq Basin receives 50-200 mm of annual precipitation (Henton et al., 2017; Maher et al., 2021). To date, studies have formed fecal stanol population reconstructions from lake and wetland sediments, but to our knowledge this project is the first application of the method in dryland sediments or within the confines of an archaeological site.

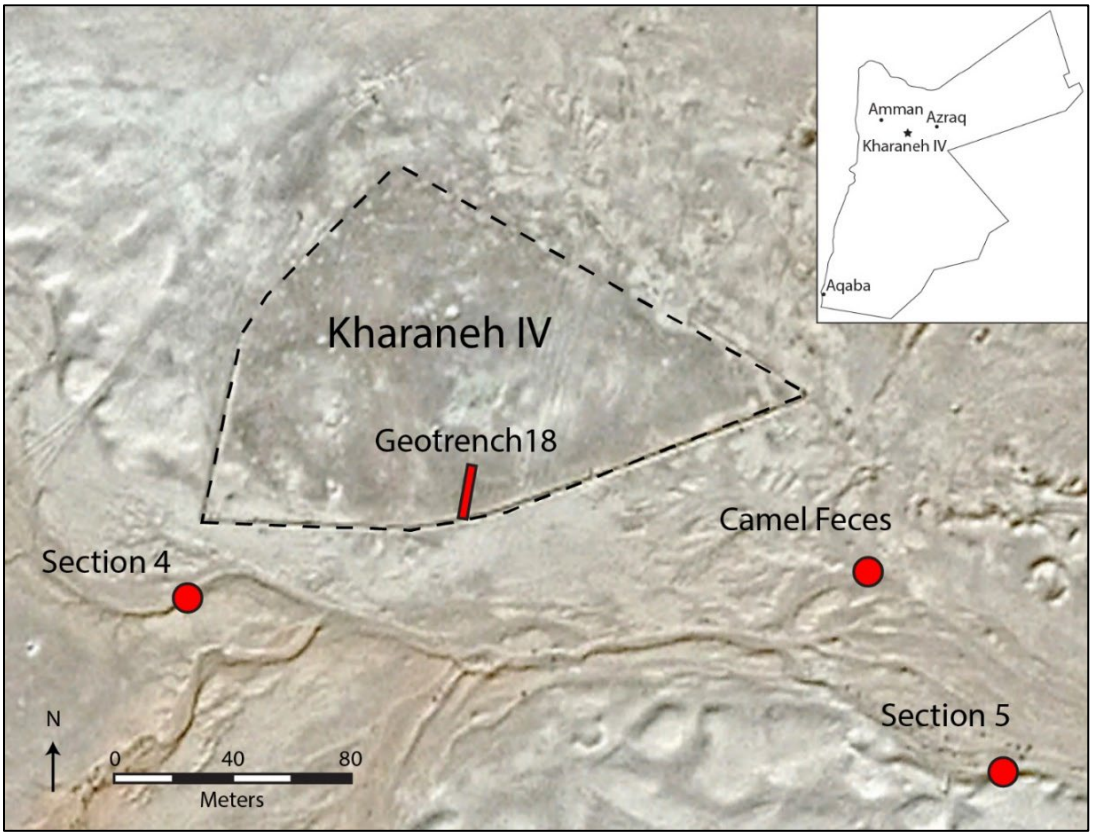

Figure 2.2. Annotated satellite image from Google Earth showing Kharaneh IV and the sampling locations used in this study.

Researchers have excavated at Kharaneh IV since the 1980s, beginning with work by Muheisen (1983; Muheisen and Wada, 1995) and continuing now under the Epipaleolithic Foragers in Azraq Project (EFAP), which has investigated multiple areas of the site and produced a large volume of data about subsistence strategies, cultural interactions and behaviors, technological changes, and environmental conditions during the Early and Middle Epipaleolithic (Henton et al., 2017; Jones et al., 2016; Macdonald et al., 2018; Macdonald and Maher, 2022; Maher, 2021; Maher et al., 2021, 2012; Ramsey et al., 2018). Although there are many excavated locations at the site to conduct fecal stanol analysis, we targeted units at the site's periphery for two reasons. First, the site's periphery is near a topographic low that presumably would have collected fecal material, but it is also above the wadi floor and more protected from erosional processes. Second, we expect the initial deposition of fecal material at Kharaneh IV to have been similar to defecation practices of modern small-scale societies. Observations of the Hadza in Tanzania showed that a defecation belt develops approximately 20-40 m outside of the camp after several days of occupation (Jones, 2016) and Yellen (1977) noted that a typical Ju/Huansi camp contains a communal area, a special activities area, and a peripheral area of unpleasant activities, including defecation (Figure 2.3). Kharaneh IV's periphery is approximately 30 m from the site's center. While acknowledging the limitations of ethnographic analogy, the site's periphery is a topographically and culturally fitting location to attempt to obtain fecal stanol samples.

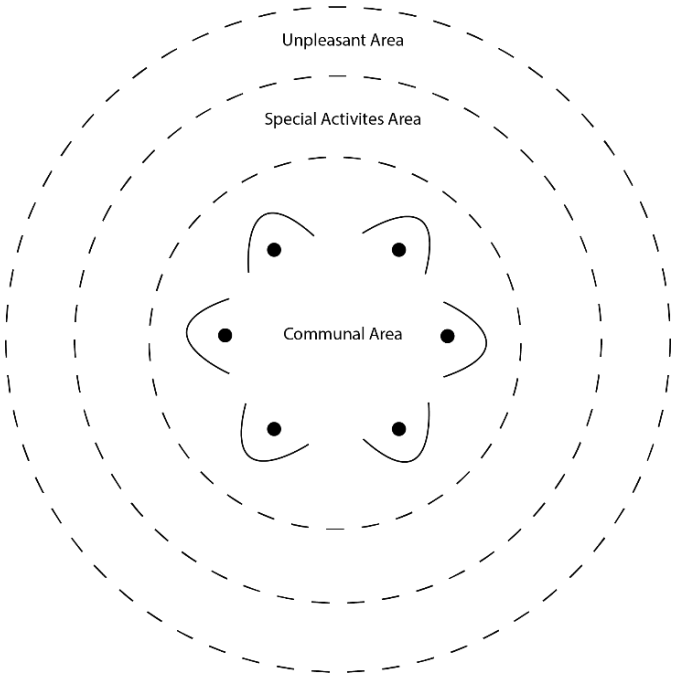

Figure 2.3. Yellen's (1977) ring model for hunter-gatherer settlement patterns, adapted to include the peripheral location for "unpleasant" activities, including defecation (Adapted from Lane 2014).

Methods

Sample Collection

We analyzed 22 sediment samples obtained from Kharaneh IV during the 2018 EFAP excavation season. We collected 16 onsite samples from a geological exploration trench (Geotrench18) dug perpendicular to the southern slope and boundary of the site (Figure 2). We excavated Geotrench18 to expose a 13 m-long, 0.6 m-wide cross section running from near the center of the site to its periphery (Figure 2.4). Within the geotrench we collected six samples at 10 cm intervals from 5 to 55 cm in depth at location GT12 and four samples at depths of 5, 15, 25, and 40 cm at locations GT3 and GT8 to determine changes in fecal stanol concentration with depth, and two additional samples to determine lateral changes in concentration at a depth of 16 cm at location GT0 and a depth of 19 cm at location GT5 (Figure 2.5).

Figure 2.4. Field photographs of sampling locations S5, S4, and Geotrench18, respectively. The contact between brown, permeable silts and white, impermeable marl is clearly visible in S4.

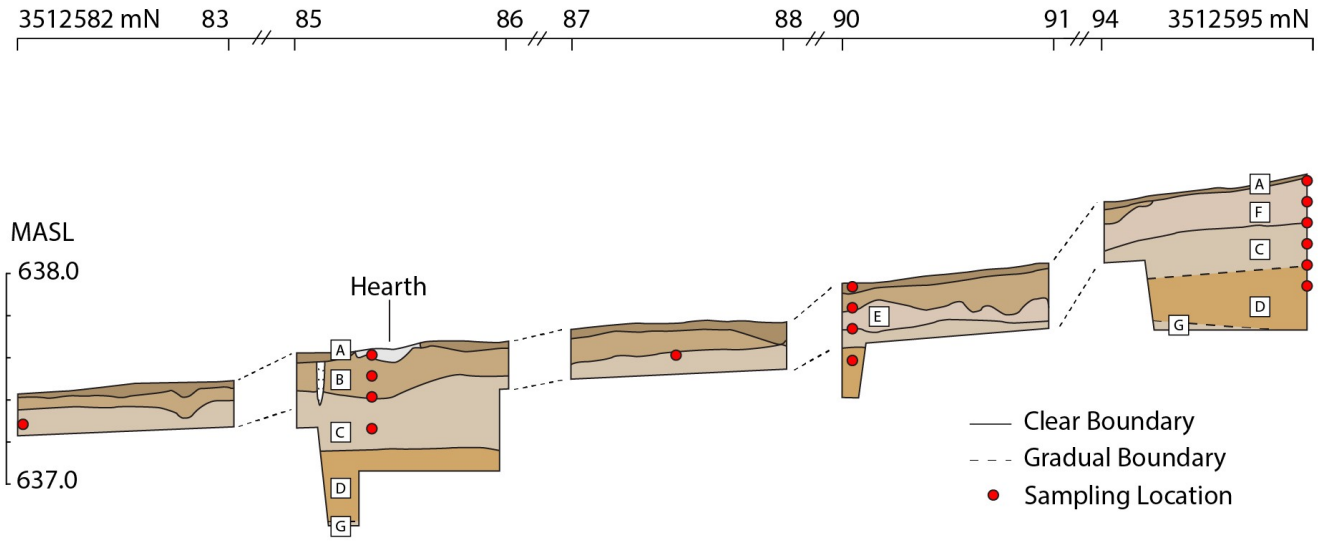

Figure 2.5. Geotrench profile showing sampling locations (red circles) and stratigraphy.

We collected six sediment samples from two offsite locations dug into culturally sterile wadi floor and wetland deposits previously studied by Jones et al. (2016), S4 and S5 (Figures 2 and 4). S4 is 90 m southwest of Kharaneh IV and Location S5 is 165 m southeast of Kharaneh IV. We chose these locations to incorporate sedimentological data and descriptions from Jones et al. (2016). Jones et al. (2016) describe S4 sediments as 27 cm of very pale brown (10YR 7/4) and brownish-yellow (10YR 6/6) fine sand (wadi floor deposit) overlying light yellowish-brown (10YR 6/4) clayey silt (wetland deposit) to depth and S5 sediments as very pale brown (10YR 7/3, 10YR 7/4, 10YR 8/2) silts (wetland deposit) to depth beneath a 10 cm-thick weathering surface. We collected four samples at depths of 0, 15, 30, and 60 cm at location S4 and two samples at depths of 0 and 60 cm at location S5. The offsite locations serve as control samples because the exposed wetland deposits predate the site (20-22 Ka BP; Jones et al., 2016) and the wadi floor deposits postdate the site (4.5 Ka BP) and are expected to contain little to no human-derived stanol molecules.

During the 2018 EFAP summer season, we obtained two surface samples of dromedary camel (*Camelus dromedarius*) feces from recent camel droppings located immediately outside the southern boundary of Kharaneh IV (Figure 2). Because camel herds frequently traverse the site, we were concerned that camels may produce fecal stanol molecules that could contaminate cultural deposits at the site and complicate the interpretation of fecal stanols in archaeological soils.

Laboratory Methods

Prior to analysis, we processed sediment samples with weights ranging from 9 to 14 g and added 5 g of anhydrous sodium sulfate to each sample to remove any remaining water. We prepared two dried camel fecal samples weighing 0.15 and 0.57 g. We followed an extraction procedure similar to White et al. (2018), employing soxhlet extraction to soak sediment samples contained in cellulose thimbles (Whatman) with 200 mL of dichloromethane (DCM) overnight. We concentrated samples to a final volume of 0.5 mL using rotary evaporators (Büchi) and

evaporation under a nitrogen stream. We derivatized stanols into their trimethlysilyl (TMS) ethers through a reaction with N,O-Bistrifluoroacetamide (BSTFA) for one hour at 70 °C. Due to the high stanol content in the camel fecal samples, we performed a 1:10 dilution of the derivatized extract to produce smaller and more clearly defined spectra peaks. We injected the derivatized samples using an autosampler (7683B series, Agilent Technologies, Santa Clara, California, USA) into an Agilent gas chromatograph (GC; 6890N series) equipped with a mass selective detector (MSD; Agilent 5973 inert series) and a Supelco fused silica capillary GC column (0.25mm ID x 30m×0.25 μm film thickness). We programmed the temperature profile of the GC oven to rise from 45 °C to 225 °C at 25 °C/min, then to 285 °C at 1.5 °C/min and held for 12 min. We set the injector temperature at 285 °C. We used helium as a carrier gas, and we used the MSD in the Electron Ionization (EI) mode. The source and quadrupole temperatures were set at 230 °C and 150 °C, respectively.

We identified stanol and sterol compounds (coprostanol, epicoprostanol, 5α-cholestanol, sitosterol, and stigmasterol) by comparing characteristic mass spectra fragmentation patterns and gas chromatographic retention times of samples and blank spikes with the chemical standard solutions of these compounds (Sigma Aldrich). We generated data for analysis using the Agilent Environmental Chem Station software. We determined concentrations by comparing peak areas with a calibration curve and the relative response factor of an internal standard (anthracene-d10 and benzo(g,h,i) perylene-d12; AccuStandard).

Results and Discussion

Stratigraphically, we identified seven sedimentary units in Geotrench18 (Table 2.2), which can be organized into two groups by compaction and compositions: loose, upper deposits that contain artifacts in a matrix of silt and fine sand (Layers A, B, E, and F) and very compact, lower deposits with few artifacts in a clay-rich marl (Layers C, D, and G). The contact between these groups is abrupt and recognizable by a sudden increase in compaction (Figures 4 and 5). Similarly, the contact between upper reddish silty sand and lower clayey silt at offsite location S4 is abrupt and marked by an increase in compaction. The contact between the upper weathering surface and lower silts at offsite location S5 is gradual.

Table 2.2. Summary of Geotrench18 stratigraphy

Layer	Munsell	Color	Compaction	Avg. Thickness (cm)	Lower Boundary	Description
A	10YR 6/4	Light brown	Loose	< 5	Abrupt, smooth	Deflated, surface palimpsest, high artifact density covering brown silt
B	10YR 7/4	Reddish brown	Moderate	15	Abrupt, wavy-irregular	Reddish silt, lower boundary is a disconformity
C	10YR 8/2	Light gray	Compact	25	Clear-gradual, smooth	Pale colored marl, contains small crystals near top, breaks in large aggregates/blocky texture
D	10YR 7/6	Brown	Compact	30	Gradual, smooth	Similar texture to C, but contains root traces and

						darker color, mottled in places breaks in large aggregates/blocky texture
E	2.5YR 8/2	Very light gray	Loose	10	Gradual, smooth	Very loose light-colored unit, interfingers with B, grades laterally into F
F	2.5YR 8/2	Light gray	Moderate	15	Clear, smooth	Same level as E, but more compact and high artifact density, likely edge of site
G	10YR 8/2	Light gray	Compact	na	na	Identical to C, but beneath D

Coprostanol values ranged from 0.00 to 25.25 ng/g (Table 2.3). Within the geotrench, coprostanol was high near the surface, absent or lower at 15 cm deep, consistently highest at 25 cm deep, and absent or lower below 25 cm (Figure 2.6). The highest coprostanol values occurred at or slightly above the contact between upper porous silt and sand and lower, less permeable marl. With the exception of one sample from location GT3 measuring 2.45 ng/g at 40 cm depth, we did not identify coprostanol below the contact. We propose two hypotheses to explain this relationship: a) coprostanol measured at Kharaneh IV is *in situ* and related to human activity during the site's occupation or b) coprostanol is mobile in Kharaneh IV sediments and accumulating at the contact with less permeable marl.

Table 2.3. Summary of Kharaneh IV fecal stanol data. Concentrations of stanols are in ng/g of dry sediment and depth is in cm.

Location	Depth	Coprostanol	Epicoprostanol	5α-Cholestanol	Stigmasterol	Sitosterol
GT12	5	8.74	0	2.27	23.1	49.18
GT12	15	5.35	0	5.08	62.53	69.04
GT12	25	17.72	1.88	23.54	30.79	68.49
GT12	35	0	0	0	0	0
GT12	45	0	0	0	0	0
GT12	55	0	0	0	0	0
GT8	5	0	0	0	0	30.96
GT8	15	0	0	0	102.63	60.89
GT8	25	25.25	0	75.31	95.37	89.1
GT8	40	0	0	0	0	13.02
GT5	19	4.4	0	8.13	103.76	80.55
GT3	5	1.43	0	0	16.8	24.97
GT3	15	0	0	0	237.45	136.9
GT3	25	5.98	0	4.96	273.75	193.12
GT3	40	2.45	0	0	82.27	70.68
GT0	16	0	0	0	208.41	132.97
S4	0	18.31	1.41	10.07	78.23	263.68
S4	15	0	0	0	293.91	401.13
S4	30	9.76	0.91	8.79	131.27	151.27
S4	60	0	0	0	62.81	65.32
S5	0	9.52	1.51	3.58	35.33	46.58
S5	60	0	0	0	0	10.58

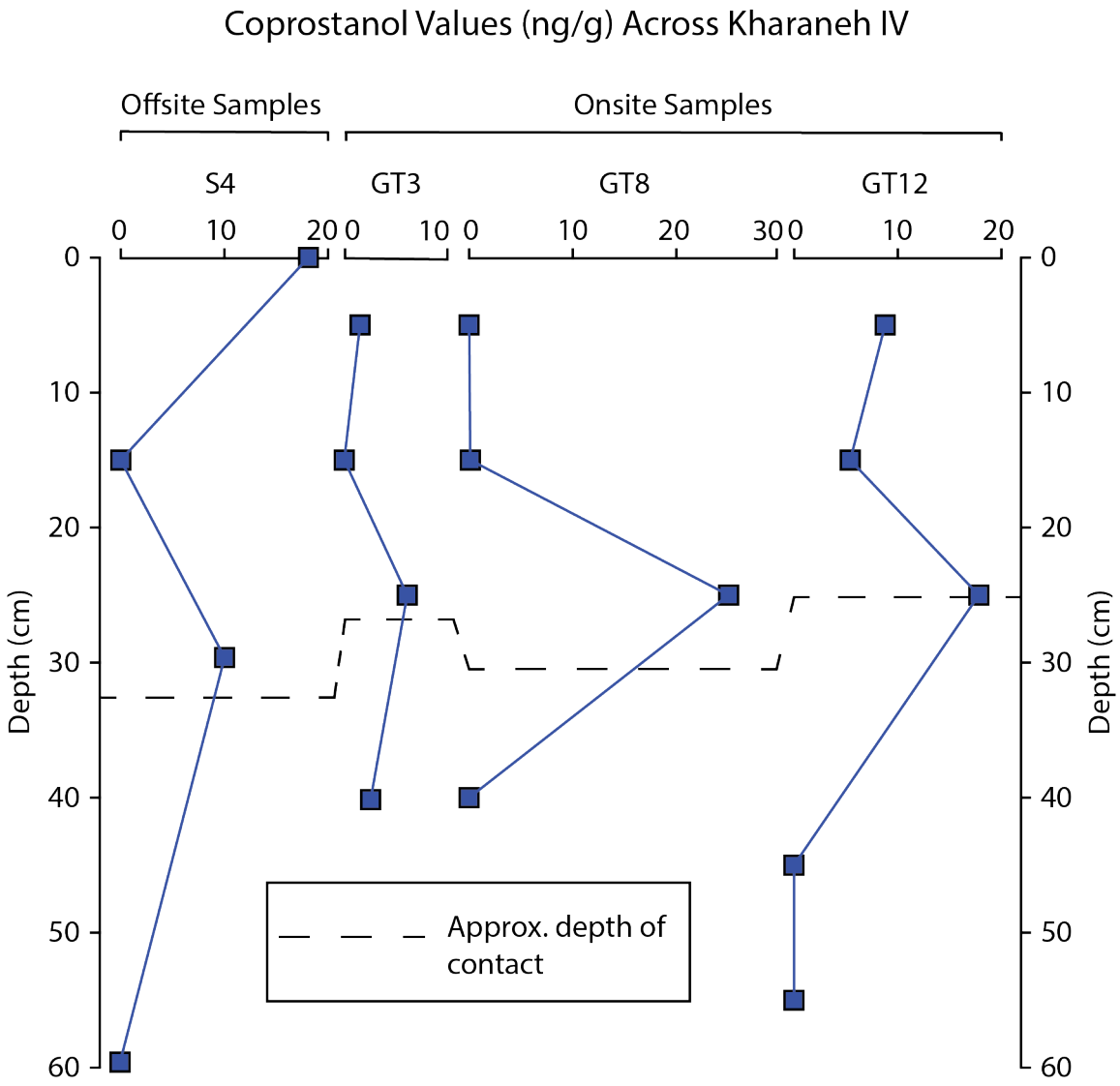

Figure 2.6. Coprostanol values across Kharaneh IV sampled locations. The dashed line is the approximate depth of the contact with less permeable marls at each location. Locations with less than three samples (S5, GT0, and GT5) are not plotted.

If coprostanol is *in situ* within Kharaneh IV sediments, then we would expect it to be absent or present at lower values in offsite samples that are further away from the site's population center and that postdate and predate the site. Coprostanol values at location S4 show a similar trend to onsite sampling locations, with high values near the surface and at the contact with less permeable marls at 30 cm deep and no detectable coprostanol at 15 cm and 60 cm deep. If these sediments were contemporaneous with Kharaneh IV, then it would be possible that offsite coprostanol values relate to the occupation of Kharaneh IV as modern hunter-gather groups often defecate at a distance from the group's activity center (Yellen, 1977). However, Jones et al. (2016) used optically-stimulated luminescence (OSL) to date sediments just above

the contact with less permeable clays in location S4 to 4.5 ± 0.4 ka BP. The similar coprostanol trends in allochronic offsite and onsite contexts suggest that coprostanol is not *in situ* within Kharaneh IV sediments.

The distinct increase in coprostanol above the contact of permeable silts and sands with less permeable marls in both onsite and offsite contexts suggest coprostanol is mobile in porous sediments and is accumulating at the contact with less permeable layers. Experimental data from Yager et al. (2014) indicate that coprostanol can be mobile in terrestrial surficial sediments, with migration of coprostanol through a sandy loam to depths over 1 m possible in under two years. While coprostanol is hydrophobic (Bull et al., 2002) and unlikely to undergo transportation dissolved in water, it may move in association with particulate matter within the porous upper sediments of Kharaneh IV. If coprostanol is migrating downwards at Kharaneh IV, then it requires a modern source in an area of low human activity.

Although Kharaneh IV does not appear to have supported a sustained human occupation following its abandonment at c. 18.4 ka BP (Richter et al., 2013), contamination of Kharaneh IV sediments with more recent coprostanol is possible from millennia of local grazing activity, including sheep, goat, and most notably camel. Because we could not identify published camel fecal stanol data we collected and tested two samples of camel feces. Camel fecal coprostanol values averaged 145.73 µg/g ± 41.06 (Table 2.4). The identification of coprostanol in camel feces shows that dromedary camels can produce coprostanol in amounts similar to other herbivorous mammals, less than sheep and pigs, but more than horses and donkeys (Figure 2.7; Table 2.5). The results indicate that the dromedary camel produces meaningful amounts of coprostanol that may complicate the interpretation of archaeological fecal stanol data as a nonhuman source. This is an important consideration in archaeological studies throughout North Africa and Southwest Asia.

Table 2.4. Summary of dromedary camel fecal sterol and stanol content.

	Sample 1 (µg/g)	**Sample 2 (µg/g)**	**Average (µg/g)**
Coprostanol	104.66	186.79	145.73
Epicoprostanol	11.79	20.59	16.19
Cholesterol	39.00	65.84	52.42
5a-Cholestanol	47.16	82.30	64.73
Stigmasterol	28.55	49.10	38.82
Sitosterol	73.93	116.20	95.07

Table 2.5. Survey of animal coprostanol content in modern stools (Leeming et al., 1996; Prost et al., 2018, 2017; Shah et al., 2007; Sherblom et al., 1997).

	Author	**Shah et al.**	**Leeming et al.**	**Prost et al.**	**Prost et al.**	**Sherblom et al.**	**This study**
	Year	2007	1996	2017	2018	1997	-
		All values in µg/g					
Animal	Human		3432	6940			
Herbivorous Mammals	Pig	530	353	772			
	Sheep	336	170	524			
	Cow	72	213	251	142		
	Horse	90	43	82	51		

	Donkey	131		92			
	Goat			63			
	Water Buffalo	15					
	Dromedary Camel						146
	Rabbit	507					
Carnivorous Mammals	Dog	1.5	8				
	Dingo	47					
	Cat		397				
Marsupials	Kangaroo	83					
	Koala	15					
	Possum		219				
Birds	Chicken	0.6	12				
	Duck	1	29				
	Turkey	1					
	Magpie		7				
	Seagull		13				
	Goose			15			
Aquatic Mammals	Manatee					1368	
	Dolphins					2.5	

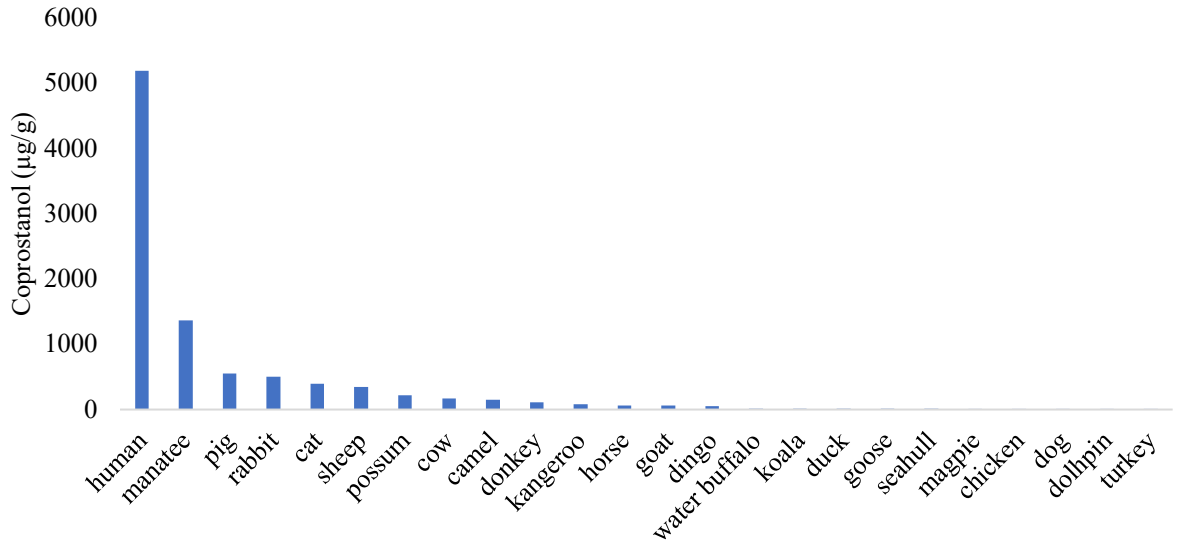

Figure 2.7. Coprostanol production in sampled animal stools (Leeming et al., 1996; Prost et al., 2018, 2017; Shah et al., 2007; Sherblom et al., 1997; this study) from highest to lowest. Values are averaged where multiple published data exist for one animal.

Epicoprostanol is only present in quantifiable amounts within four samples, all located above the contact with less permeable marls, and is absent in all other samples (Table 2.3). 5α-cholestanol displays a similar trend in concentration with depth as coprostanol, with its highest

values occurring at the permeability change contact in on and offsite locations, further suggesting a downward mobility pattern (Table 2.3). 5α-cholestanol is traditionally understood as a degradation product of cholesterol that is formed primarily by microbial communities outside the guts of animals in the open environment (White et al., 2018). However, we measured 5α-cholestanol in appreciable amounts within camel feces (Table 2.4), indicating camels as a likely source of 5α-cholestanol at Kharaneh IV. Additionally, the existence of 5α-cholestanol in camel feces suggests that there are multiple pathways to its production and this fact complicates the use of the molecule in stanol ratios that assume it represents a background level of stanol input and decay (*sensu* Bull et al., 1999, 2002; White et al., 2018).

The plant sterols measured in this study, sitosterol and stigmasterol, display similar depth trends to coprostanol, with higher concentrations above the contact than below it (Figure 2.8). However, while sitosterol and stigmasterol values are diminished beneath the contact, they are present at values greater than zero. This suggests that the contact is either not completely impermeable and that some sitosterol and stigmasterol from more recent herd animal contaminants reach the marl layers, or that they are *in situ* molecules produced by Late Pleistocene wetland flora.

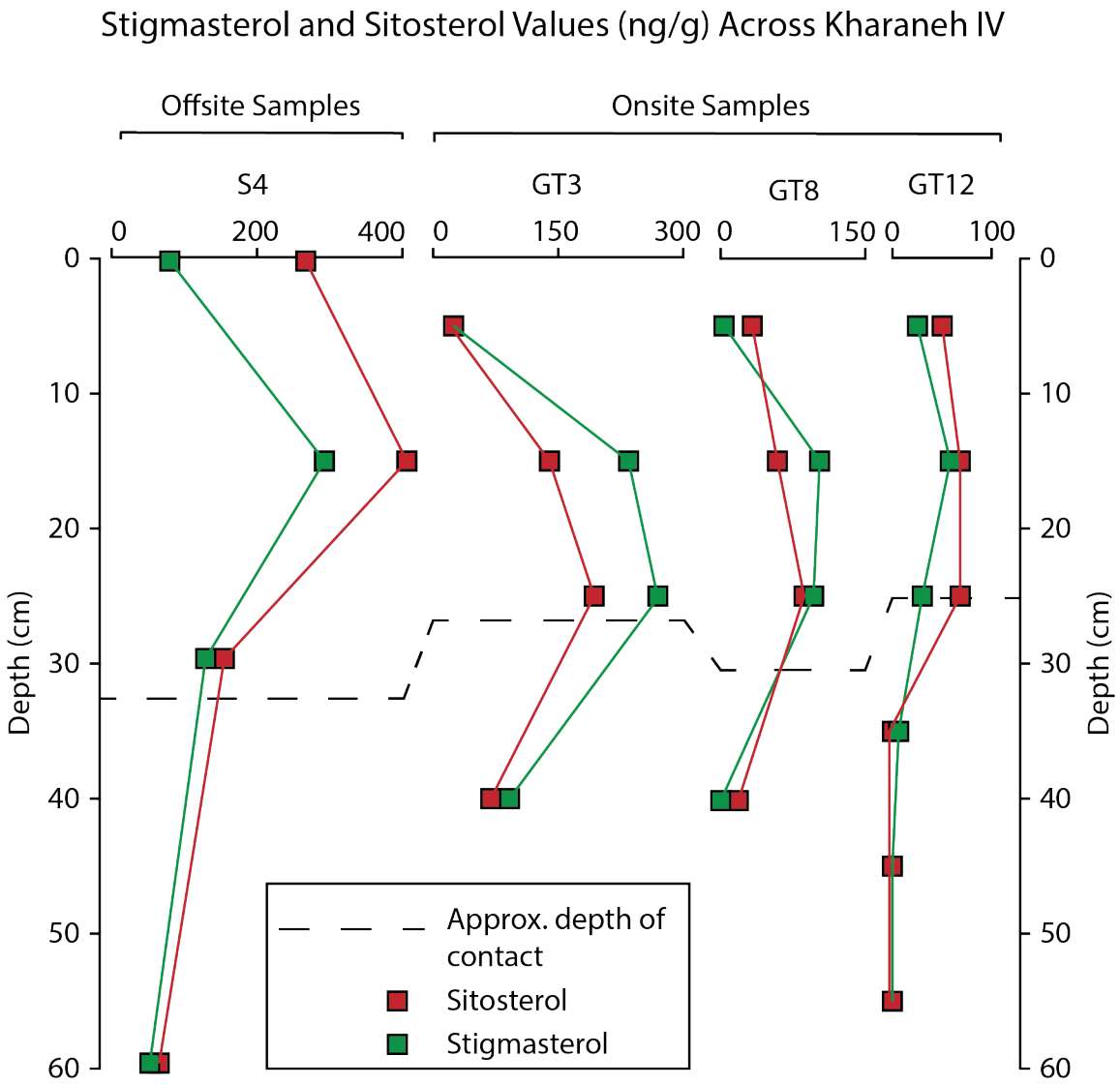

Figure 2.8. Stigmasterol (green) and sitosterol (red) values across Kharaneh IV sampled locations. The dashed line is the approximate depth of the contact with less permeable clays at each location. Locations with less than three samples (S5, GT0, and GT5) are not plotted.

Conclusion and Recommendations

The similar, allochronic on-site and off-site trends in coprostanol at Kharaneh IV, frequent coprostanol deposition from camel defecation, and experimental evidence from Yager et al. (2014) that indicates coprostanol can be mobile in dryland sediments, suggest that coprostanol at Kharaneh IV is likely not *in situ*. Few archaeological studies have considered fecal stanol mobility in terrestrial contexts. The possibility of coprostanol migration through porous sediments is a major limitation of its use as a biomarker in archaeological studies due to potential mixing with modern contaminants and a loss of temporal context. While coprostanol may be mobile in terrestrial sediments through percolation and bioturbation, it does not appear to be

mobile in aqueous sediments (Peng et al., 2002). We recommend that archaeological studies attempting to use coprostanol as an indicator of ancient population change target aquatic depositional contexts, such as lakes, ponds, and marshes, where post-depositional movement of coprostanol is expected to be low. The mobility of fecal stanols in soils raises questions of how these molecules are transported across a landscape. It is unclear how much fecal material is lost to soils before it is deposited in an aquatic depositional center, how long it takes to reach a deposition point, if this process is uniform, and if these factors need to be considered in the interpretation of fecal stanol data. This study and experimental data (Yager et al., 2014) demonstrate vertical stanol mobility, but additional research should be conducted on the rate of lateral stanol mobility to account for delays between the timing of stanol production and their ultimate deposition. The occurrence of coprostanol in camel feces highlights the need for investigators to consider all potential nonhuman contributors to a region's fecal stanol record and to expand the list of animals known to produce coprostanol. We recommend that future studies obtain and analyze fecal samples from animals within their study area that may contribute to its fecal stanol record, thereby increasing confidence in data interpretation and contributing to our overall understanding of fecal stanol abundance in the animal kingdom. Finally, we note that the presence of 5α-cholestanol in camel feces indicates multiple pathways to the molecule's formation that calls into question its utility as a marker of environmental stanol input and preservation.

Chapter 3

Gazelle Tooth Enamel Isotopic Record as a Proxy of Paleoclimatic Conditions at Kharaneh IV, Jordan

Abstract

Previous studies at the Epipaleolithic aggregation site Kharaneh IV have been limited in reconstructing paleoenvironmental conditions during the site's occupation due to the erosion of contemporary sedimentary features. This study presents gazelle tooth enamel O and C isotope values from multiple stratigraphic contexts at Kharaneh IV to determine if diachronic isotopic variation is related to changes in local paleoclimate. We find little variation in values between the site's older Area B and younger Area A occupations, indicating relatively stable conditions over the course of the site's thousand-year history, and supporting notions of Kharaneh IV as a reliable persistent place. However, a -2% excursion in Middle Epipaleolithic Area A $\delta^{18}O$ values suggests a temporary period of enhanced precipitation that may be related to continuity in the site's archaeological assemblage.

Introduction

A major problem in environmental archaeology derives from limitations in our ability to correlate archaeological and paleoclimatic datasets. Sources of paleoenvironmental data, including ocean, lake, and ice cores, speleothems, and tree rings, operate at different temporal and geographical scales (Figure 3.1). When applying these data to archaeological sites, the extent to which regional and global climatic conditions and events affected the lives of people at the local scale is unclear and, possibly, negligible. Chronometric error becomes compounded when multiple paleoclimatic datasets are correlated to an archaeological site that has its own chronometric uncertainties, whether from artifact-based chronologies, radiocarbon dating, or the indistinctness of human behaviors as tracked in post-depositional processes. A reliance on external correlations limits our ability to understand the complexities of human-environmental dynamics at the site level and invites allegations of 'neo-environmental determinism' (Ellen, 1982; Erickson, 1999; Livingstone, 2012; Meyer and Guss, 2017).

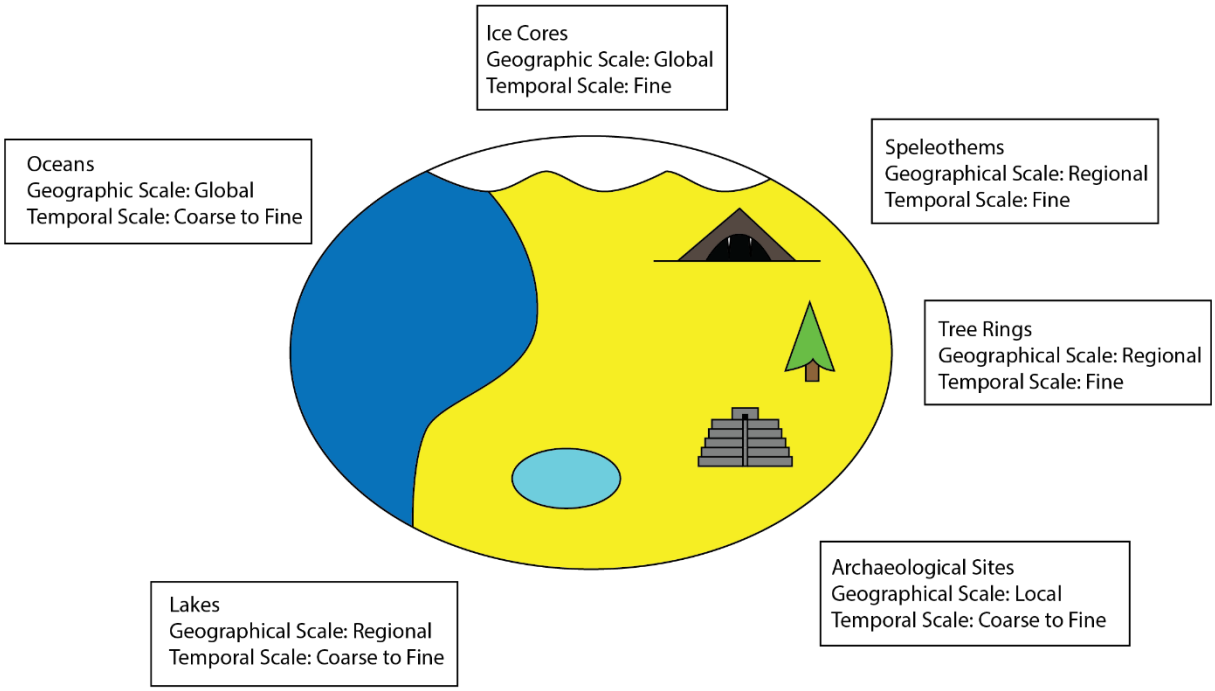

Figure 3.1. Schematic showing different geographic scales and distances of paleoenvironmental proxies in relation to archaeological sites.

A solution to this problem is to obtain paleoclimatic and archaeological information from the same sedimentary archive, which reduces problems of geographical scale by using samples from the same location and chronological problems by allowing for direct stratigraphic comparison. Researchers have thus turned to a variety of near or onsite sources of paleoclimatic data, including pollen (Mariotti Lippi et al., 2010; Mercuri et al., 2015, 2013), fecal molecules (D'Anjou et al., 2012; Keenan et al., 2021; White et al., 2019; see Chapter 2), archaeological sediments (Xiong et al., 2023), and human and animal bone and tooth hydroxyapatite (Heaton et al., 1986; Hedges et al., 2004; Sarkar et al., 2016; Schwarcz et al., 2010).

In archaeological contexts with prevalent faunal remains, stable isotope analysis of animal tooth hydroxyapatite can provide valuable paleoclimatic data (Henton et al., 2017; Leng and Melanie, 2006; Naito et al., 2022). The oxygen isotopic composition ($\delta^{18}O$) of tooth enamel hydroxyapatite reflects the $\delta^{18}O$ values of ingested water, either as drinking water or food water, which in turn corresponds to regional temperature and precipitation conditions within an organism's habitat (Dansgaard, 1964; Habinger et al., 2020; Iacumin and Longinelli, 2002; Kohn et al., 1998; Naito et al., 2022). The carbon isotopic composition ($\delta^{13}C$) of tooth enamel hydroxyapatite is derived from an organism's diet. Plants with C_3, C_4, and CAM photosynthetic pathways have distinct differences in fractionation of ^{13}C during photosynthesis, which impacts the composition of hydroxyapatite depending on the type of vegetation an organism ingests (DeNiro and Epstein, 1978; Hoppe et al., 2006; O'Leary, 1981; Smith and Epstein, 1971; Zazzo et al., 2010). Variations in the carbon and oxygen isotopic composition of tooth enamel in different specimens through time may relate to changes in local paleoclimate (Naito et al., 2022).

Kharaneh IV

This study applies tooth enamel isotope analyses to animal remains from the Kharaneh IV archaeological site in eastern Jordan (Figure 2). Kharaneh IV is a large, Epipaleolithic hunter-gatherer aggregation site located in Jordan's Azraq Basin that was occupied from approximately 19,800 to 18,600 BP (Macdonald et al., 2018; Maher et al., 2012; Richter et al., 2013). Paleoenvironmental reconstructions indicate the presence of a wetland in the vicinity of Kharaneh IV that evaporated at some point during or following the site's use (Besancon et al., 1989; Garrard et al., 1985; Jones et al., 2016; Maher et al., 2021). The Kharaneh wetland was central to the subsistence and settlement practices of hunter-gatherer groups in that it provided a range of wetland plants for food and building materials (Bode et al., 2022; Ramsey et al., 2018, 2016) and water for people and a diverse set of prey (Macdonald et al., 2018; Martin et al., 2010; Spyrou et al., 2019) that supported at least multi-seasonal occupations throughout its history (Henton et al., 2017). Multiple studies have investigated the environmental events that occurred leading up to the site's initial occupation (Jones et al., 2016; Maher et al., 2021), but there is no sedimentological archive to reconstruct the paleoenvironment during the site's occupation due to the erosion of contemporary sedimentary features (Jones et al., 2016).

The paucity of concurrent paleoclimatic and archaeological data complicates our understanding of human-environmental relations at Kharaneh IV. The site's eastern excavated units in Area B contain Early Epipaleolithic artifacts and date to 19,830 and 18,730 cal. BP (Richter et al., 2013). The site's western excavated units in Area A contain Early and Middle Epipaleolithic artifacts and the Middle Epipaleolithic contexts are generally younger, dating to 18,850-18,600 cal. BP (Figure 3.2) (Macdonald et al., 2018; Richter et al., 2013). Over 30 radiocarbon dates from throughout the site deposits indicate no major hiatuses in occupation between or within phases. There are distinct differences in the archaeological assemblages of the two areas. Area B has multiple hut structures that contain caches of ochre, shell, and gazelle horn cores, and human burials (Maher et al., 2012). The lithic assemblage in Area B deposits is defined by non-geometric microliths prepared in a mostly uniform manner (Macdonald et al., 2018). Area A contains numerous postholes and hearths, which Spyrou et al. (2019) and Maher and Macdonald (2020) consider to be associated with meat drying activities.

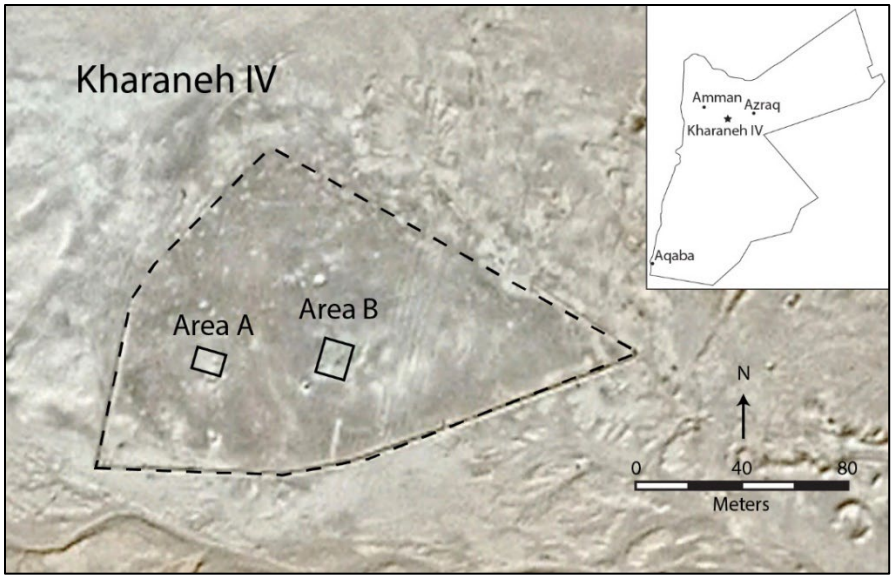

Figure 3.2. Annotated satellite image from Google Earth showing Kharaneh IV and the sampling locations used in this study.

Unlike the Early Epipaleolithic levels in Areas A and B, the geometric microliths in the Middle Epipaleolithic levels of Area A are highly variable in form and suggest a variety of technological traditions present at one time (Macdonald et al., 2018). Artifact density in Area A Middle Epipaleolithic contexts is much higher than underlying Early Epipaleolithic contexts (Macdonald et al., 2018). Taken further, the variability in microlith form and increase in artifact density may indicate the amalgamation of different cultural groups at Kharaneh IV during later periods of aggregation. Macdonald et al. (2018) noted that this technological transition occurred during a change in the sedimentology of Area A, from lower compact wetland marls containing non-geometric Early Epipaleolithic microliths to sandy loams containing geometric Middle Epipaleolithic microliths. Previous work interpreted the loss of Kharaneh IV's wetland marls as an indicator of desiccation (Jones et al., 2016; Maher et al., 2021), suggesting that the technological transition in Area A was a response to aridification in the local environment that may have continued through the site's abandonment (Macdonald et al., 2018). Phytolith data presented by Ramsey et al. (2016) suggests that Area A may have experienced wetter conditions during the Middle Epipaleolithic, but additional evidence is needed to support this finding and Area A's upper units are so dense with cultural material that it is not possible obtain paleoenvironmental information using sedimentological data alone.

To address this problem, we investigated the use of gazelle tooth enamel O and C isotopes as proxies of paleoclimatic conditions at Kharaneh IV. While the site's dense habitation layers lack naturally deposited strata useful for traditional paleoenvironmental studies, they contain the remains of many butchered goitered gazelle (*Gazella subgutturosa*). Gazelle teeth are prevalent throughout the site's occupation deposits as isolated teeth no longer within a mandible, but we chose to focus on third mandibular molars (M_3), from both within mandibles and as isolated specimens, in this study because they are most easily identifiable and best preserved due to their large size (Figure 3.3). Third molar enamel in modern gazelle populations form between the first 9 and 18 months of an individual's life and, thereby, reflect close to a year of seasonal

change as the organism incorporated isotopic signatures of its surroundings (Davis, 1980; Henton et al., 2017). Kohn et al. (1998) demonstrated this isotopic pattern of seasonality within modern gazelle populations by showing a progression in $\delta^{18}O$ enamel values that tracked annual variation in the $\delta^{18}O$ of local surface water. The interpretation of gazelle tooth enamel isotopes is complex because gazelles are nonobligate drinkers that may migrate large distances, requiring $\delta^{18}O$ values to be understood within the context of plant tissue $\delta^{18}O$ and possibly meaning that their isotopic signature reflects regional, not local, conditions. However, Henton et al. (2017) demonstrated that gazelle tooth $^{87}Sr/^{86}Sr$ values from Kharaneh IV remains are consistent with $^{87}Sr/^{86}Sr$ values of local soils, suggesting that gazelle stayed near the site year-round.

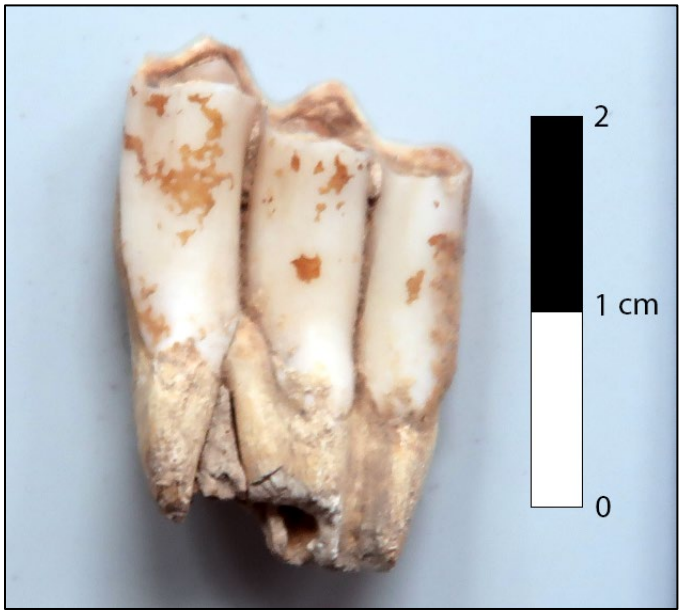

Figure 3.3. Third mandibular gazelle molar prior to cleaning and sample preparation.

For this study, we compared the range of $\delta^{18}O$ and $\delta^{13}C$ gazelle tooth enamel values reported by Henton et al. (2017) and new data from this project from Kharaneh IV's younger Area A with data we obtained from Area B to determine if there is diachronic variation in gazelle tooth isotope values and to assess if this variation is related to changes in local climate.

Methods

We obtained 14 Area B M_3 specimens and seven Area A M_3 specimens from bulk > 4 mm material collected over multiple field seasons by the Epipaleolithic Foragers in Azraq Project (EFAP) (Table 3.1). We removed dirt and plaque using a dental pick and brush and used a handheld Foredom rotary tool with a diamond coated drill bit to sample enamel at 5 mm increments beyond the enamel:root junction (ERJ). Due to size differences, the number of samples yielded per tooth ranged from 1-4 (5-20 mm from ERJ). Following the methods of Miller (2016), we bathed the samples in 1 mL of sodium hypochlorite for 24 hours, rinsed them with 1 mL of ultrapure water, bathed the samples in 1 mL of 0.1 M hydrochloric acid for 12 hours, then rinsed them with water 10 times to remove latent salts that initially disrupted mass spectrometer analysis (Yang et al., 2005). Following drying in an oven at 60° C for 4 hours, we

submitted the samples to the Center for Stable Isotope Biogeochemistry (CSIB) at the Department of Integrative Biology, University of California at Berkeley for analysis.

Table 3.1. Analyzed tooth specimens with archaeological context information.

Tooth ID	Square	Area	Locus	n. Samples
AQ3	AQ42	A	3	2
AQ4	AQ42	A	2	1
AR1	AR40	A	8	4
AR2	AR42	A	8	2
AR3	AR37	A	35	3
AS2	AS38	A	3	3
AS3	AS42	A	8	1
Area A = 7 Specimens				
AX1	AX74	B	88	1
AX2	AX74	B	88	1
AY2	AY73	B	41	3
AY3	AY74	B	88	3
R4	R/S2/60/P3	B	115	2
R5	R/S2/60/P3	B	115	3
R6	R/S2/60/P3	B	115	3
R7	R/S2/60/P3	B	139	3
R8	R/S2/60/P3	B	4	2
R9	R/S2/60/P3	B	27	3
R10	R/S2/60/P3	B	27	2
R11	R/S2/60	B	115	3
R12	R/S2/60/P3	B	124	3
R13	R/S2/60/P1	B	60	2
Area B = 14 Specimens				

We originally reacted bulk enamel powder samples containing about 10 to 100 micrograms of calcite or aragonite with 100% H_3PO_4 at 90° C for 10 mins to generate CO_2 gas for both carbon and oxygen isotope analyses ($\delta^{13}C$ and $\delta^{18}O$) using a GV IsoPrime mass spectrometer with Dual-Inlet and MultiCarb systems at CSIB. We included several replicates of one international standard, NBS19, and two lab standards, $CaCO_3$-I & II, in each run. However, samples ran with the dual inlet MultiCarb device and reacted with 100% H_3PO_4 at high temperature (90° C) displayed the 'salt effect' (Yang et al., 2005). To eliminate the salt effect, we ran these samples using continuous flow via a GasBench device at room temperature and 85% H_3PO_4. In this new approach, most of the non-CO_2 gases (such as SO_2 and HCl) generated from significant soluble salts (such as sulfate and chloride) can be converted to liquid acids with 15% H_2O in 85% H_3PO_4 at room temperature (Yang et al., 2005) and a possible small portion of the non-CO_2 gases mixed with the CO_2 can be further separated via the GC column through the

GasBench device. This procedure removed the salt effect such that non-CO_2 gases no longer affected the CO_2 generated from carbonate in 'salty' samples during the carbonate isotope analysis. The overall external analytical precision is $\pm$0.2‰ for both $\delta^{13}C$ and $\delta^{18}O$.

We incorporated 14 relevant data points from Henton *et al.* (2017) that are comparable in ERJ distance to the samples presented in this study (Table 3.2). To best compare datasets, we chose Henton *et al.* samples with an ERJ distance within 1.5 mm of the 5 mm ERJ intervals used in our samples and rounded the ERJ distance to 5, 10, or 15 mm when plotting Henton *et al.* data alongside the results from this study. While Henton *et al.* primarily analyzed gazelle tooth specimens from Area A, we note that one specimen, tooth 79, should be reclassified as from Area B.

Table 3.2. Henton et al. (2017) data incorporated in this study.

Tooth ID	Area	Square	Locus	ERJ (mm)	Rounded ERJ (mm)	$\delta^{18}O$	$\delta^{13}C$
2	A	AR36	100	5.3	5	-1.73	-9.2
2	A	AR36	100	8.9	10	-0.14	-9.11
2	A	AR36	100	15.9	15	-2.50	-7.03
4	A	AR35	110	6	5	4.92	-10.79
4	A	AR35	110	15	15	-0.41	-6.20
30	A	AR36	34	5.2	5	-0.02	-8.77
30	A	AR36	34	14.9	15	-4.24	-5.85
31	A	AR36	34	5.5	5	1.82	-9.72
31	A	AR36	34	10.3	10	0.96	-10.12
35	A	AS42	99	6.2	5	4.54	-9.31
35	A	AS42	99	10.3	10	1.71	-8.21
79	B	AW73	158	6.1	5	4.88	-10.3
79	B	AW73	158	9.5	10	3.54	-10.62
79	B	AW73	158	14.2	15	-0.81	-9.14

Results

The results of the study show that Area A $\delta^{18}O$ samples range from -2.81 to 7.14‰ and Area B $\delta^{18}O$ samples range from -3.31 to 6.53‰ (Table 3.3; Figure 3.4). Area A $\delta^{13}C$ samples range from -10.78 to -3.56‰ and Area B $\delta^{13}C$ samples range from -11.40 to -3.15‰. The $\delta^{18}O$ and $\delta^{13}C$ envelopes for Area A and Area B samples are notably similar, with less than 1‰ difference in their maximum and minimum extents. The Area A samples from this study are slightly more positive than those reported in six comparable Area A M_3 specimens by Henton *et al.* (2017), which range from -4.24 to 4.92‰ $\delta^{18}O$ and -10.79 to -5.85‰ $\delta^{13}C$ (Figure 3.5). This discrepancy could be due to low sample sizes in comparable data from Henton *et al.* (M_3 = 6) and this study (M_3 = 7), quantitative differences arising from different analytical equipment, or reflect actual diversity within Area A samples.

Table 3.3. Results of O and C isotope analyses.

Sample ID	Area	ERJ Dist (mm)	$\delta^{18}O$	$\delta^{13}C$
AQ3.1	A	5	7.14	-8.71
AQ3.2	A	15	1.26	-6.40
AQ4.1	A	5	5.18	-9.14
AR1.1	A	5	5.88	-9.39
AR1.2	A	15	0.41	-5.78
AR1.3	A	10	2.74	-8.23
AR1.4	A	20	-2.67	-3.56
AR2.1	A	5	5.74	-9.10
AR2.2	A	15	-0.13	-6.51
AR3.1	A	5	1.41	-8.52
AR3.2	A	15	-2.81	-3.79
AR3.3	A	10	-1.59	-4.94
AS2.1	A	5	5.48	-10.78
AS2.2	A	15	-0.39	-6.52
AS2.3	A	10	2.74	-8.46
AS3.1	A	5	5.31	-10.04
AX1.1	B	5	6.03	-9.68
AX2.1	B	5	3.49	-10.52
AY2.1	B	5	3.19	-11.40
AY2.2	B	15	-0.29	-7.53
AY2.3	B	10	-0.18	-9.15
AY3.1	B	5	1.84	-8.81
AY3.2	B	10	0.96	-8.32
AY3.3	B	15	-1.23	-6.57
R4.1	B	5	4.85	-10.41
R4.2	B	15	-1.25	-7.79
R5.1	B	5	5.52	-7.37
R5.2	B	15	-0.65	-4.10
R5.3	B	10	-0.04	-5.82
R6.1	B	5	6.53	-9.47
R6.2	B	15	0.59	-9.32
R6.3	B	10	2.09	-9.66
R7.1	B	5	6.14	-11.28
R7.2	B	15	2.99	-9.84
R7.3	B	10	4.05	-11.24
R8.1	B	5	2.80	-7.77
R8.2	B	15	-1.30	-5.02
R9.1	B	5	1.90	-7.39

R9.2	B	15	-1.10	-4.48
R9.3	B	10	-0.16	-5.84
R10.1	B	5	2.85	-5.90
R10.2	B	15	-1.56	-3.15
R11.1	B	5	6.47	-10.09
R11.2	B	15	-0.66	-6.25
R11.3	B	10	2.57	-9.16
R12.1	B	5	1.96	-8.37
R12.2	B	15	-3.31	-4.42
R12.3	B	10	-0.99	-5.02
R13.1	B	5	4.01	-10.95
R13.2	B	10	1.50	-9.37

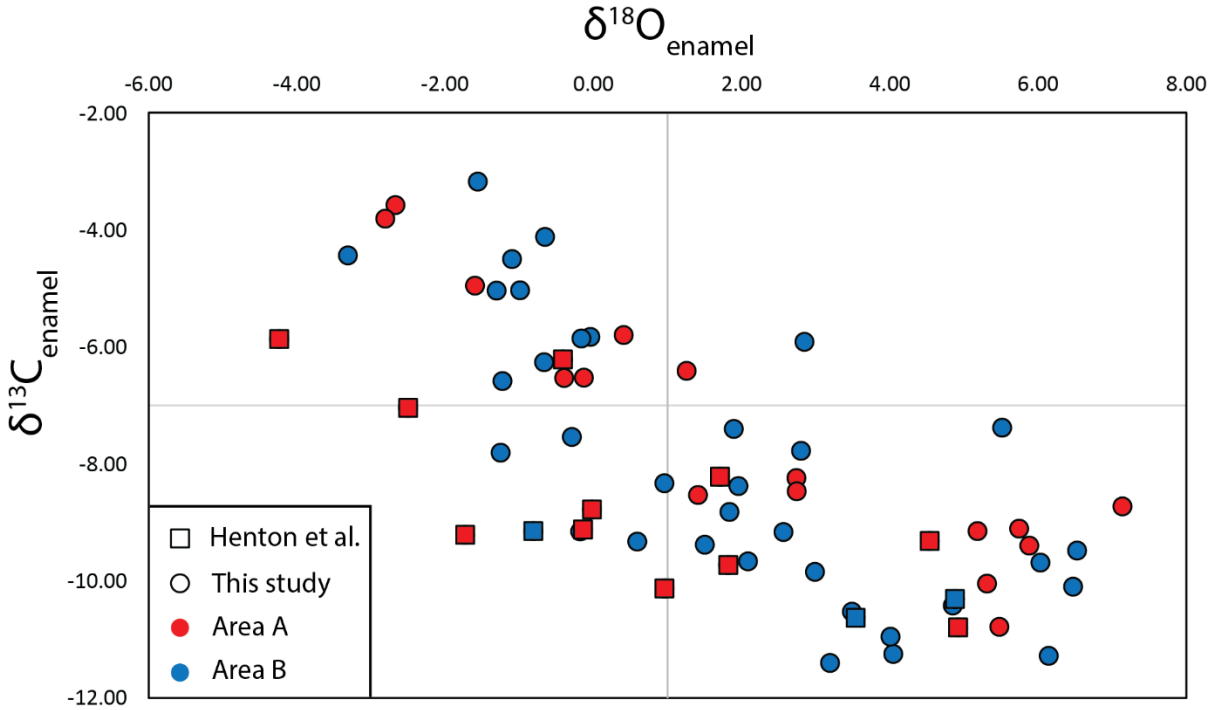

Figure 3.4. Plot of $\delta^{18}O$ and $\delta^{13}C$ values in Area A (red) and Area B (blue) samples. Data points include relevant samples from Henton et al. 2017 (squares) along with data from this study (circles).

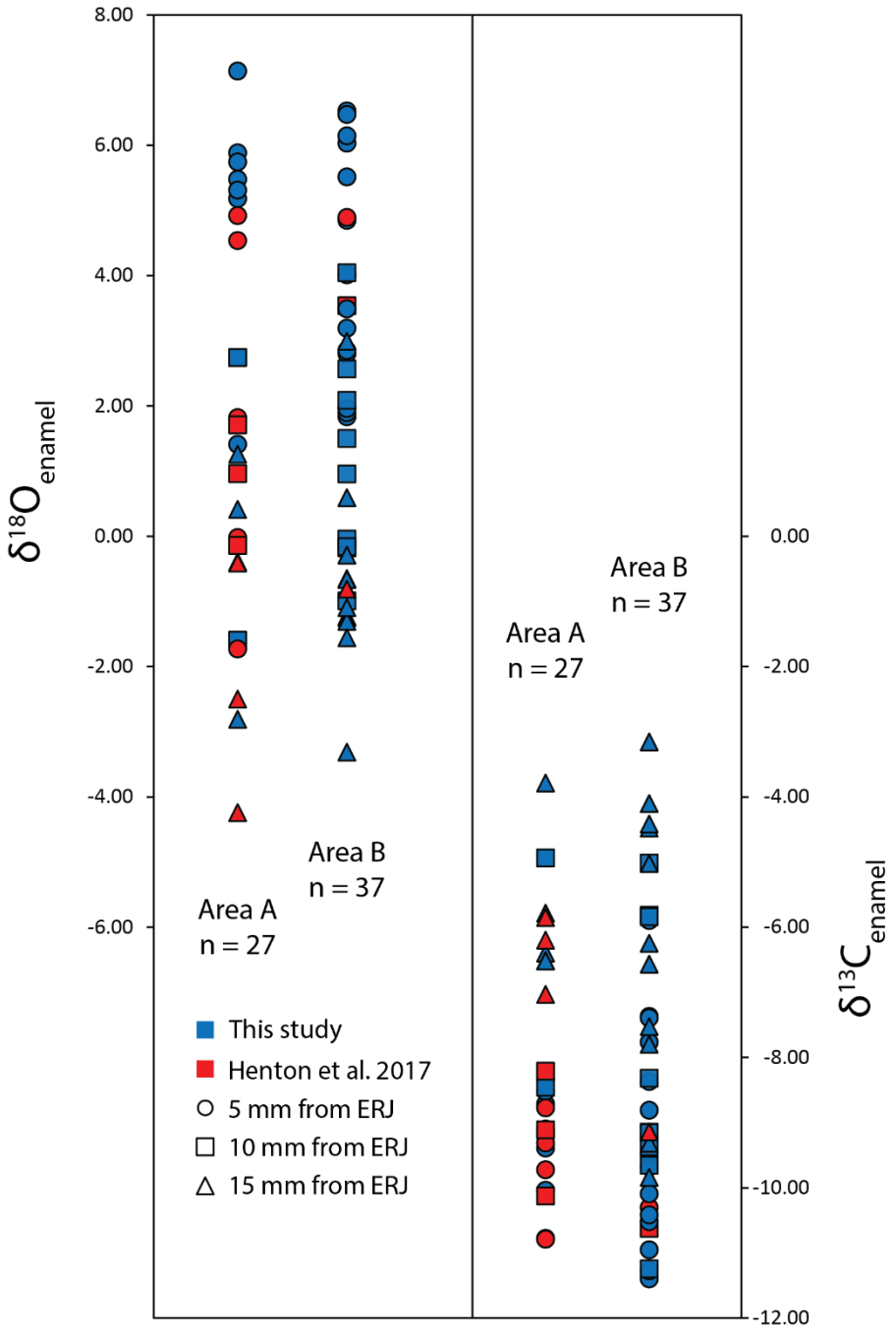

Figure 3.5. Range of $\delta^{18}O$ (left) and $\delta^{13}C$ (right) values in Area A and Area B samples according to ERJ distance (data point shapes). Data from Henton et al. 2017 are shown in red and data from this study are shown in blue.

The Area A samples selected for this study are stratigraphically higher (Loci 002-035; locus number generally increases with depth at Kharaneh IV) than those presented in Henton *et al.* (Loci 034-110) and, therefore, represent later and earlier Area A occupation levels, respectively. Both sets of Area A samples presented here are stratigraphically above the Early to

Middle Epipaleolithic transition identified by Macdonald et al. (2018) in Locus 115 and thus date to the Middle Epipaleolithic Area A context (18,850-18,600 cal. BP). Notably, three negative $\delta^{18}O$ outliers in Area A samples are from the same tooth specimen, AR3 (Figure 3.6). AR3 is from a locus depth (Locus 035) that is comparable to the levels analyzed by Henton *et al.* (2017) and its $\delta^{18}O$ values are more similar to the lower $\delta^{18}O$ envelope presented in Henton *et al.* (2017) than the higher $\delta^{18}O$ envelope in the rest of the Area A samples analyzed in this study. This suggests that differences in Area A samples between this study and Henton *et al.* (2017) relate to actual differences within the stratigraphy of Area A and do not result from separate analytical equipment or procedures of the two studies.

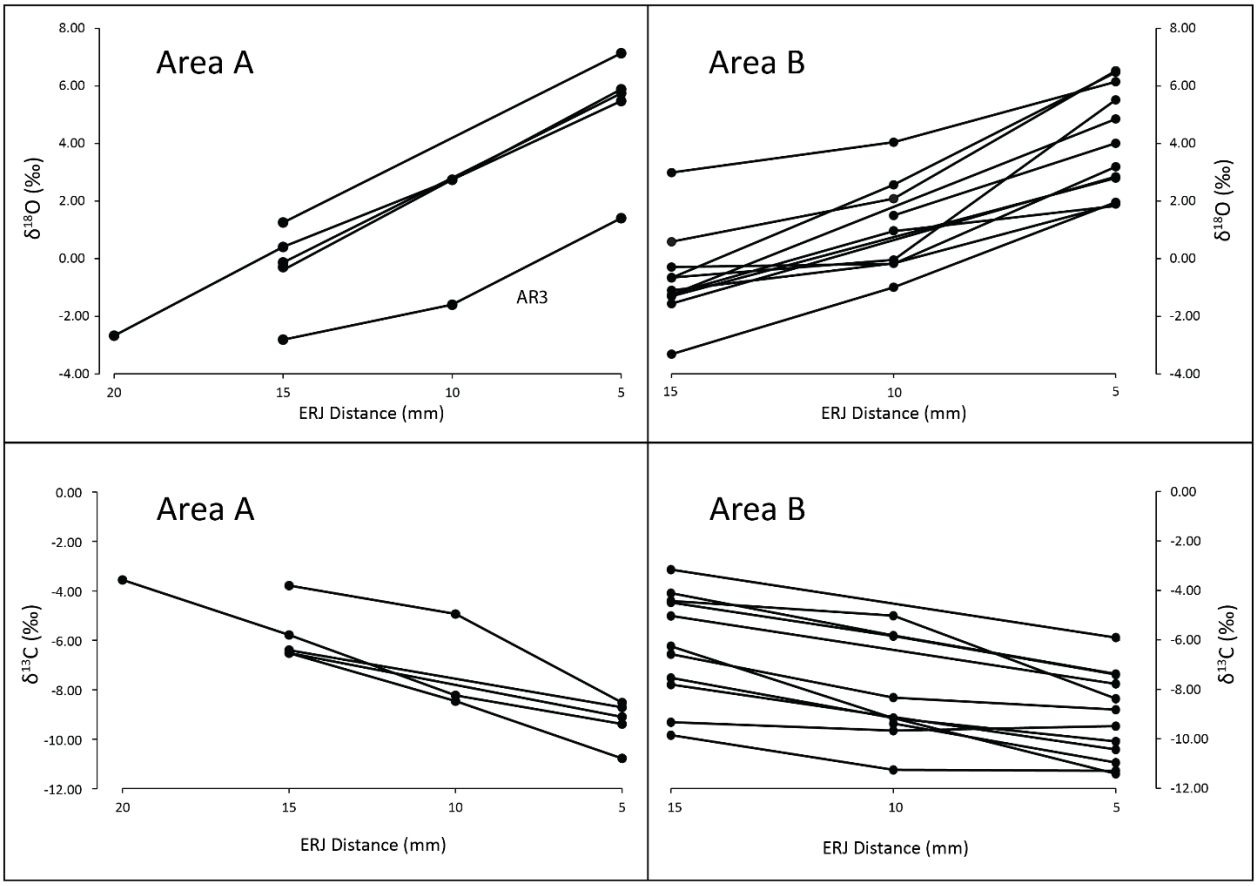

Figure 3.6. $\delta^{18}O$ (top) and $\delta^{13}C$ (bottom) plots for individual tooth specimens (black lines).

Individual teeth that yielded multiple samples consistently have highest enamel $\delta^{18}O$ values at 5 mm from the ERJ, lowest $\delta^{18}O$ values at 15-20 mm from the ERJ, and intermediary $\delta^{18}O$ values at 10 mm from the ERJ, displaying a negative correlation between $\delta^{18}O$ and ERJ distance (Figure 6). Henton *et al.* (2017) identified the same correlation in $\delta^{18}O$ and ERJ distance and attributed the relationship to seasonal differences in local water as enamel formation progressed. Meteoric water in the Azraq Basin today averages between 0.33‰ $\delta^{18}O$ in September and -6.36‰ $\delta^{18}O$ in January, with maxima over 6‰ and minima under -12‰ over the past 50 years (Table 4.4) (Henton *et al.*, 2017; IAEA/WMO, 2022). The negative correlation

between $\delta^{18}O$ and ERJ distance is interpreted to correspond to low $\delta^{18}O$ values at the 20 mm ERJ distance in M_3 samples with enamel formation during the late winter and high $\delta^{18}O$ values at the 5 mm ERJ distance with enamel formation during the summer, encapsulating approximately three seasons of growth (Figure 3.7). The correlation between enamel growth period and the $\delta^{18}O$ seasonality of modern rainfall and that the envelope of $\delta^{18}O$ values in each area of Kharaneh IV (Area A = 11.38‰; Area B = 9.84‰) is within the maximum and minimum range of modern meteoric water $\delta^{18}O$ variation (18.69‰) over a period of just 50 years (IAEA/WMO, 2022) suggest that the Kharaneh IV gazelle tooth enamel isotope record reflects, and would record, changes in local paleoclimate.

Table 3.4. Meteoric water $\delta^{18}O$ measurements from the Azraq Basin. Data from the GNIP Database (IAEA/WMO, 2022).

Date	**$\delta^{18}O$**
1967-10-31	-1.08
1967-11-30	-1.77
1968-01-31	-9.77
1968-02-29	-3.69
1968-03-31	-2.19
1968-05-31	5.53
1968-11-30	-2.58
1968-12-31	-4.57
1969-01-31	-3.28
1969-03-31	-4.61
1969-04-30	-0.82
1989-12-31	-2.75
1990-01-31	-6.84
1990-02-28	-5.36
1990-10-31	0.68
1990-12-31	-1.02
1991-01-31	-7.66
1991-03-31	-5.36
1991-10-31	2.85
1991-11-30	-9.33
1992-01-31	-12.23
1992-02-29	-12.4
1992-03-31	-5.96
1992-11-30	-3.24
1993-01-31	-4.24
1993-02-28	-9.96
1993-03-31	-2.74
1994-01-31	0.3
1994-03-31	-2.42
1994-09-30	0.33

1994-10-31	-4.72
1994-12-31	-4.9
1996-12-31	-0.88
1997-01-31	-5.57
1997-02-28	-3.12
1997-11-30	-2.94
1998-01-31	-4.91
1998-02-28	-5.75
1998-04-30	-1.73
1999-01-31	-3.13
1999-02-28	-1.72
1999-03-31	6.29
2000-01-31	-11.63
2000-10-31	3.47
2001-02-28	-3.22
2002-11-30	-3.445
2003-01-31	-7.32
2003-02-28	-2.29

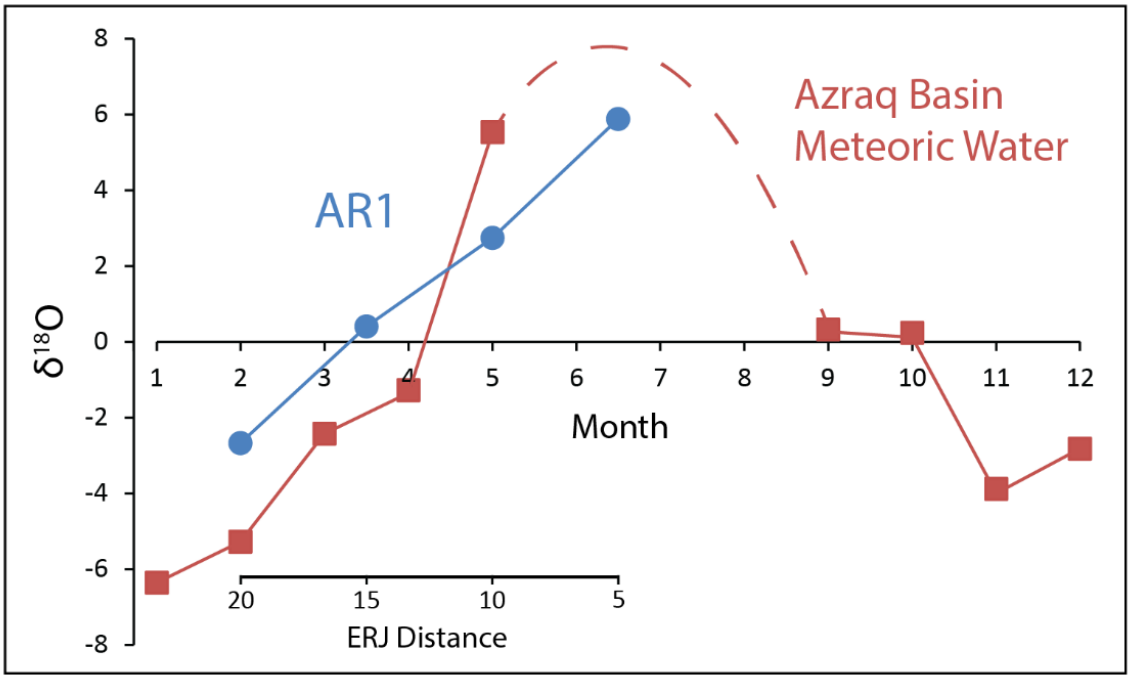

Figure 3.7. Tooth specimen AR1 $\delta^{18}O$ values (blue) plotted with Azraq Basin meteoric water $\delta^{18}O$ values (red; IAEA/WMO, 2022) showing seasonal relationships in tooth enamel growth and precipitation. Dashed line projects summer rainfall isotopic values, for which modern data is unavailable (IAEA/WMO, 2022).

Discussion

With the interpretation that the gazelle tooth enamel isotope record presented here reflects local meteoric water and vegetation isotopic values, we find that there was relatively little paleoclimatic change between the occupations of Area A and Area B, with perhaps an episode of warmer or wetter conditions following the beginning of Area A's Middle Epipaleolithic occupation. A stable local environment is supported by regional climate datasets from Lake Lisan (Bartov et al., 2003), Soreq Cave, Israel (Bar-Matthews et al., 2003; Grant et al., 2012), and Sofular Cave, Turkey (Fleitmann et al., 2009) which show little change during this period. The offset in $\delta^{18}O$ values between the stratigraphically lower Henton *et al.* (2017) Area A dataset and the Area A samples from this study suggests a period of climatic instability, which may relate to a brief negative excursion in speleothem $\delta^{18}O$ values from Soreq Cave centered on 18,800 BP (Figure 3.8) (Grant et al., 2012).

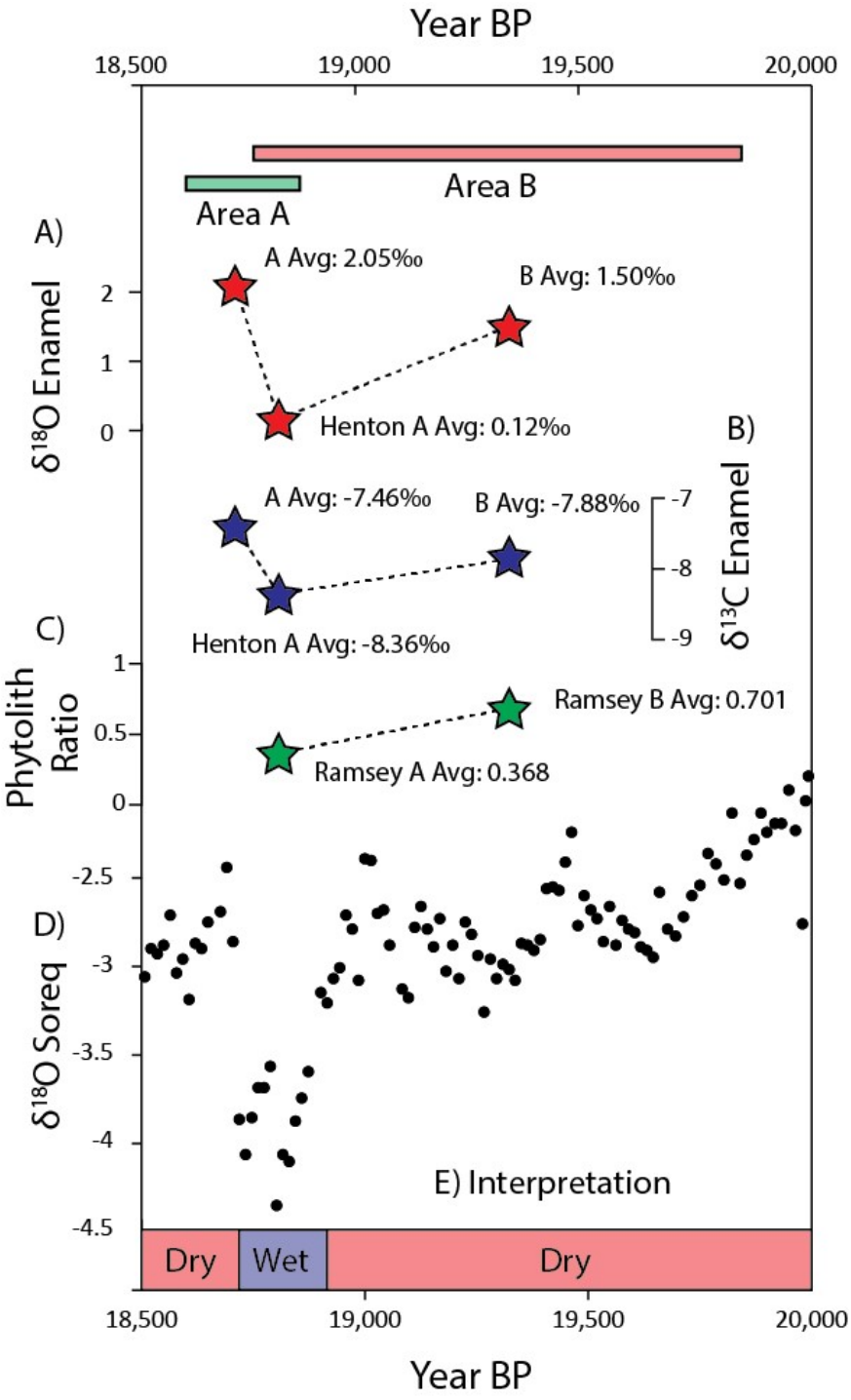

Figure 3.8. A) Averaged Kharaneh IV gazelle tooth enamel $\delta^{18}O$ values across Area A (Henton et al. 2017 and this study) and Area B (red stars), B) averaged Kharaneh IV gazelle tooth enamel $\delta^{13}C$ values across Area A (Henton et al. 2017 and this study) and Area B (blue stars), C) averaged chloridoid to chloridoid and panicoid grass ratio values (Ramsey et al. 2016) (green stars), D) Soreq Cave speleothem $\delta^{18}O$ values (black circles; Grant et al., 2012), and E) paleoclimatic interpretation. The occupation dates for Area A and B are shown above as colored bars (Richter et al., 2013; Maher et al., 2016).

In comparison to recent gazelle populations, the Kharaneh IV samples have higher M_3 $\delta^{18}O$ values than modern gazelle teeth obtained from the Lake Turkana and Nairobi regions of Kenya, (Kohn et al., 1996; 1998) (Table 3.5; Figure 3.9). While acknowledging that Kenya is climatologically distinct from Jordan, the comparison shows that the Kharaneh IV samples are only slightly higher than the Lake Turkana specimens, which inhabit a much warmer (29°C average temperature) and drier (200 mm annual precipitation) area than the Nairobi region specimens (19°C average temperature; 800 mm annual precipitation) (Kohn et al., 1998). This suggests that the Kharaneh IV samples represent a relatively dry paleoenvironment, but a direct comparison with modern gazelle in Jordan is not possible from available data.

Table 3.5. Comparison of archaeological Kharaneh IV and modern African gazelle M_3 specimen $\delta^{18}O$ values averaged across each tooth. The data from Kohn et al. (1996; 1998) have been converted from VSMOW to VPDB using the following transformation VPDB = ($\delta^{18}O$ VSMOW – 30.86)/1.03086 (Friedman and O'Neil 1977; Werner and Brand 2001).

Region	**Study**	**Sample ID**	**$\delta^{18}O$ (‰)**
Lake Turkana	Kohn et al. 1996	GG2090 #1	-0.17
Lake Turkana	Kohn et al. 1996	GG2090 #2	-0.39
Lake Turkana	Kohn et al. 1998	GG2109-1A	-0.18
Lake Turkana	Kohn et al. 1998	GG2109-1C	-0.35
Nairobi	Kohn et al. 1998	Gazelle-1	-8.96
Nairobi	Kohn et al. 1998	Gazelle-2	-5.50
Nairobi	Kohn et al. 1998	Gazelle-2-M3	-6.58
Kharaneh IV	Henton et al.	Area A (n=6)	0.12
Kharaneh IV	This study	Area A (n=7)	2.05
Kharaneh IV	This study	Area B (n=14)	1.5

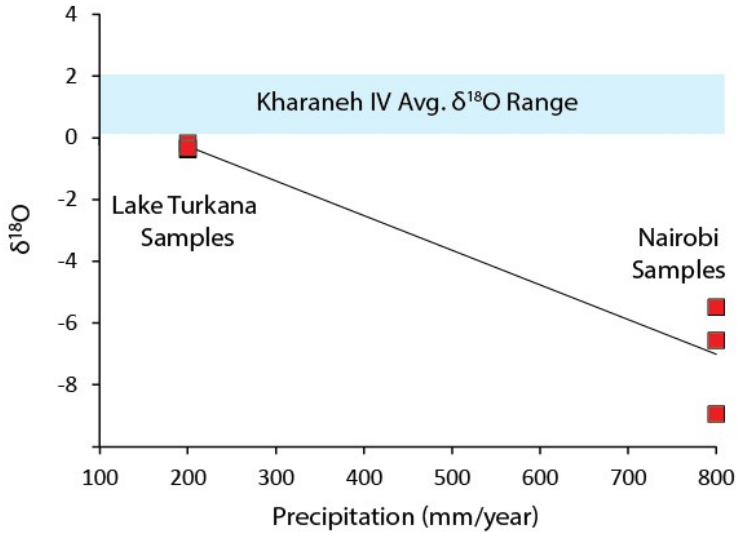

Figure 3.9. The relationship between annual precipitation and gazelle enamel $\delta^{18}O$ value in modern samples (red squares; Kohn et al., 1996; 1998) and the average range of $\delta^{18}O$ values in

Kharaneh IV samples, plotted across the chart because precipitation data are not available for archaeological samples.

Regionally, modern $\delta^{18}O$ data from Soreq Cave, Israel, show a negative correlation between annualized average $\delta^{18}O$ values and annual rainfall amount (Bar-Matthews et al., 2003). Additionally, negative $\delta^{18}O$ values from Soreq Cave and Peqi'in Cave, Israel, are associated with cave water level highs and correlate temporally with warm interglacial periods (Bar-Matthews et al., 2003; Grant et al., 2012). The negative excursion in Kharaneh IV gazelle tooth enamel $\delta^{18}O$ values following the beginning of Area A's Middle Epipaleolithic occupation may indicate a temporary period of increased precipitation. Bar-Matthews *et al.* (2003) found that a decrease of 1‰ in modern annualized rainfall $\delta^{18}O$ in neighboring Israel corresponded to a 200 mm increase in local annual precipitation. While acknowledging the limitations of applying modern trends to paleoenvironmental data, the strong relationship between negative $\delta^{18}O$ values and high precipitation observed by Bar-Matthews *et al.* (2003) suggests that the 2‰ offset between earlier and later Area A samples is related to a period of enhanced precipitation at the onset of Kharaneh IV's Area A occupation (Table 3.6; Figure 3.8).

Table 3.6. Averaged Kharaneh IV gazelle tooth enamel $\delta^{18}O$ and $\delta^{13}C$ values.

ERJ Distance	Variable	Avg. 5 mm	Avg. 10 mm	Avg. 15 mm	Total Avg.
Area A (this study)	$\delta^{18}O$	5.16‰	1.30‰	-0.30‰	2.05‰
Area A (Henton et al.)	$\delta^{18}O$	1.90‰	0.84‰	-2.38‰	0.12‰
Area B	$\delta^{18}O$	4.11‰	1.10‰	-0.70‰	1.50‰
Area A (this study)	$\delta^{13}C$	-9.38‰	-7.21‰	-5.80‰	-7.46‰
Area A (Henton et al.)	$\delta^{13}C$	-9.56‰	-9.15‰	-6.36‰	-8.36‰
Area B	$\delta^{13}C$	-9.24‰	-8.17‰	-6.22‰	-7.88‰

The interpretation of wetter conditions during Kharaneh IV's Middle Epipaleolithic occupation is also supported by phytolith evidence from Ramsey et al. (2016), which show lower chloridoid to chloridoid and panicoid grass ratio values in Middle Epipaleolithic Area A samples, suggesting a decrease in aridity (Figure 3.8). While both chloridoid and panicoid grasses generally use the C_4 photosynthetic pathway, chloridoids tolerate arid conditions better than panicoids and the ratio of chloridoids to panicoids can be interpreted as a precipitation signal, with higher and lower values corresponding to greater or less arid conditions (Ramsey et al., 2016). A shift in local plant communities resulting from increased precipitation may be apparent in the Kharaneh IV gazelle tooth enamel isotope record, wherein earlier Henton et al. (2017) $\delta^{13}C$ values are on average 0.9‰ lower than later Area A $\delta^{13}C$ values generated by this study (Table 5; Figure 8). This modest difference may relate to gazelle consuming slightly more abundant C_3 plants during a period of increased precipitation, although Ramsey et al. (2017) reported similar amounts of C_3 pooid grass phytoliths between Area A and Area B samples, so the offset in isotopic $\delta^{13}C$ values likely does not reflect a significant change in local vegetation.

From stratigraphic relationships, it appears that this climatic shift occurred after the Early to Middle Epipaleolithic transition in the site's archaeological record described by Macdonald et al. (2018), but before the site's eventual abandonment. While previous environmental research at

the site has largely emphasized desiccation over the course of the site's latter occupation (Jones et al., 2016; Macdonald et al., 2018; Maher et al., 2021), the data presented here, including regional isotopic evidence (Grant et al., 2012), site-scale phytolith (Ramsey et al., 2016) and faunal isotopic data (Henton et al., 2017; this study) point to a temporary and, possibly, substantial increase in rainfall during some of Kharaneh IV's Middle Epipaleolithic occupation. Our findings highlight the importance of using a multiproxy and multiscale approach in archaeological paleoclimatic research to identify the nuances of short-term and subtle environmental changes that may be missed using singular proxies and large geographic scales.

It is notable that the expansion in artifact density and technology types identified by Macdonald et al. (2018) suggesting greater and more diverse populations at Kharaneh IV occurred before the Middle Epipaleolithic increase in precipitation discussed here. This supports Macdonald et al.'s (2018) finding that if environmental change was related to the Early to Middle Epipaleolithic transition at Kharaneh IV, then it was related to wetland desiccation, not expansion. When this drying trend temporarily reversed during the site's Middle Epipaleolithic occupation, Kharaneh IV's inhabitants continued to invest heavily in the site, developing food processing stations (Spyrou et al., 2019), conducting communal hunting (Martin et al., 2010) and knapping activities (De Peña, 2022; Macdonald and Maher, 2022; Maher and Macdonald, 2020), creating artistically incised objects (Macdonald and Maher, 2022), and maintaining connections across the broader landscape through the curation and possible exchange of Mediterranean and Red Sea shells (Whitehurse, 2021), despite a presumed greater accessibility to water at other locations throughout the region.

The continued occupation of Kharaneh IV through Middle Epipaleolithic climatic change highlights and supports two main findings from previous work at the site: 1) the Kharaneh wetland was important for its reliability as a resource-rich environment (Ramsey et al., 2016) and 2) Kharaneh IV was a persistent place on the Epipaleolithic landscape (Macdonald and Maher, 2022; Maher, 2021, 2019, 2018). Increased precipitation during the Middle Epipaleolithic Kharaneh IV occupation may have enhanced the local wetland through greater water availability and more opportunities to obtain wetland fauna and flora. But it also would have allowed hunter-gatherers to exploit risky resources, such as wild cereals, grasses, and other seasonal resources, located at further distances in the surrounding steppe and grasslands, while maintaining access to reliable wetland resources, such as sedges and reeds (Ramsey et al., 2016). Epipaleolithic hunter-gatherers had no way to know how long the new, wetter conditions would last, so maintaining activities at a reliable wetland was part of a resilient resource strategy of balancing risky and reliable resources (Ramsey et al., 2016).

Soon enough, arid conditions returned to the site toward the end of the Middle Epipaleolithic occupation (Figure 3.8). While this later desiccation event may be related to the site's eventual abandonment, multiple dense cultural deposits near the site's surface suggest that occupation at Kharaneh IV continued in the face of a shifting climate. Despite this later period of oscillation, the continuity in $\delta^{18}O$ and $\delta^{13}C$ gazelle tooth enamel values between Area B and later Area A samples suggests that climatic conditions were largely dry, but stable for much of the site's occupation. This finding supports previous characterizations of the Kharaneh IV wetland as a reliable "persistent place" for Epipaleolithic hunter-gatherers over a thousand-year period (Macdonald and Maher, 2022; Maher, 2019; Ramsey et al., 2016). The contemporary

paleoclimatic data presented here contribute to our understanding of Kharaneh IV by demonstrating that the mostly stable local environment was punctuated by a time of increased precipitation during the site's Middle Epipaleolithic occupation, despite the wetland's eventual desiccation discussed in previous work (Jones et al., 2016; Macdonald et al., 2018; Maher et al., 2021).

Conclusion

Site-specific paleoclimatic data enhance our ability to understand human-environmental dynamics in the past. At Kharaneh IV, older strata beneath and adjacent to the site have allowed researchers to reconstruct the environmental events that occurred leading up to the site's initial occupation, but the subsequent erosion of these features have made it difficult to obtain paleoclimatic data contemporary with the site's use (Besancon et al., 1989; Garrard et al., 1985; Jones et al., 2016). The data presented here comprise a paleoclimatic record that can be directly compared to changes in Kharaneh IV's archaeological record. Overall, the similarities in gazelle tooth enamel isotopic data between Area A and Area B indicate that local environmental conditions were stable throughout much of the site's occupation. However, the 2‰ offset between later Area A samples analyzed in this study and earlier Area A data presented by Henton et al. (2017) and phytolith evidence from Ramsey et al. (2016) suggest that Kharaneh IV experienced a period of increased precipitation during its Middle Epipaleolithic occupation. While this may have expanded resource opportunities elsewhere throughout the region, Kharaneh IV's inhabitants chose to continue a close connection to the site, as evidenced through dense, concurrent cultural deposits and archaeological signatures of communal and artistic behaviors (De Peña, 2022; Macdonald et al., 2018; Macdonald and Maher, 2022; Martin et al., 2010; Spyrou et al., 2019). It is important to note that after $\delta^{18}O$ values rebounded to levels even higher than the Area B average during the later Area A occupation, intense occupation of Kharaneh IV continued. Sustained aggregation as the wetland ostensibly contracted with rising $\delta^{18}O$ values demonstrates that the relationship of Epipaleolithic hunter-gatherers at Kharaneh IV and the environment is complex and supports the understanding of Kharaneh IV as a persistent place on the Epipaleolithic landscape of eastern Jordan.

Chapter 4

Interweaving Persistent Place Theory and Paleoclimatology: The Paleoenvironmental Record of Kharaneh IV

Abstract

As an exercise in forming new bonds between archaeological method and theory, we suggest that paleoclimatic and paleoenvironmental data are pertinent to understanding the processes that form persistent places. This chapter presents new physical and chemical geoarchaeological data from Kharaneh IV, a large Early to Middle Epipaleolithic site in eastern Jordan, and aggregates existing data to define the site's 'unique' (*sensu* Schlanger, 1992) environmental qualities to form a narrative of local climatic change on the Kharaneh landscape. We find that the site's nearby wetland does not appear to have had a particularly unique hydrological setting that set it apart from the surrounding region, but its reliability over a thousand-year period encouraged continued reoccupations of the site that contributed to the formation of a persistent place.

Introduction

When applied to human-environment relations in the past, paleoclimatic research benefits from the frameworks of archaeological theory by providing a means of integrating data with intangible complexities of human culture. Archaeological theories in turn benefit from data that can be used to model the paleoenvironments in which individuals and groups operate. However, the integration of paleoclimatic data and theoretical frameworks can be challenging, in part because we are still forming theoretical and methodological pairings. This paper explores how paleoclimatic and paleoenvironmental data can be implemented in applications of persistent place theory to better understand how environments and cultures interact over geologically measurable timeframes (Shaw et al., 2016).

Schlanger (1992:92) defined persistent places as repeatedly used locations with long occupations that "structure the use and reuse of the larger landscape." Schlanger (1992) associated persistent places with three main qualities; they 1) possess unique qualities that are conducive to certain activities, 2) contain features that encourage further reoccupation and reuse, and 3) are formed through extensive use and revisitation. Researchers have applied the theoretical framework of persistent places in numerous ways since Schlanger's introduction of the concept, ranging in time from the Middle Pleistocene in Western Europe (Shaw et al., 2016) to the Colonial Period in California (Schneider, 2015) and in geographical scale from the size of massive shellmounds (Fish et al., 2013) to individual burials (Littleton and Allen, 2007). Methodologically, Thompson et al. (2011) integrated remote sensing techniques with persistent place theory in what they call 'inquiry-based archaeogeophysics,' and Maher (2019) demonstrated how geoarchaeological methods can help to understand place-making at the Epipaleolithic aggregation site Kharaneh IV in eastern Jordan.

This paper continues Maher's (2019) integration of persistent places and geoarchaeology by noting that paleoclimatic and paleoenvironmental analyses are particularly suited to

understanding place-making. Specifically, paleoclimatic and paleoenvironmental analyses can be used to quantitatively describe the 'unique qualities' of Schlanger's (1992) first property of persistent places, and they may be pertinent to understanding the cultural decisions that result in further reoccupation and revisitation. This paper uses physical and chemical descriptions of recently and previously excavated sedimentary contexts, geological survey observations, and previously published archaeological and paleoclimatic data from Kharaneh IV and the surrounding region to constrain the unique environmental qualities of the site, document its climatic history, and contribute to our understanding of Kharaneh IV as a persistent place.

Kharaneh IV and its Geological and Environmental Context

Kharaneh IV is an Early to Middle Epipaleolithic site in eastern Jordan that forms an approximately 22,000 m^2, 2.5 m-high tell on the landscape (Figure 4.1). It is notable for its large size, deemed by some to be a 'megasite' (Richter et al., 2013; Spyrou et al., 2019), its well preserved hut structures (Maher et al., 2012; Ramsey et al., 2018), some of the earliest artistic objects identified in Jordan (Macdonald and Maher, 2022), a complex lithic assemblage that suggests interactions of multiple Epipaleolithic groups and cultures (Maher and Macdonald, 2013; Macdonald et al., 2018a, 2018b), and a strong research potential for understanding hunting (Henton et al., 2017; Martin et al., 2010; Spyrou et al., 2019) and knapping (de La Torre et al., 2019; De Peña, 2022; Macdonald et al., 2018b; Macdonald and Maher, 2022; Maher and Macdonald, 2020) activities during the Early and Middle Epipaleolithic. Kharaneh IV is situated in the low-lying valley of Wadi Kharaneh, an ephemeral wash that drains into the Azraq Basin approximately 40 km to the northeast. Modern annual precipitation in the Azraq Basin watershed ranges from 200 mm in the northwest to 50 mm in the southeast, with rainfall in the Kharaneh region falling between 50 and 100 mm per year (Henton et al., 2017; Suleiman and Al-Bakri, 2011). Precipitation in the Azraq Basin primarily originates to the west in the Mediterranean Sea, but winter storms lose strength due to the rain shadow effect of the Judaean Mountains (Enzel et al., 2008; Garbrecht and Peleg, 1994). Temperatures in the Azraq Basin are highly variable, ranging from 45 °C in the summer to −10 °C in the winter (Henton et al., 2017).

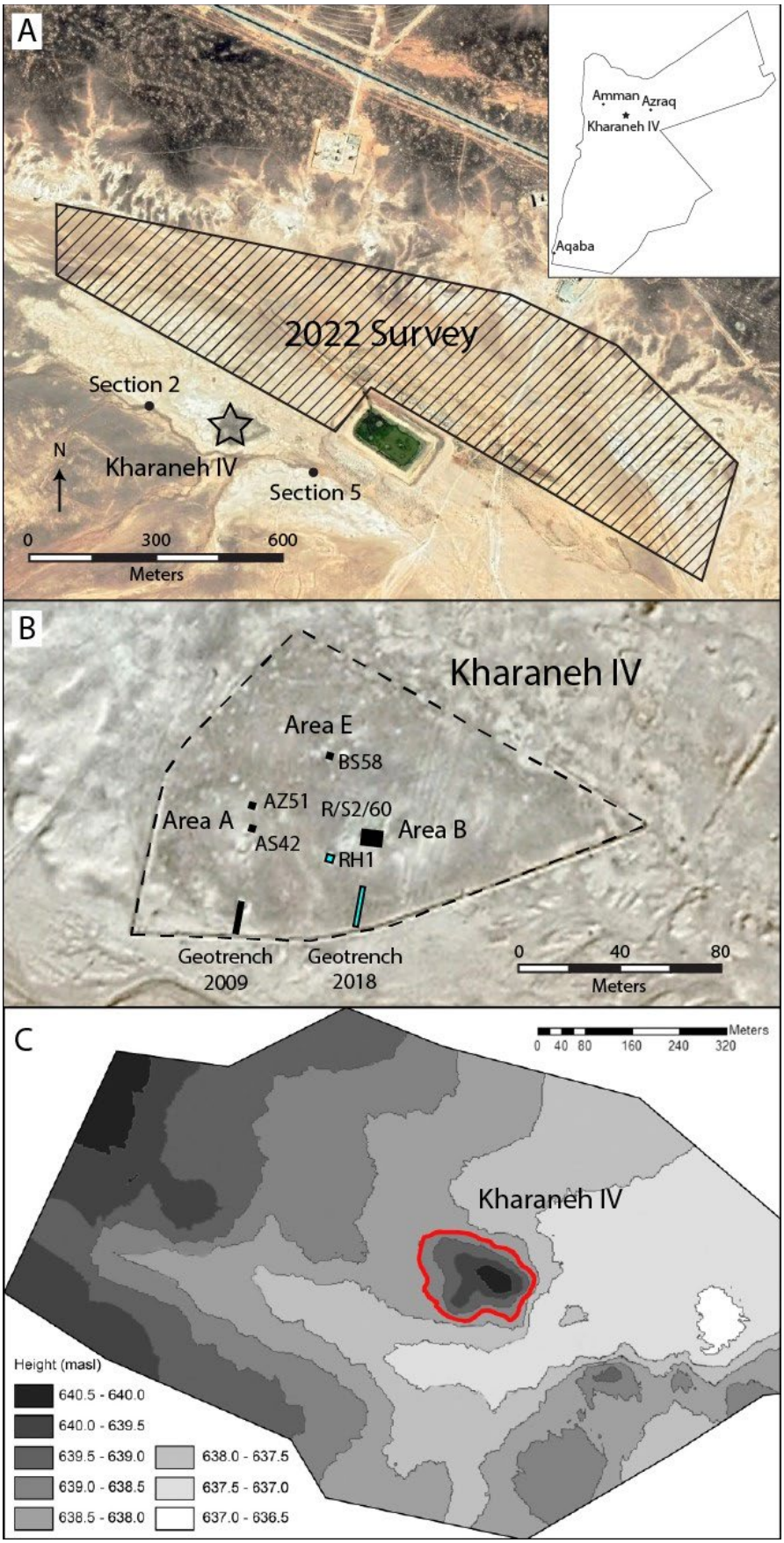
A
Amman
Azraq
Kharaneh IV
Aqaba
2022 Survey
Section 2
Kharaneh IV
Section 5
N
0
300
600
Meters
B
Kharaneh IV
Area E
BS58
AZ51
R/S2/60
Area A
Area B
AS42
RH1
Geotrench 2009
Geotrench 2018
0
40
80
Meters
C
Meters
0 40 80 160 240 320
Kharaneh IV
Height (masl)
640.5 - 640.0
640.0 - 639.5
639.5 - 639.0
639.0 - 638.5
638.5 - 638.0
638.0 - 637.5
637.5 - 637.0
637.0 - 636.5

Figure 4.1. Geological survey area and offsite excavation locations (A), with closeup of Kharaneh IV (B) showing relevant excavation locations (blue = excavated by this study; black = earlier excavation) and topographic map of the Kharaneh IV landscape (C), modified from Jones et al. (2016).

Geologically, the Kharaneh landscape is set upon chalk and limestone bedrock that was deposited in a shallow sea during the Eocene (Al-Hunjul, 2001; Al-Tamimi et al., 2021; Fadda, 1998; Qudaira, 2000). Chalk bedrock of the Wadi Shallala Formation outcrops along the northern edge of Wadi Kharaneh and forms steep hillsides, while it is obscured by Pleistocene gravels on the gradual alluvial slopes to the south (Al-Hunjul, 2001; Qudaira, 2000) (Figure 4.2). Structurally, geologists have identified numerous NW-SE striking normal faults in eastern Jordan and Kharaneh IV is located approximately 5 km east of the Malalih Fault and 3 km west of the Wadi Kharana-Dab'i Fault (Al-Hunjul, 2001; Besancon et al., 1989; Qudaira, 2000) (Figure 4.2). The immediate vicinity of Kharaneh IV is mapped as Quaternary alluvium and Pleistocene gravels (Al-Hunjul, 2001; Qudaira, 2000), but more detailed observations of the Kharaneh landscape have shown its geological context to be much more complex.

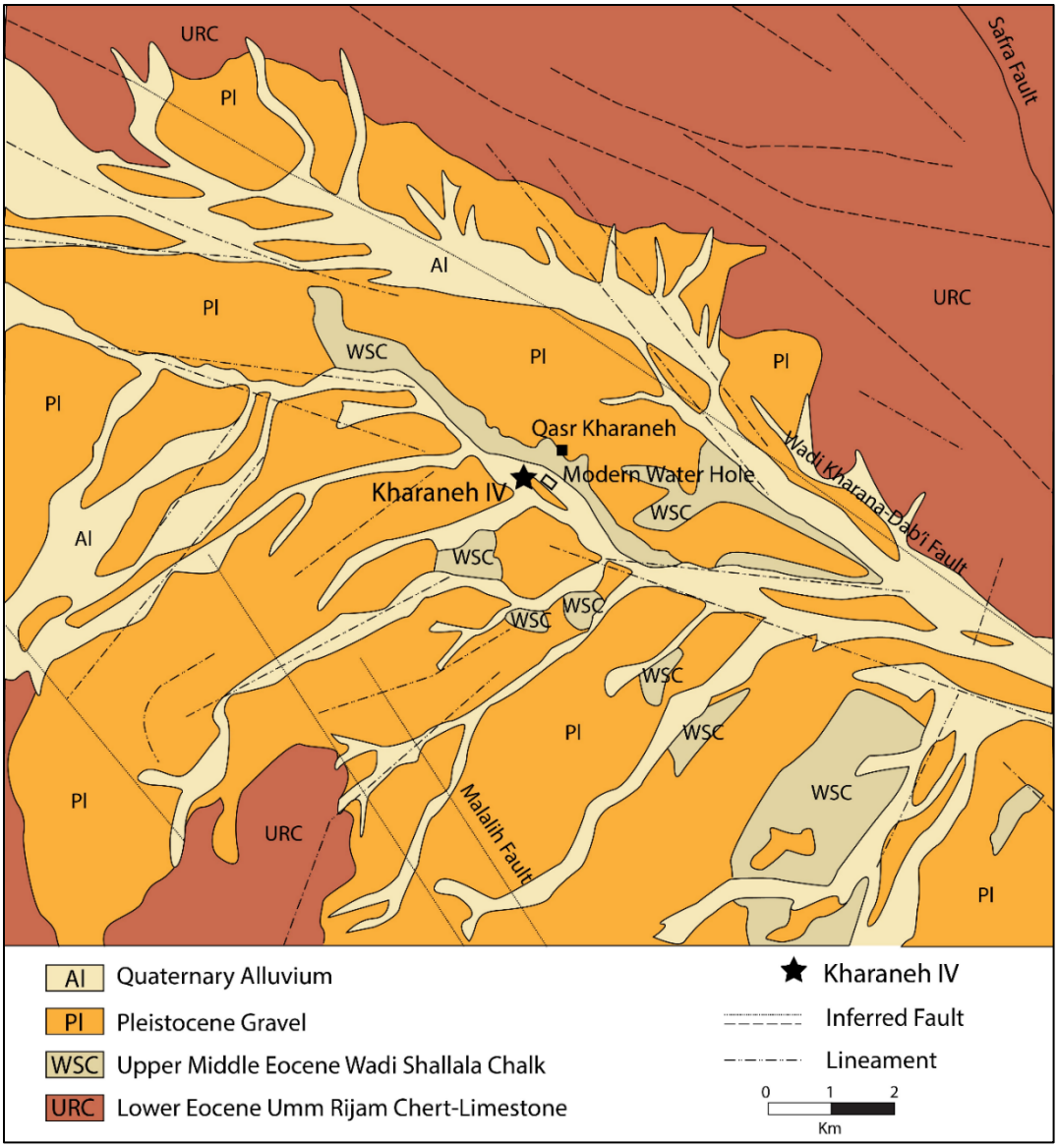

Figure 4.2. Geologic map of the study area after Al-Hunjul (2001) and Qudaira (2000), showing numerous local northwest-southeast trending faults and lineaments.

Garrard et al. (1985) characterized Kharaneh IV's local stratigraphy as lower gravel deposits containing Upper Palaeolithic artifacts, overlain by clays of a possible lacustrine origin that form the terrace that contains Kharaneh IV. The authors noted that there are no obvious signs of a basin or bedrock barrier to have allowed the formation of a lake but posited that calcreted wadi gravels may have acted as a dam. Garrard et al. (1985) reported a homogenous sandy loam above the clays that is possibly a loess similar to deposits they identified in nearby Wadi Jilat. They interpreted this sequence as representing an initial wet period with greater vegetation than at present that occurred during the deposition of clays, followed by a dry period marked by the deposition of loess that coincided with the occupation of Kharaneh IV. At some point after the deposition of cultural deposits at Kharaneh IV, the wadi became an erosional environment characterized by increased incision and terrace formation.

Besançon et al. (1989) identified distinct terraces in Wadi Kharaneh: An upper terrace of unknown age, a middle terrace with Late Acheulian bifaces, and a lower terrace that includes Kharaneh IV. They described the stratigraphy of the lower terrace as 30 cm of fine, light beige silt containing Epipalaeolithic artifacts above a clay horizon containing white-to-greenish particles of calcareous material, traces of roots and rare, possibly Late Palaeolithic artifacts. Below the clay is a basal pebble layer of large, unpatinated flints, including some Late Palaeolithic artifacts. Besançon et al. (1989) noted that although the wadi has likely existed for some time, the wadis have only incised the area approximately 20 m below the bedrock platform on which Qasr Kharaneh is located. They attribute this minimal downcutting to both low annual rainfall in the region throughout the Holocene and a low gradient in this part of the Azraq Basin. Besançon et al.'s (1989) study highlights the complexity of Wadi Kharaneh's history; although the pebble layer is likely an old and intact basal depositional layer (perhaps the remains of a former channel), the wadi has experienced multiple depositional and erosional phases, filling in and being exhumed with changes in regional climate.

Jones et al. (2016) conducted a landscape survey of the area around Kharaneh IV, geological excavations of onsite and offsite contexts, and the results of geochemical analyses and radiocarbon and optically stimulated luminescence (OSL) dating to characterize the environmental setting of Kharaneh IV. They identified two main depositional units at the site, Holocene wadi fills and Pleistocene wetland deposits, that both displayed lateral variations. They found that grain size is similar in on-site and off-site samples and is predominantly silts and clays, although on-site samples are slightly coarser. On-site samples display much higher magnetic susceptibility, which Jones et al. (2016) attributed to high levels of cultural burning in virtually all archaeological contexts. Off-site samples have lower percentages of SiO2 and MgO but higher percentages of CaO and carbonate content, which Jones et al. (2016) used to interpret off-site terrace deposits as carbonate-enriched wetland sediments. Jones et al. (2016) dated off-site terrace deposits by OSL to approximately 23,000–19,000 BP, suggesting that wetland conditions existed at Kharaneh IV over that range and likely overlapped with the beginning of the site's occupation. Jones et al. (2016) addressed Garrard et al.'s (1985) concern for how a body of water could have collected in Wadi Kharaneh when there are no signs of a basin or bedrock barrier to have allowed the formation of a small lake by suggesting that wetland marls formed as groundwater discharge deposits.

This paper builds on the aforementioned paleoenvironmental studies by presenting new geoarchaeological and paleoenvironmental data from investigations during the 2018, 2019, and 2022 Epipaleolithic Foragers in Azraq Project (EFAP) field seasons and archived sediment samples from earlier EFAP field seasons, and by incorporating published data from past Kharaneh IV studies (Jones et al., 2016; Macdonald et al., 2018a) and regional paleoclimate archives (Bar-Matthews et al., 2003; Bartov et al., 2003; Grant et al., 2012; Torfstein et al., 2013) to construct a narrative of environmental change at Kharaneh IV. We then analyze the hydrological conditions of the Kharaneh wetland that made it a 'unique quality' (Schlenger 1992) in the development of Kharaneh IV as a persistent place.

Methods

Locations

We excavated two new onsite units, Geotrench2018 and RH1, re-excavated two earlier offsite units first dug by Jones et al. (2016), Sections 2 and 5, and present new and existing data from previously excavated units AS42, AZ51, BS58, and Geotrench2009 (Figure 4.1). In 2018, we excavated an exploratory geoarchaeological unit, Geotrench2018, from the site's southern boundary to a point 13 m north near the site's Area B deposits (Figure 4.3). Geotrench2018 measured 13 m long, 0.6 m wide, and varied between 20 and 84 cm deep (Table 4.1). We re-excavated two offsite sampling locations, Sections 2 and 5, within the slope of the wadi terrace to link our results with the data and chronology presented by Jones et al. (2016). Offsite sampling locations dug into the terrace slope were approximately 50 cm wide and ranged from 100 cm deep in Section 2 to 135 cm deep in Section 5.

Figure 4.3. Geotrench2018 (left), Section 2 (center), and Section 5 (right).

Table 4.1. Summary of locations excavated by this study.

Location	UTM E	UTM N	Surface Elev. (MASL)	Max Length (m)	Max Width (m)	Max Depth (m)
Geotrench 2018	258769.0	3512582.0	637.418	13.0	0.6	0.84
	258769.0	3512595.0	638.338			
Section 2 2018	258493.7	3512651.7	639.472	na	0.5	1.35
Section 5 2018	258923.5	3512541.3	637.864	na	0.5	0.85
RH1	258758.1	3512603.3	639.459	1.4	1.4	2.24
	258757.7	3512601.4	639.245			

In 2019, we transformed a previously disturbed, 50 cm-deep looter's pit located approximately 15 m southwest of Area B into a deep sounding unit, Robber Hole 1 (RH1) (Figure 4.4). We continued RH1 to a total depth of 2.24 m, with an initial width of 1.4 m at the surface of the looter's pit, a 1 m width at the onset of our excavations, and a 0.5 m width at its base to create an access step. Although the site's grid is along a N-S axis, we maintained the looter hole's original orientation to limit additional disturbance, which formed a square offset approximately 40° west of north. In 2022, we conducted a geological survey of an approximately 65-hectare area north and east of Kharaneh IV to better characterize the local geology (Figure 4.4).

Figure 4.4. RH1 (left) and inspection during 2022 geological survey (right).

Field Methods

We used shovels and pickaxes to excavate compact geological deposits in the trench and offsite locations and used trowels and brushes to expose sidewall stratigraphy. We used small tools, brushes, and trowels to excavate loose cultural deposits in upper RH1 levels and hand picks and shovels to excavate compact geological deposits in lower RH1 levels. We collected bulk sediment samples at 5 cm vertical intervals at three locations along the west wall of Geotrench2018, at 351285.2 m N, 351290.05 m N, and 351294.8 m N and along the NE wall of RH1, and by sedimentary unit in Sections 2 and 5. We employed flotation in the upper cultural levels of RH1 and a portion of lower RH1 geological levels to sort deposits into >4 mm, >2 mm, and >1mm fractions of cultural materials and a mesh to collect a light fraction of botanical and microfaunal remains. We drew cross-sections of Geotrench2018's west wall and RH1's northeast and northwest walls. We recorded the Munsell soil color and basic sediment properties of each layer. During 2022 geological investigations, we performed a four-person unsystematic pedestrian survey and followed bedrock exposures in the wadi and foothills. We used a pickaxe, shovel, and hoe to determine the subsurface presence of bedrock and further reveal surface exposures.

Laboratory Methods

We selected 97 sediment samples from six onsite and two offsite contexts for loss-on-ignition (LOI) analysis (Ball, 1964; Davies, 1974; Heiri et al., 2001; Shuman, 2003; Wang et al., 2011). We used a 5 cm sampling interval for RH1 samples to provide an understanding of changes with depth and sampled by unit for the remaining contexts to characterize lateral changes across the site where bulk samples were available. We measured 1-2 g of sediment per sample (min = 0.86 g; max = 2.59 g; mean= 1.58 g) and placed samples in ceramic crucibles before progressively heating them to 100°C for 12 hours to remove water, 550°C for 4 hours to remove organic carbon, and 900°C for 2 hours to remove carbonate. We used a Thermolyne 30400 furnace muffle oven for heating samples and an Ohaus GA200D balance to weigh samples. We removed crucibles at each heating interval to weigh and record the amount lost during each burn and calculate the percent organic, carbonate, and mineral content of each sample. We used a stereo microscope with magnification up to 4.5x to identify ostracod remains collected in the light fraction during flotation of RH1 sediment. We estimated ostracod density by counting the number of ostracods visible within a 15.2 mm^2 view area of the microscope, repeating the count four times, averaging the value for each float sample, and dividing the averaged count by the number of liters excavated within each layer to allow for comparison by locus. To analyze lithic artifacts in RH1, Dr. Felicia de Peña sorted debitage using a modified type list based off Wilke and Quintero (1994) and classified tools and other retouched pieces using modified typologies developed by Bar-Yosef (1970) and Goring-Morris (1987). We incorporate additional lithic artifact data from Macdonald et al. (2018).

Results

Geotrench 2018

We identified seven distinct sedimentological units in Geotrench2018 (Table 4.2; Figure 4.5). All units gently slope southward at 4° and are laterally continuous except for Layers E and F. The discontinuity of Layers E and F indicates that there is some lateral variability in Kharaneh IV strata, which may reflect a diverse paleoenvironmental landscape or highly localized weathering and depositional events, or both. We encountered lithic artifacts in each layer, but deposits with frequent artifacts are only present in Layer F. Layer A is a thin (< 5 cm) surface palimpsest of lithic artifacts and loose brown sediment that covers the length of the trench. Lithic artifacts are concentrated at the surface of Layer A above an aeolian dust horizon (Figure 4.7), suggesting that the lithic pavement that covers Kharaneh IV formed through the displacement and gradual upward migration of lithics by intruding aeolian dust. Carbonate content is high in Layer A (average = 11.54%), likely from aeolian deposition of carbonate sediments, and organic content is moderate (9.66%) (Table 4.3; Figure 4.6). Although Layer A is disturbed by biological activity in the form of rodent and insect holes and surficial geomorphological processes, it contains buried lithic artifacts and an *in situ* combustion feature in its west wall at 3512585.4 m N (Figure 4.5). The combustion feature is approximately 25 cm wide and 5 cm deep (Figure 4.7). While the combustion feature suggests that the layer is of some antiquity and not completely

disturbed, it is likely younger than uppermost layers in the rest of the site due to the inferred age of Layer B that postdates Kharaneh IV's occupation.

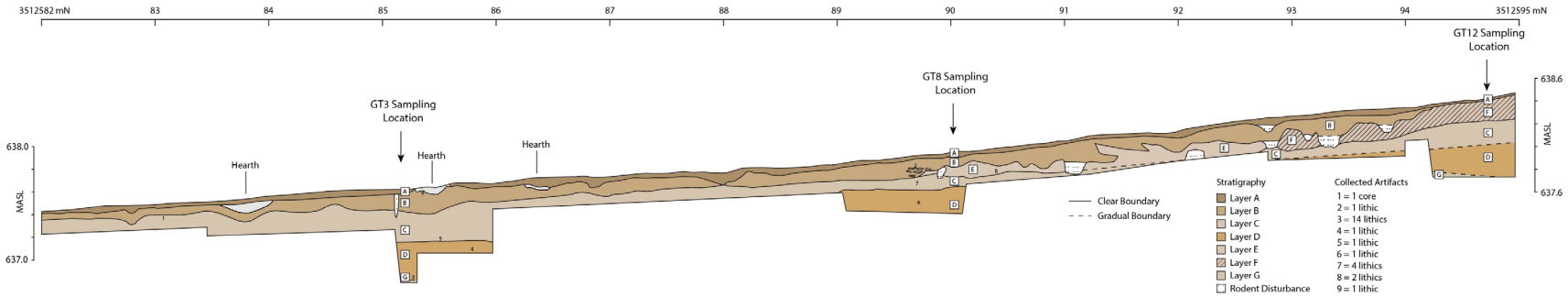

Figure 4.5. Cross section of Geotrench2018 W wall.

Table 4.2. Summary of Geotrench2018 stratigraphy.

Layer	Munsell	Color	Compaction	Avg. Thickness (cm)	Lower Boundary	Charcoal	Bone	Lithics	Notes
A	10YR 6/4	Light brown	Loose	< 5	Abrupt, smooth	Present	Absent	Present	Deflated, surface palimpsest, high artifact density covering brown silt
B	10YR 7/4	Reddish brown	Moderate	15	Abrupt, wavy-irregular	Present	Absent	Present	Reddish silt, lower boundary is a disturbed by bioturbation, possible unconformity
C	10YR 8/2	Light gray	Compact	25	Clear-gradual, smooth	Absent	Absent	Present	Pale colored marl, contains visible evaporites near top, breaks into large aggregates/blocky texture
D	10YR 7/6	Brown	Compact	30	Gradual, smooth	Absent	Absent	Present	Similar texture to C, but contains root traces and darker color, mottled in places breaks in large aggregates/blocky texture
E	2.5YR 8/2	Very light gray	Loose	10	Gradual, smooth	Absent	Absent	Present	Very loose light-colored unit, eroded by B, grades laterally into F
F	2.5YR 8/2	Light gray	Moderate	15	Clear, smooth	Present	Present	Present	Same level as E, but more compact and high artifact density, likely edge of site
G	10YR 8/2	Light gray	Compact	na	na	Absent	Absent	Present	Identical to C, but beneath D

Table 4.3. Summary of Geotrench2018 LOI data.

Location	Depth (cm)	Locus	Organic %	Carbonate %	Mineral %
GT3	2.5	A	10.15	11.98	77.88
GT3	7.5	B	12.85	6.84	80.32
GT3	12.5	B	12.45	7.30	80.25
GT3	17.5	B	13.71	5.69	80.59
GT3	22.5	B	13.92	4.26	81.82
GT3	27.5	C	12.05	7.39	80.56
GT8	2.5	A	10.13	12.71	77.17
GT8	7.5	B	12.10	10.79	77.12
GT8	12.5	B	17.76	6.36	75.88
GT8	17.5	E	10.98	14.39	74.63
GT8	22.5	B	19.53	6.24	74.23
GT8	27.5	C	13.41	8.37	78.22
GT8	32.5	C	13.42	5.07	81.51
GT8	37.5	C	12.62	5.44	81.94
GT8	42.5	D	13.66	4.55	81.80
GT8	47.5	D	11.01	8.67	80.32
GT12	2.5	A	8.69	9.94	81.36
GT12	7.5	F	6.65	9.13	84.22
GT12	12.5	F	9.84	6.12	84.04
GT12	17.5	F	11.31	6.19	82.50
GT12	22.5	F	13.27	6.42	80.31
GT12	27.5	C	12.99	6.54	80.47
GT12	32.5	C	13.67	5.16	81.17
GT12	37.5	C	12.82	6.21	80.97
GT12	42.5	C	15.68	3.63	80.69
GT12	47.5	D	13.58	7.76	78.66
GT12	52.5	D	13.53	7.55	78.92
GT12	57.5	D	12.67	8.06	79.27

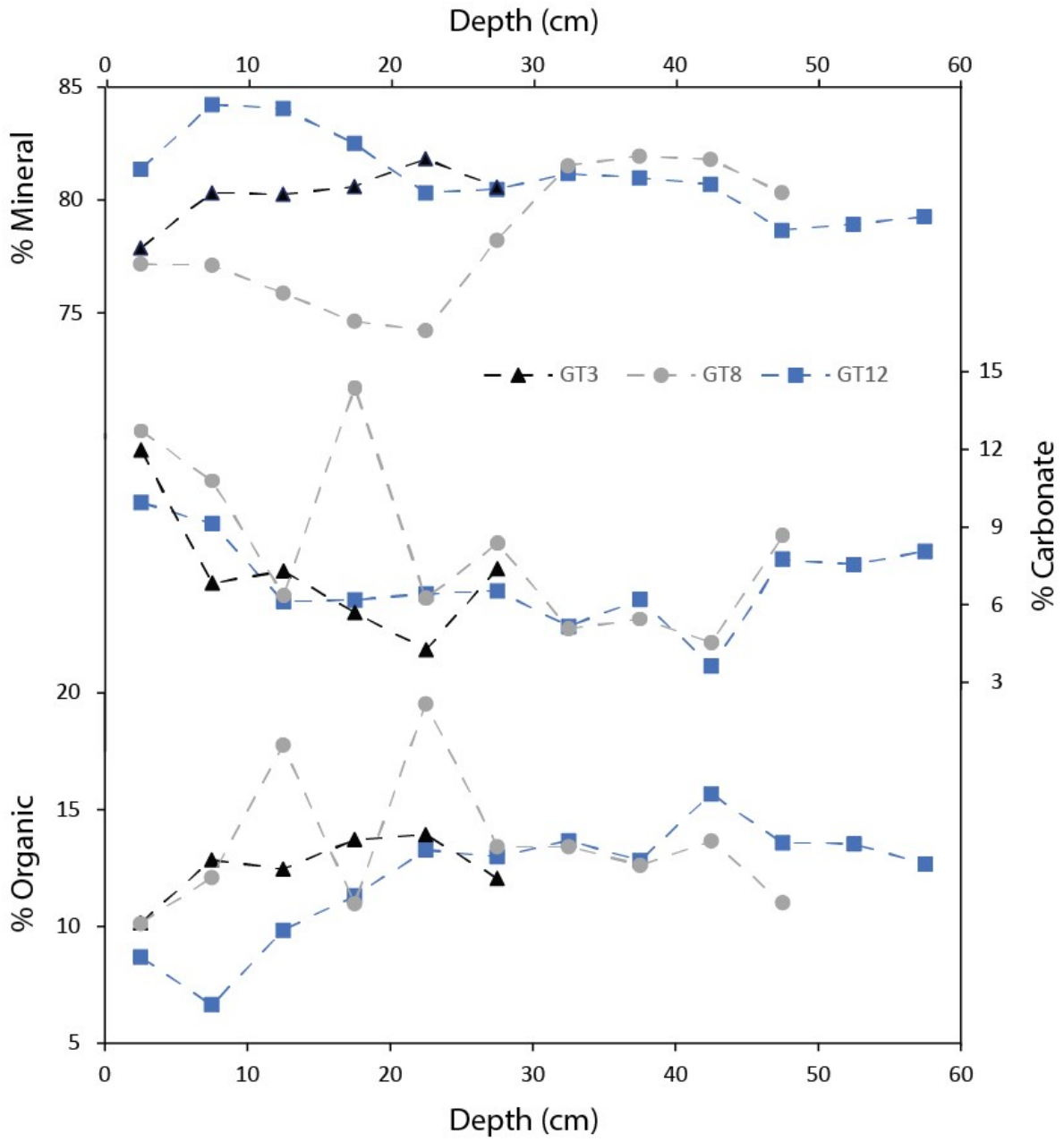

Figure 4.6. Geotrench2018 LOI values at three locations along the trench, GT3, GT8, and GT12.

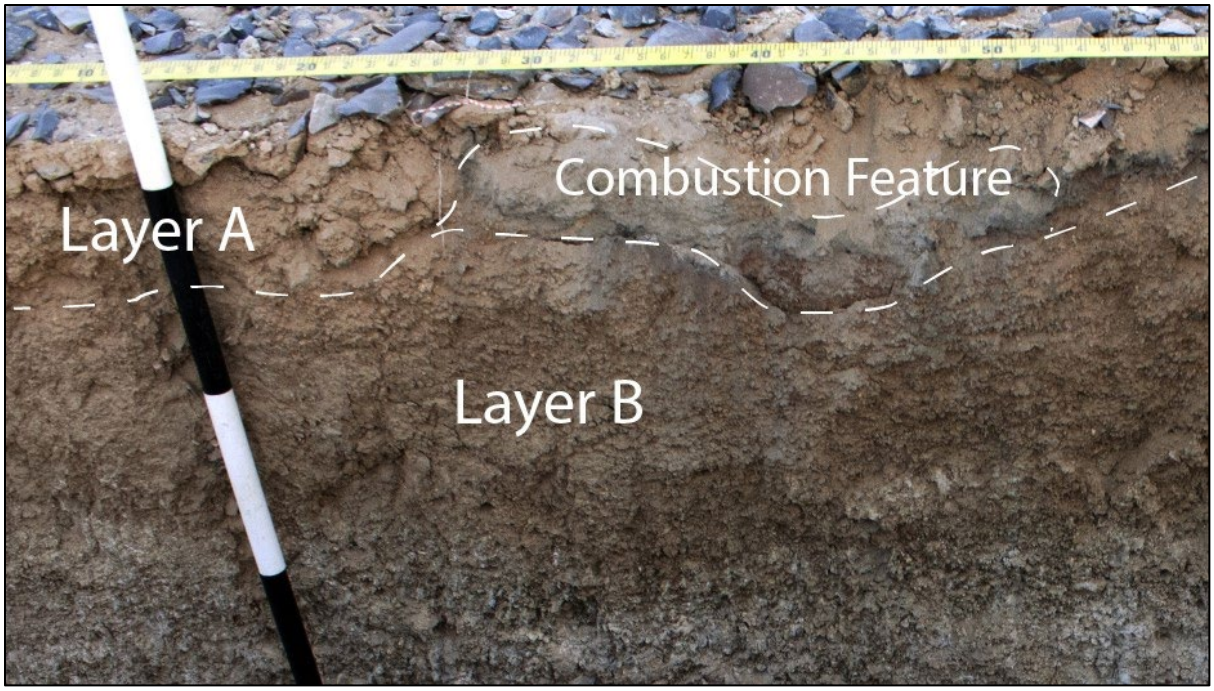

Figure 4.7. Detail of combustion feature within Layer A.

Layer B is a 15 cm-thick, reddish-brown silt that underlies Layer A for most of the trench and is equivalent to the "wadi silt" described by Jones et al. (2016) as Locus 2 in Geotrench2009. Layer B has a granular soil structure and is more compact than Layer A, but much looser than underlying Layer C. Layer B contains two *in situ* combustion features in its west wall at 3512583.8 mN and 3512586.4 mN (Figure 4.8). The more southern Layer B combustion feature is approximately 40 cm wide and 10 cm deep and the more northern combustion feature is 15 cm wide and 4 cm deep. Layer B's lower contact is abrupt and wavy and appears disturbed through bioturbation in the form of rodent and insect burrows. Its contact likely resulted from both pedogenic processes, in the form of illuviation, and erosional processes, through wadi alluvial erosion and subsequent aggradation. Red surficial soils similar in appearance to Layers A and B are common in Jordan and frequently result from the leaching of carbonate (Lucke et al., 2014), leaving rubified upper horizons characteristic of Mediterranean Terra Rossa soils (Durn, 2003). A loss in carbonate through leaching is visible in Layer B's LOI profile, which decreases in carbonate content from a high of 10.79% near the surface to a low of 4.26% above the layer's lower, hardpan contact (Table 4.3; Figure 4.6). The contact is likely also an unconformity because it grades laterally into Layer E, leaving erosional features suggestive of wadi expansion and aggradation. Jones et al. (2016) used Optically Stimulated Luminescence (OSL) to date Geotrench2009 Locus 2 to 15 ± 1 ka BP; while Layer B cannot be securely tied to this date without further dating attempts, the strong similarities between Locus 2 and Layer B suggest that Layer B dates to a similar age.

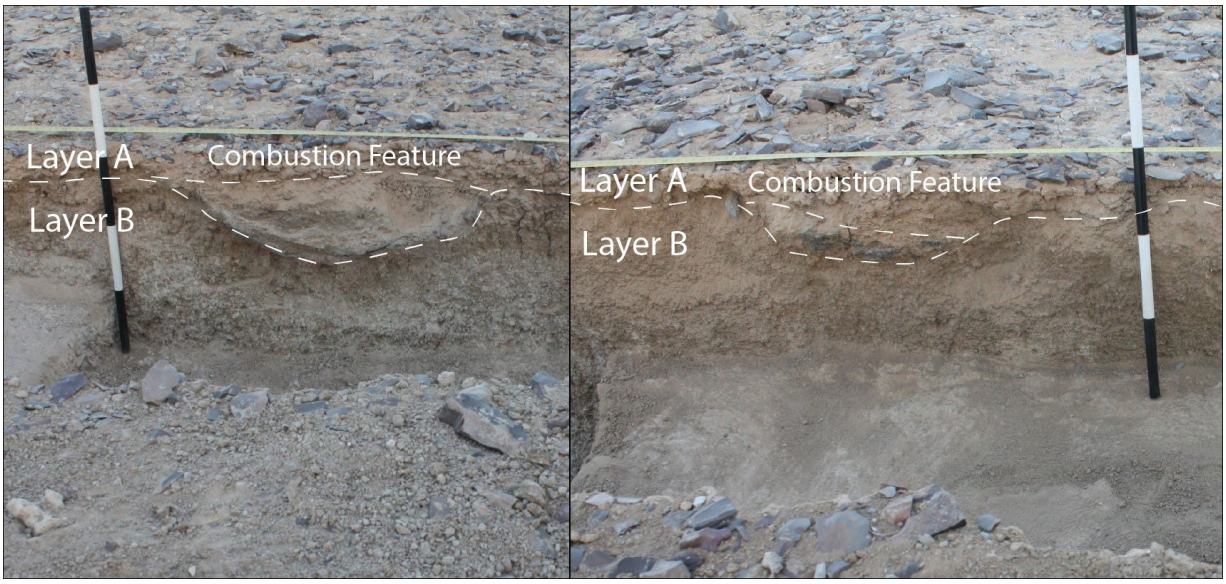

Figure 4.8. Detail of more southern combustion feature (left) and more northern combustion feature (right) within Layer B.

Layer C is a light grey, 25 cm-thick marl that extends through the length of the trench beneath Layer B. The layer is significantly more compact than overlying units, breaks into large aggregates, and contains visible gypsum and carbonate evaporite crystals at its upper contact. Its soil structure is variable, ranging from massive near its upper contact with Layer B to a strong blocky to prismatic structure below. Its prismatic structure suggests the layer at times experienced wet-dry cycles. The contact also presents a change in porosity, with more porous silts and sands in Layer B and less porous, clay-rich marls in Layer C and below (Figure 4.9). Previous studies at Kharaneh IV have identified similar deposits at depth throughout the site (Jones et al., 2016; Macdonald et al., 2018a; Maher et al., 2021b), and Jones et al. (2016) interpreted equivalent units in Geotrench2009 as ground water discharge deposits. Ground water discharge deposits are somewhat common in deserts throughout the world and form where the water table meets the surface, often at the edge of an alluvial fan or where ground water is forced to the surface by a fault or change in bedrock topography (Pigati et al., 2014). As Jones et al. (2016:101) note, the marls at Kharaneh IV are similar to a specific type of ground water discharge deposit, wetland marls. Wetland marls, as defined by Pigati et al. (2014:70), are high in carbonate content from alkaline rich waters, are massive to blocky in structure, and form in flat, marshy areas.

Mineral content in Layer C is uniform throughout the trench (average = 81.22%), but organic content rises from 12.82% at its upper contact to 15.68% at its lower contact and carbonate values decrease with depth from a high of 8.37% at its contact with Layer B to 3.63% near its contact with Layer D (Table 4.3; Figures 4.6 and 4.9). The change in carbonate amount with depth possibly indicates upward carbonate migration associated with groundwater evaporation during the wetland's Late Glacial Maximum desiccation (Finstad et al., 2016) or downward carbonate migration through illuviation and leaching of soluble minerals from porous Layers A and B into Layer C over time (Casby-Horton et al., 2015), or both, as these processes

are mutually inclusive possibilities. We noted several lithic artifacts within Layer C, indicating a human presence at the wetland before the site was occupied intensively.

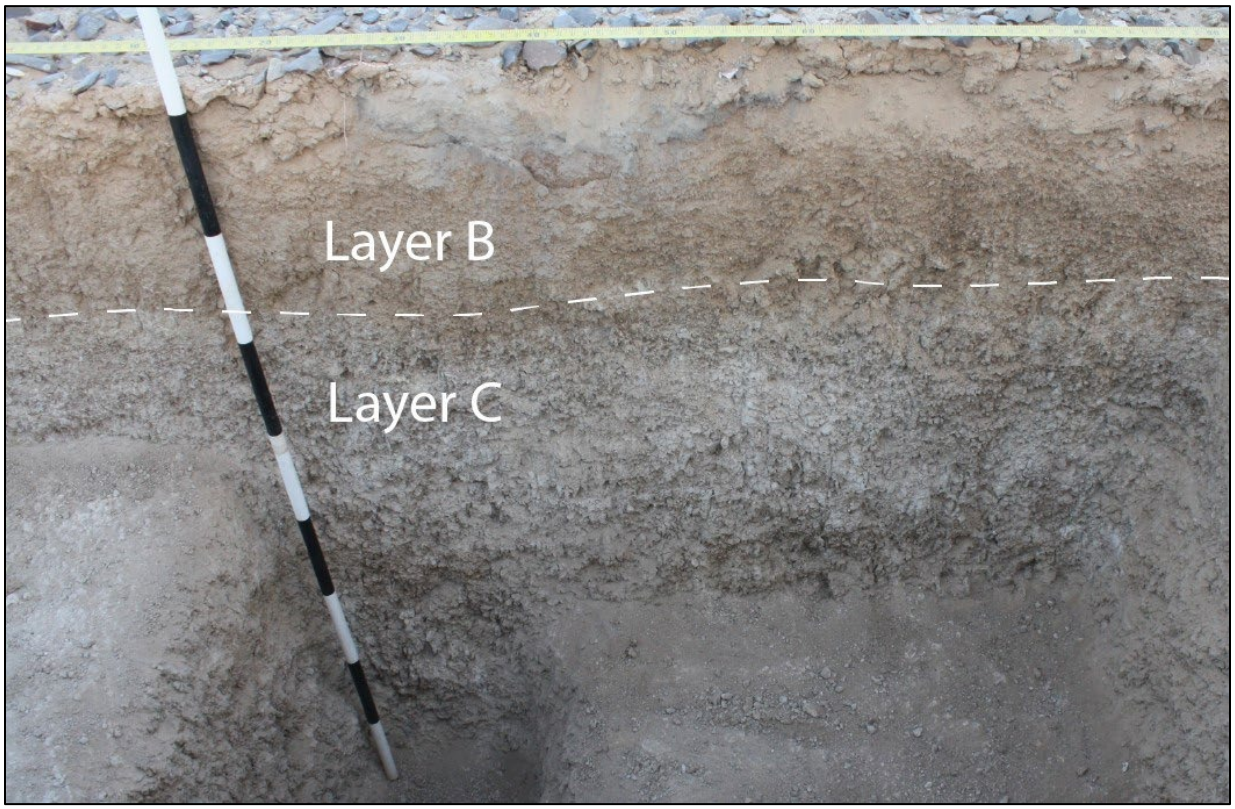

Figure 4.9. Contact between Layer B silt and sand and Layer C marl.

Layer D underlies Layer C and is similar in compaction, texture, and its prismatic structure, but its color is dark brown and it contains root traces that indicate a higher organic content than in other layers. It is relatively high in organic (average = 13.26%) and carbonate (average = 8.01%) content, and somewhat low in mineral content (average = 78.95%) (Table 4.3; Figure 4.6). Changes in marl color and root trace amount between Layers C and D suggest that the spatial extent of vegetated and unvegetated areas shifted with time, becoming less vegetated and likely drier during the deposition of Layer C. Jones et al. (2016) noted similar variation in Geotrench2009 marls and OSL dated Locus 5, a brown marl equivalent in depth and structure to Layer D, to 22 ± 1 ka BP. Stratigraphic correlation suggests that Layer D is of a similar age.

Due to time constraints and the difficulty of penetrating through compact marl layers, we stopped digging at the upper centimeters of a white marl, Layer G, similar in appearance and composition to Layer C (Figure 4.10). Although all other layers contain a small number of lithic artifacts (Table 4.2), it is notable that we observed a concentration of 14 lithic artifacts near the contact of Layers D and G approximately 3 m north along the trench. This is consistent with Macdonald et al.'s (2018) finding that early cultural deposits exist at depth within the site and that the area was known and utilized before its dense occupation at Areas A and B. Additionally, the location of this cluster near the edge of the Kharaneh IV site boundary demonstrates that

artifact concentrations may occur away from the center of the site and that Epipaleolithic activities took place throughout the Kharaneh landscape (Maher et al., 2021b).

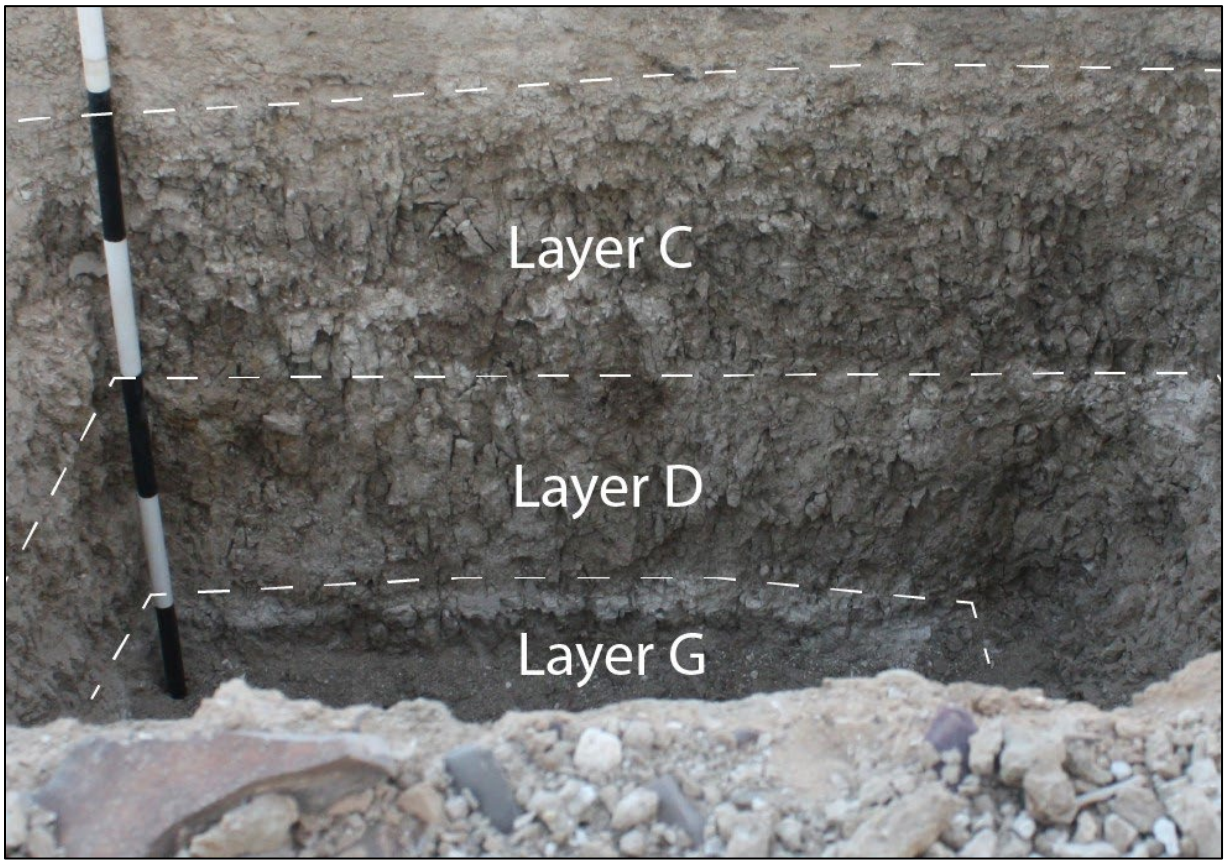

Figure 4.10. Kharaneh wetland marl: Layers C, D and G.

Toward the north terminus of Geotrench2018, we encountered two layers, E and F, between Layers B and C. Layer E is white in color, very loose, and displays a granular structure. At 14.39%, Layer E has the highest carbonate content in Geotrench2018 (Table 4.3; Figure 4.6). Layer E grades laterally into Layer B, producing several thin, isolated segments of Layer E that resemble sedimentary interfingering or onlap (Figure 4.11). To the north, Layer B material intrudes beneath Layer E in multiple locations, producing angular splinters of Layer E atop Layer B (Figure 4.5). Much of the layer's unusual appearance can be attributed to rodent burrows and subsequent infilling by overlying Layer B, but its lateral discontinuity with Layer B cannot be explained by bioturbation alone. While true interfingering would suggest concurrent deposition of Layers B and E, which is difficult to explain considering their different composition, the layer also resembles sedimentary onlap, wherein younger sedimentary units overlie angular erosional surfaces from transgressive activity (Christie-Blick, 1991). It is possible that aggradational fluvial and alluvial processes after the site's occupation eroded Layer E and subsequently filled in the erosional surface with wadi silts during the deposition of Layer B. Layer E's loose compaction, high carbonate content, and lateral discontinuity are distinct from other layers in the trench. While it likely is a groundwater discharge deposit due to its high

carbonate content, its loose compaction is similar to the upper levels of offsite Sections 2 and 5 in the surrounding marl terraces, which are exposed to surface conditions and soft in their upper 20-30 cm but compact below. The loose compaction of Layer E and its compact underlying layers suggests that it was similarly once exposed to surface conditions prior to burial and further suggests that its upper contact with Layer B is an unconformity.

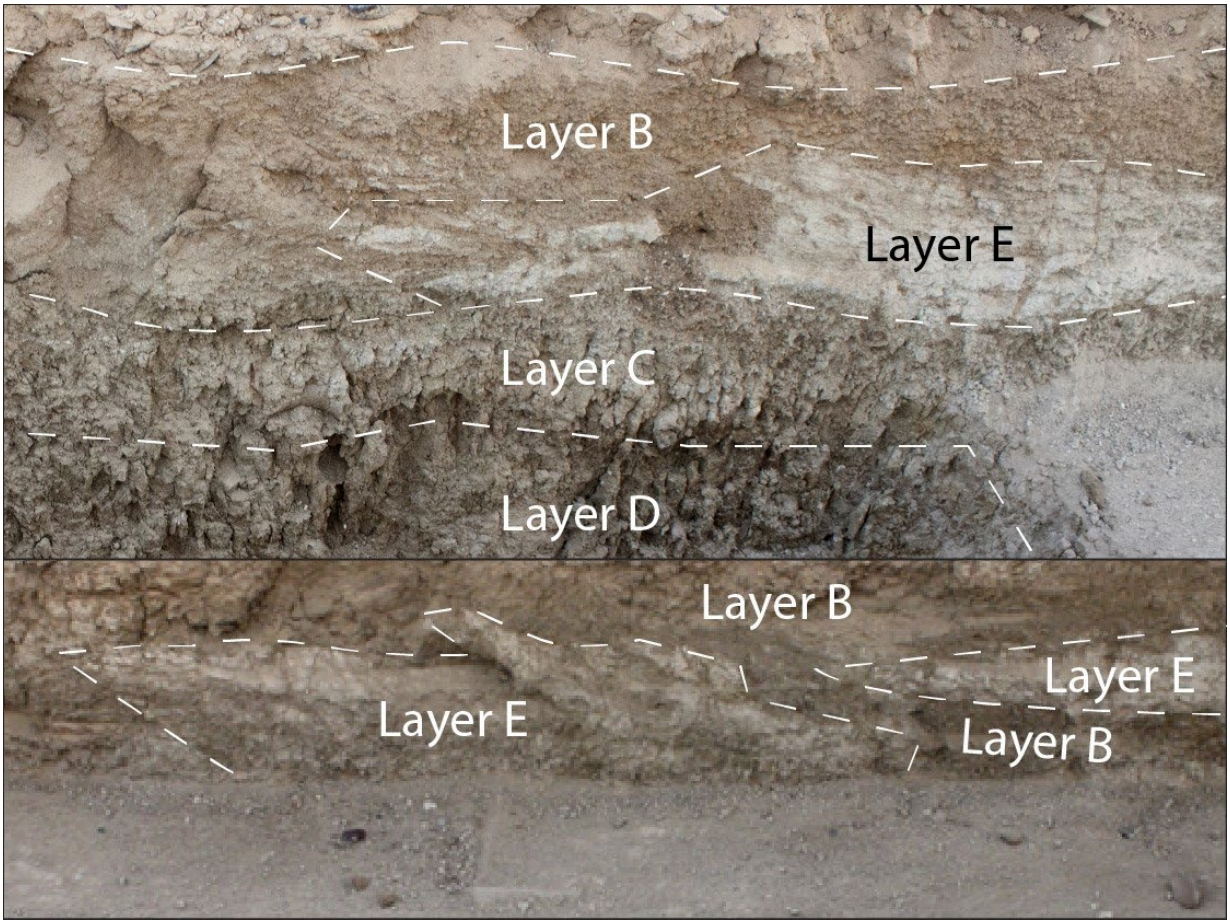

Figure 4.11. Top: contact of Layers B and E that resembles interfingering. Bottom: Layer B material beneath Layer E.

Layer F is a lateral continuation of Layer E that is defined by the regular appearance of *in situ* artifacts that we began to encounter approximately 11 m north into the trench (Figure 4.12). It is more compact than Layer E, but not nearly as compact as its underlying marls. Layer F thickens and Layer B gradually thins out toward Geotrench2018's northern terminus, suggesting that the aggradational deposition of Layer B ceased at this point. Organic content in Layer F increases with depth from 6.65% near the surface to 11.31% at its lower contact, carbonate content decreases from 9.13% to 6.19%, and mineral values decrease slightly with depth from 84.22% to 82.50% (Table 4.3; Figure 4.6). Layer F is the only layer in the trench observed to contain bone, in addition to lithics and charcoal. The occurrence of a higher number and larger variety of artifacts suggests that Layer F marks the site boundary of Kharaneh IV and confirms that site activities were focused on a small, but intensively used area (Maher et al., 2021).

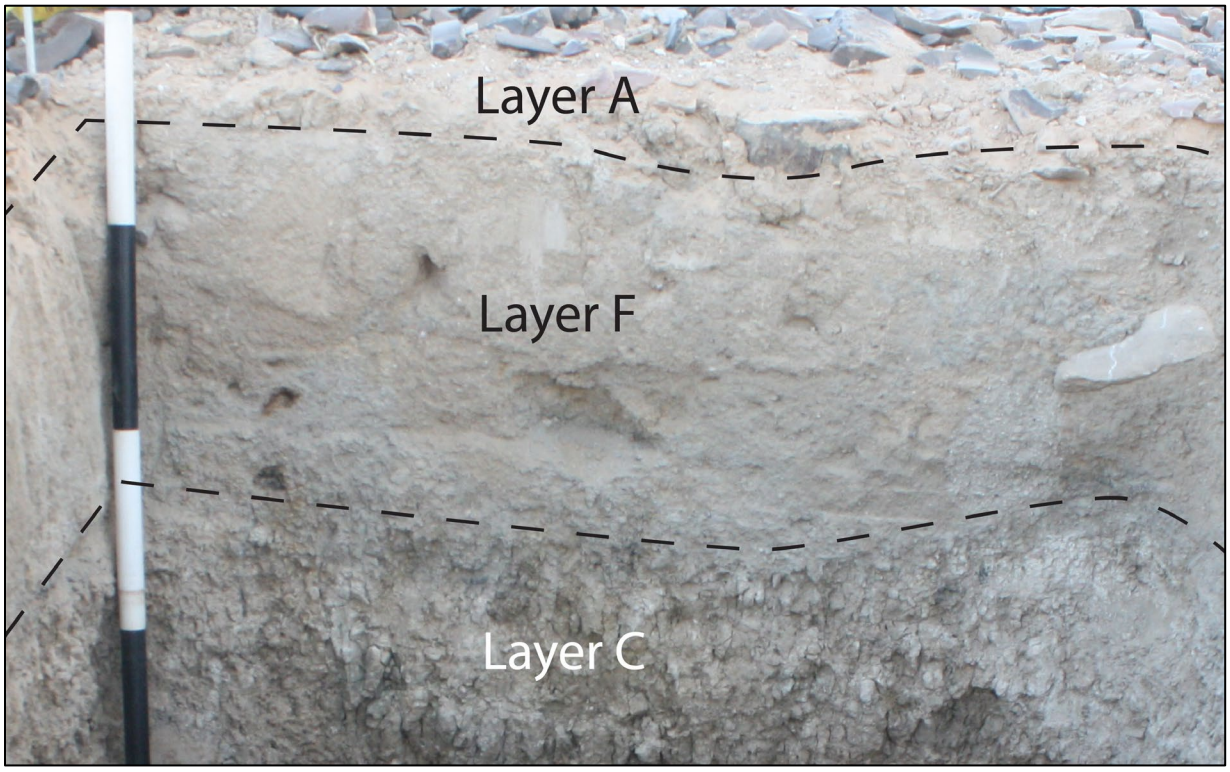

Figure 4.12. Layer F, showing contacts with underlying marl Layer C and overlying palimpsest Layer A. Note visible, *in-situ* artifacts within Layer F.

RH1

We identified 12 distinct sedimentological units in RH1, displaying a high degree of stratigraphic diversity and reflecting a dynamic paleolandscape (Figure 4.13; Table 4.4). Layers 1-4 are dense cultural deposits that were heavily disturbed by looting activity to a depth of 40 cm. LOI values in Layers 1-4 are uniformly low in carbonate content (average = 5.28%), high in mineral content (average = 84.28%) and show a slight increase in organic content with depth, from 8.30% in Layer 1 to 13.00% in Layer 4 (Table 4.5; Figure 4.14). Layer 5 is a 15 cm-thick, light gray, compact clay marl that was partially disturbed by looting activity. Like Layers 1-4, it is low in carbonate and organic content and high in mineral content. It has a medium grade soil structure and forms angular, blocky peds greater than 1 cm in diameter when broken apart. Layer 5 is more compact than overlying layers and contains bone, charcoal, and lithic artifacts. At 70.69 lithics/liter excavated sediment, its lithic density is much higher than underlying units, suggesting that Layer 5 is related to intense use of the Kharaneh wetland during with the site's Area B Early Epipaleolithic occupation (Table 4.6; Figure 4.14). The predominance of non-geometric microliths (n = 18; 94.7% of microliths) and narrow-faced cores (n = 5; 83.3% of cores) is consistent with Early Epipaleolithic artifact assemblages at Kharaneh IV (Macdonald et al., 2018a).

Table 4.4. Summary of RH1 stratigraphy.

Layer	Munsell	Color	Compaction	Thickness (cm)	Lower Boundary	Charcoal	Bone	Lithics
1-4	na	na	Loose	40	Clear, wavy	Present	Present	Present
5	10YR 7/2	Light gray	Compact	15	Clear, wavy	Present	Present	Present
6	10YR 7/6	Yellow	Compact	25	Clear, wavy	Present	Present	Present
7	10YR 7/3	Pale brown	Moderate	10	Clear, smooth	Present	Present	Present
8	10YR 8/4	Pale brown	Compact	10	Clear, smooth	Trace	Trace	Trace
9	10YR 6/3	Pale brown	Compact	35	Clear, smooth	Absent	Trace	Trace
10	2.5 Y 8/1	White	Moderate	35	Abrupt, smooth	Absent	Absent	Trace
11	10YR 7/4	Pale brown	Compact	25	Clear, smooth	Absent	Absent	Trace
12	10YR 7/3	Pale brown	Compact	na	na	Absent	Absent	Absent

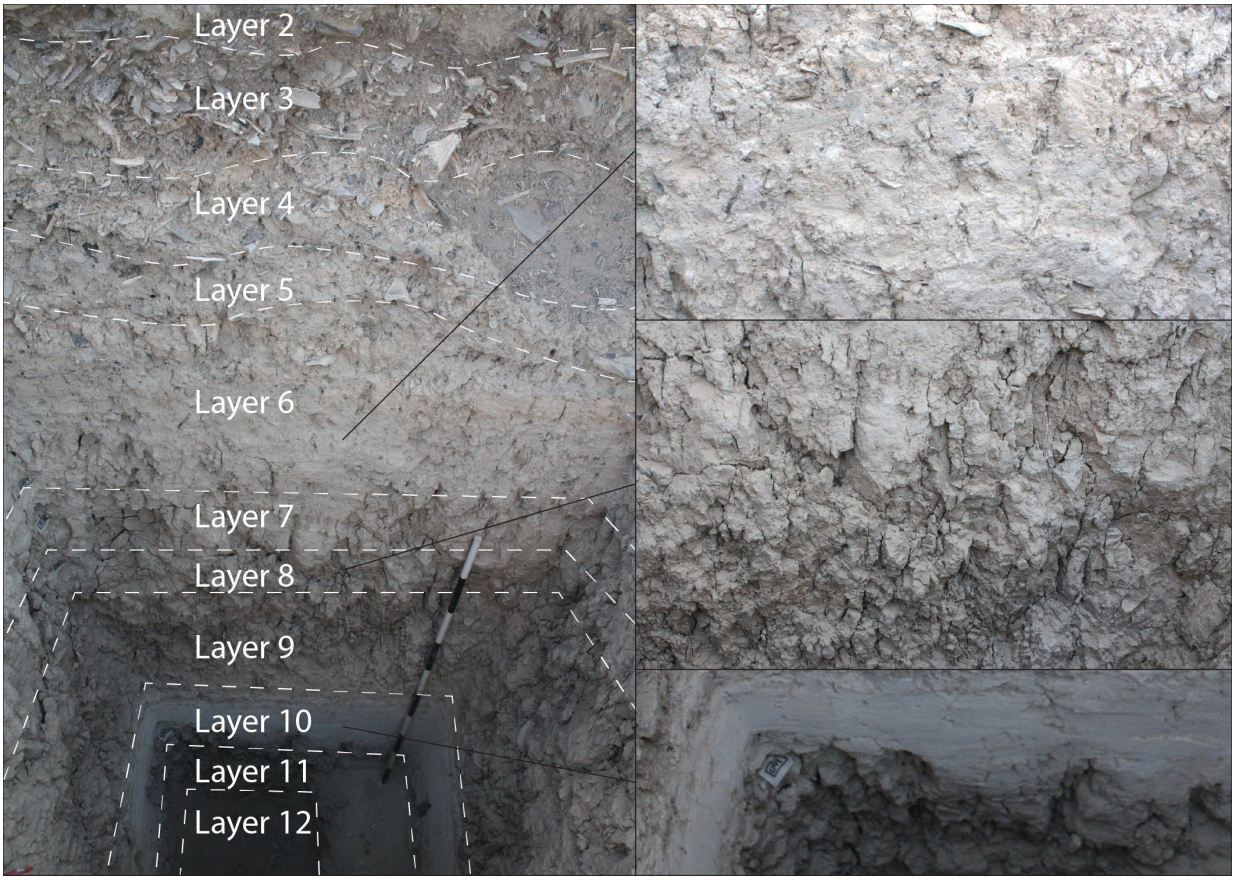

Figure 4.13. Annotated photograph of the northeastern section of RH1 (left), showing detail of structural diversity from top to bottom: massive to blocky Layer 6, prismatic Layers 7 and 8, and granular Layer 10 (right).

Table 4.5. Summary of RH1 LOI data.

Location	Depth (cm)	Layer Number	Organic %	Carbonate %	Mineral %
RH1	5	1	8.30	8.45	83.25
RH1	10	2	9.18	5.73	85.10
RH1	15	2	8.10	5.84	86.06
RH1	20	3	10.54	5.17	84.29
RH1	25	3	11.54	5.59	82.87
RH1	30	3	10.93	3.96	85.11
RH1	35	4	11.95	4.15	83.90
RH1	40	4	13.00	3.36	83.63
RH1	45	5	11.88	4.78	83.34
RH1	50	5	11.57	5.77	82.66
RH1	55	6	13.78	3.18	83.05
RH1	57.5	6	11.76	5.49	82.76
RH1	60	6	15.99	3.40	80.62
RH1	70	6	16.73	4.97	78.30
RH1	75	6	13.52	7.51	78.97
RH1	80	6	15.04	7.79	77.17
RH1	85	7	13.15	10.12	76.73
RH1	90	7	14.61	10.53	74.86
RH1	95	8	10.96	14.62	74.42
RH1	100	8	11.41	8.79	79.79
RH1	105	9	11.69	7.12	81.18
RH1	110	9	11.36	5.80	82.84
RH1	115	9	11.96	4.90	83.14
RH1	120	9	11.63	4.31	84.07
RH1	125	9	11.98	5.20	82.82
RH1	130	9	12.26	6.21	81.53
RH1	135	9	13.19	7.65	79.16
RH1	145	10	10.83	15.62	73.55
RH1	150	10	14.13	15.36	70.51
RH1	155	10	11.27	22.33	66.40
RH1	160	10	11.53	26.11	62.36
RH1	165	10	6.17	32.67	61.16
RH1	170	10	9.03	28.03	62.93
RH1	175	11	8.22	24.71	67.06
RH1	180	11	10.25	15.96	73.79
RH1	185	11	9.97	14.43	75.60
RH1	190	11	13.68	9.16	77.16
RH1	195	11	11.72	8.33	79.95

RH1	200	11	18.89	3.13	77.97
RH1	205	12	11.53	7.65	80.82
RH1	210	12	13.79	5.68	80.54

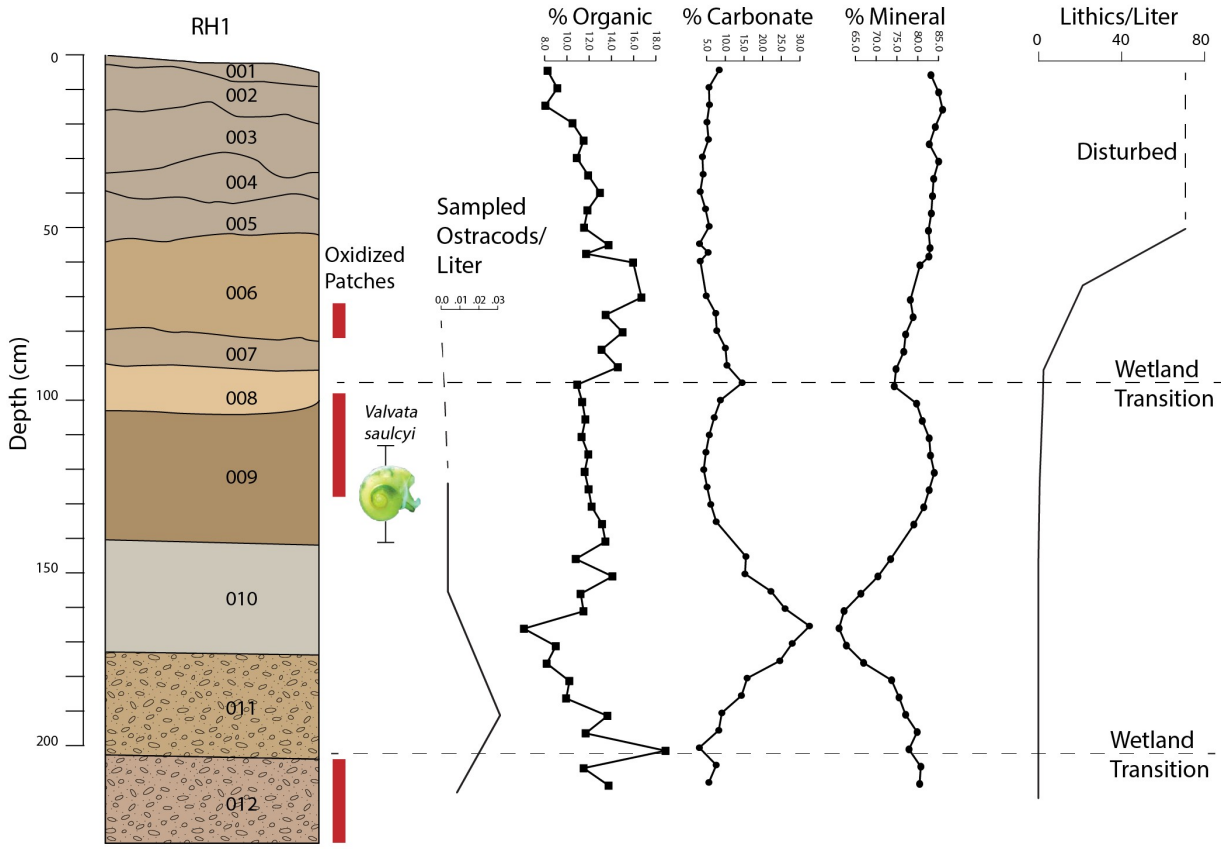

Figure 4.14. RH1 stratigraphy, oxidation stains, ostracod counts, LOI, and lithic data.

Table 4.6. Summary of RH1 lithic artifacts. No data are presented for Layers 1-4 due to disturbance associated with looting activity. Analysis conducted by Dr. Felicia de Peña.

Layer		**5**	**6**	**7**	**8**	**9**
Flakes		349	1074	47	67	30
Blades		118	106	15	22	4
Tools	Geometric microliths	1	7	0	0	0
	Nongeometric microliths	18	11	0	2	0
	Microlith fragments	3	14	0	3	1
	Scrapers	2	13	0	0	1
	Multi-tools	1	0	0	0	0
	Heavy-duty tools	1	0	0	0	0
	Burins	1	18	0	0	1
	Microburins	0	0	0	0	1
	Truncated blades	0	0	0	0	1

	Denticulates	0	2	0	0	0
	Retouched pieces	0	8	0	2	2
Cores	Flake cores	0	5	0	0	0
	Narrow-faced cores	5	0	0	1	1
	Broad-faced cores	0	1	0	0	0
	Opposed platform cores	1	1	0	0	0
	Multi-directional cores	0	1	0	0	0
	Burin cores	0	1	0	0	0
	Core fragments	1	3	0	0	0
Burin spalls		2	14	0	0	0
Lateral core trimming		9	6	0	0	0
Core trimming elements		49	34	3	2	2
Other debitage		358	716	32	32	26
Total		**919**	**2035**	**97**	**131**	**70**
Lithics/liter		**70.69**	**21.42**	**2.43**	**2.18**	**0.50**

Layer 6 is a 25 cm-thick, compact yellow marl that contains charcoal, bone, and lithics. It mostly has a medium grade soil structure and forms angular, blocky peds greater than 1 cm in diameter when broken, but it displays some prismatic peds at its upper and lower contacts and is massive near its middle. It contains the second-highest organic content in RH1 at 16.73% and has oxidized root traces near its lower contact. Charcoal is notably abundant, but diffuse throughout Layer 6, often found within soil peds. At 21.42 lithics/liter, Layer 6 has a lower artifact density than overlying units, but a higher artifact density than underlying units, suggesting that it is a transitional layer that marks the beginning of sustained activities at Area B. With a lower percentage of non-geometric microliths (n = 11; 61.1% of microliths) and no narrow-faced cores, Layer 6's lithic artifacts are less representative of an Early Epipaleolithic assemblage than Layer 5, but variation in Early Epipaleolithic contexts at Kharaneh IV is not unusual (Macdonald et al., 2018). Layer 6's high organic matter content and root traces indicate a facies change from underlying saturated wetland deposits to wetland adjacent dryland, meadow, or phreatophyte conditions (Pigati et al., 2014). Additionally, its moderate lithic density and abundant charcoal mark a transition from low to high human activity at the site, with its high charcoal content possibly indicative of cultural burning of vegetation in preparation for greater use of the Kharaneh IV wetland (Lightfoot et al., 2021; Mariani et al., 2022), although more work is needed to explore this idea.

Layer 7 is a near sterile, thin, pale brown marl that is less compact than overlying and underlying layers. At 2.43 lithics/liter, its lithic density is only a fraction of Layer 6's assemblage and we did not identify any tools or cores among its 97 artifacts. It is high in organic (14.61%) and carbonate (10.53%) content, and relatively low in mineral content (74.86%). The layer has a uniformly prismatic structure, a dry-wet signal which continues through Layers 8 and 9. Although the unit does not contain features indicative of standing water, such as freshwater snail shells and ostracods, found in underlying deposits, its similar appearance and structure to lower units suggest that Layer 7 marks the end of saturated wetland deposits at this location and a

transition to dryland soils and cultural deposits above. The near absence of cultural material in this layer and lower units shows that Kharaneh IV's occupation occurred as the wetland was contracting as more dry land became available. However, since the number of artifacts in Layer 7 and lower units is above zero, the wetland at this location was a place of low level, but consistent human activity long before it was intensively occupied.

Layer 8 is a near sterile (2.18 lithics/liter), 10 cm-thick, very compact pale brown marl that contains the second-highest carbonate content (14.42%) in RH1. The high carbonate content in Layers 7 and 8 may be related to both downward migration of soluble carbonate in well drained upper deposits (Layers 1-5) and upward migration of soluble carbonate from the evaporation of groundwater during wetland desiccation (Finstad et al., 2016). It displays several additional evaporative signals, including visible carbonate and gypsum precipitates, a strong prismatic soil structure, and oxidized patches, further indicating that the unit formed as the Kharaneh wetland contracted.

Layer 9 is a similarly compact, near sterile (0.50 lithics/liter) 35 cm-thick marl that is mostly brown in color. It has a uniformly moderate organic content (average = 11.93%), but its carbonate content fluctuates from 8.79% at the contact with Layer 8 to 4.31% in its middle, possibly indicating upward carbonate migration and reprecipitation with proximity to the desiccation signals identified in Layer 8. Additionally, its large gypsum precipitates, prismatic soil structure, and oxidized patches suggest a continuation of Layer 8's drying sequence. Layer 9's base is marked by the appearance of freshwater snail shells (*Valvata saulcyi*, Amr and Abu Baker, 2004), pockets of gleyed soil, and ostracod shells (Figure 4.15; Table 4.7). While species identification of ostracods is beyond the scope of this study and worthy of future work at the site, their presence in addition to freshwater snail shells, gleyed soil patches, and prismatic soil structure are indicative of groundwater discharge deposits, specifically "wet meadow" or "marsh" wetland marl facies, which form in densely vegetated environments with significant and sometimes perennial standing water (Pigati et al., 2014:74-75).

Figure 4.15. Ostracod shells identified in floated material from RH1 Layer 10 (left) and freshwater snail shell anterior (top) and posterior (bottom) view from RH1 Layer 9.

Table 4.7. Ostracod counts of floated fraction normalized to volume of each RH1 layer.

Layer	Avg. Ostracod Count/15.2 mm^2	Liters of Sediment	Ostracod Count/Liter
5	0	13	0
6	0	95	0
7	0	40	0
8	0	60	0
9	0.5	140	0.00357
10	0.25	70	0.00357
11	1.25	40	0.03125
12	0.25	30	0.00833

Layer 10 is a 35 cm-thick, homogenous, sterile, white fine sand with a granular soil structure. We observed approximately 10 lithic artifacts at the contact with Layer 9 but did not observe any artifacts during further excavation nor following flotation. We identified several ostracod shells in the floated fraction and recorded probable insect burrows and black carbon stains in the layer's interior. Layer 10 is notably high in carbonate content, peaking at 32.67% near the contact with Layer 11 and fluctuates in organic material from 6.17% at its base to 14.13% at its top. The carbonate in Layer 10 is likely an *in-situ* source, and not sink, of deposited carbonate material because it is a significant component of the matrix, as opposed to material filling pore space within the matrix, and it is bounded by deposits that signal saturated conditions, as opposed to evaporative conditions that would obtain soluble carbonate through capillary action. The layer's thick, carbonate-rich marl and the presence of ostracod shells

suggest that the layer was the most saturated in RH1, and possibly represents the timing of the Kharaneh wetland's greatest extent.

Layer 11 is a compact, near sterile, 25 cm-thick, pale brown marl that contains many flint nodules approximately 1-5 cm in diameter. Nodule frequency increases with depth and we recorded several possible flakes, but most of the flint appears to be unworked naturally occurring nodules. The prismatic soil structure of Layer 11 is similar to Layer 9, but it does not contain any large gypsum and carbonate precipitates. Organic content increases with depth from 8.22% to 18.89%, the highest organic value in RH1. Layer 11 also has the most recorded ostracods counts in RH1. The high organic content and ostracod counts in Layer 11 indicate that it formed in a saturated environment with significant biological activity. Additionally, the unworked nodules in Layer 11 are similar to flint cobbles that comprise surface pavements throughout the Kharaneh region today and Layer 11's elevation (637.43-637.71 masl) is within the modern surface level (637.0-637.5 masl) of gravelly beds immediately east of Kharaneh IV, suggesting that the layer may represent a transition from an open pavement or wadi landscape to submerged wetland conditions, likely as the water table rose and eventually met the surface to create the Kharaneh wetland.

Layer 12 is a compact, sterile sandy marl with gravels and flint nodules that persist to an unknown depth. We ceased excavation approximately 20 cm into the unit due to its high compaction and flint frequency that was equally resistant to trowel, shovel, and pick removal. It is predominantly pale brown in color, but its matrix contains numerous red oxidization stains that are more prevalent with depth and suggest wet-dry conditions. We recorded a small number of ostracod shells that indicate the presence of water during the layer's formation. The ostracod shells and oxidized patches in Layer 12 further support the interpretation that RH1's lowest units show a facies change from dryland to wetland conditions, with oxidized patches at its base indicating at least partial exposure to air giving way to sediment containing ostracod shells, gleyed patches, and freshwater snail shells in Layers 9-11.

Offsite Sections

Despite being located 443 m apart on either side of Kharaneh IV and at different elevations (Section 2 = 639.472 masl; Section 5 = 637.864 masl), offsite Sections 2 and 5 are similar in texture and composition. Both sections have a loose to moderately compact, light brown 20-30 cm thick upper layer, described as a weathering surface by Jones et al. (2016:99), above a homogenous, very compact, massive to blocky light gray marl that continues with depth to the base of excavations (Section 2 depth = 1 m; Section 5 depth = 1.3 m). We note that Jones et al. (2016) documented small flint cobbles at the bottom of Section 5 that we did not encounter. While both offsite sections are similar in compaction, color, and structure to Geotrench2018 Layers C and F and RH1 Layers 6 and 7 (Figure 4.16), their apparent thickness of >1 m contrasts with the thin and diverse layers of Geotrench2018 and RH1. Additionally, Sections 2 and 5 are high in carbonate content, ranging from 12.64% in Section 2 to 16.91% in Section 5, and organic content, ranging from 10.56% in Section 2 and 12.56% in Section 5 (Table 4.8). The massive and blocky structure and high carbonate and organic content of Sections 2 and 5 are consistent with wetland marls as described by Pigati et al. (2014), and their thickness indicates that the homogenous terraces that contain Sections 2 and 5 were the regions that held the most water in

the Kharaneh wetland (Jones et al. 2016). Jones et al. (2016) dated a 56 cm-deep OSL sample from Section 2 to 20 ± 1 ka BP and a 40 cm-deep OSL sample from Section 5 to 21 ± 1 ka BP, with a second Section 5 sample from 80 cm down dated with lower confidence to 19 ± 1 ka BP due to limited datable material. It is notable that the offsite OSL samples are younger than the 22 ± 1 ka BP OSL age of wetland marl Locus 5 in Geotrench2009, suggesting that as the wetland shrank near Kharaneh IV, it maintained considerable amounts of water in the offsite locations up to and likely during the site's occupation.

Figure 4.16. Comparison of offsite Section 2 (left) and onsite Geotrench2018 Layers C and F (middle) and RH1 Layer 6 (right).

Table 4.8. Summary of offsite section and previous excavation LOI data.

Location	Depth (cm)	Locus	Organic %	Carbonate %	Mineral %
Section 2	70	-	10.56	12.64	76.80
Section 5	50	-	12.52	15.40	72.08
Section 5	100	-	12.56	16.91	70.53
GT09N	-	3	11.84	4.02	84.14
GT09N	-	4	12.09	7.26	80.65
GT09N	-	5	14.04	3.86	82.10
GT09N	-	7	13.57	6.20	80.23
GT09N	-	8	11.38	15.12	73.50
GT09S	-	3	10.92	5.70	83.38
GT09S	-	4	13.63	7.21	79.16
GT09S	-	6	15.24	7.16	77.60
GT09S	-	7	11.56	10.87	77.57
GT09S	-	8	14.88	7.92	77.20
AS42	-	115	9.76	17.59	72.65
AZ51	-	2	12.16	8.81	79.02
AZ51	-	8	9.68	9.37	80.95
AZ51	-	9	8.50	5.55	85.95
AZ51	-	11	13.58	3.18	83.25

AZ51	-	12	11.27	8.58	80.15
BS58	-	31	10.63	18.15	71.22

Comparison with Previous Kharaneh IV Excavations

When compared with other Kharaneh IV excavations, the vertical and lateral heterogeneity of sediments displayed in Geotrench2018 and RH1 appears representative of the entire site. While multiple deep excavation units, including AS42, AZ51, and BS58, in addition to RH1, have thick upper cultural deposits and compact lower marl layers, their marls vary significantly in color, thickness, and composition (Figure 4.17; Table 4.8). As others have noted (Jones et al., 2016; Maher et al., 2021b), the sedimentological diversity of wetland deposits represents a checkered landscape of vegetated, submerged, and dry patches, similar to the Azraq Oasis today approximately 40 km to the east. The stratigraphic diversity of Kharaneh IV is further complicated by deposition along a wetland gradient. While lake surfaces are flat, groundwater-fed wetlands typically are not and instead parallel the gradient of the valley floor (Pigati et al., 2014), making stratigraphic comparison by elevation less effective.

Despite these challenges, we note several trends in sedimentology across the Kharaneh IV. Although most site excavations contain dense cultural deposits above a sequence of marls that document a desiccation trend, cultural features in BS58 are located within and directly above Locus 34, a thick, white carbonate-rich marl without a desiccation sequence of overlying marls. This suggests that early cultural layers at BS58 were deposited before much of the Kharaneh wetland had contracted and may represent some of the earliest prolonged activity at the site. While acknowledging the difficulty of stratigraphic comparison at Kharaneh IV, similarities in texture, depth, and high carbonate content between the white marl of Locus 34 in BS58 and white marl of Layer 10 in RH1 and Locus 115 in AS42 (the red units in Figure 4.17) suggest that they may be a continuous and contemporaneous layer that could serve as a marker unit throughout the site, although further investigation is needed for confirmation. Finally, while most onsite units show a desiccation pattern of lower marls transitioning to artifact-dense, upper silts and sands, the offsite units are entirely composed of marls, suggesting that the Kharaneh IV site was situated on the margin of a contracting, but still extant wetland.

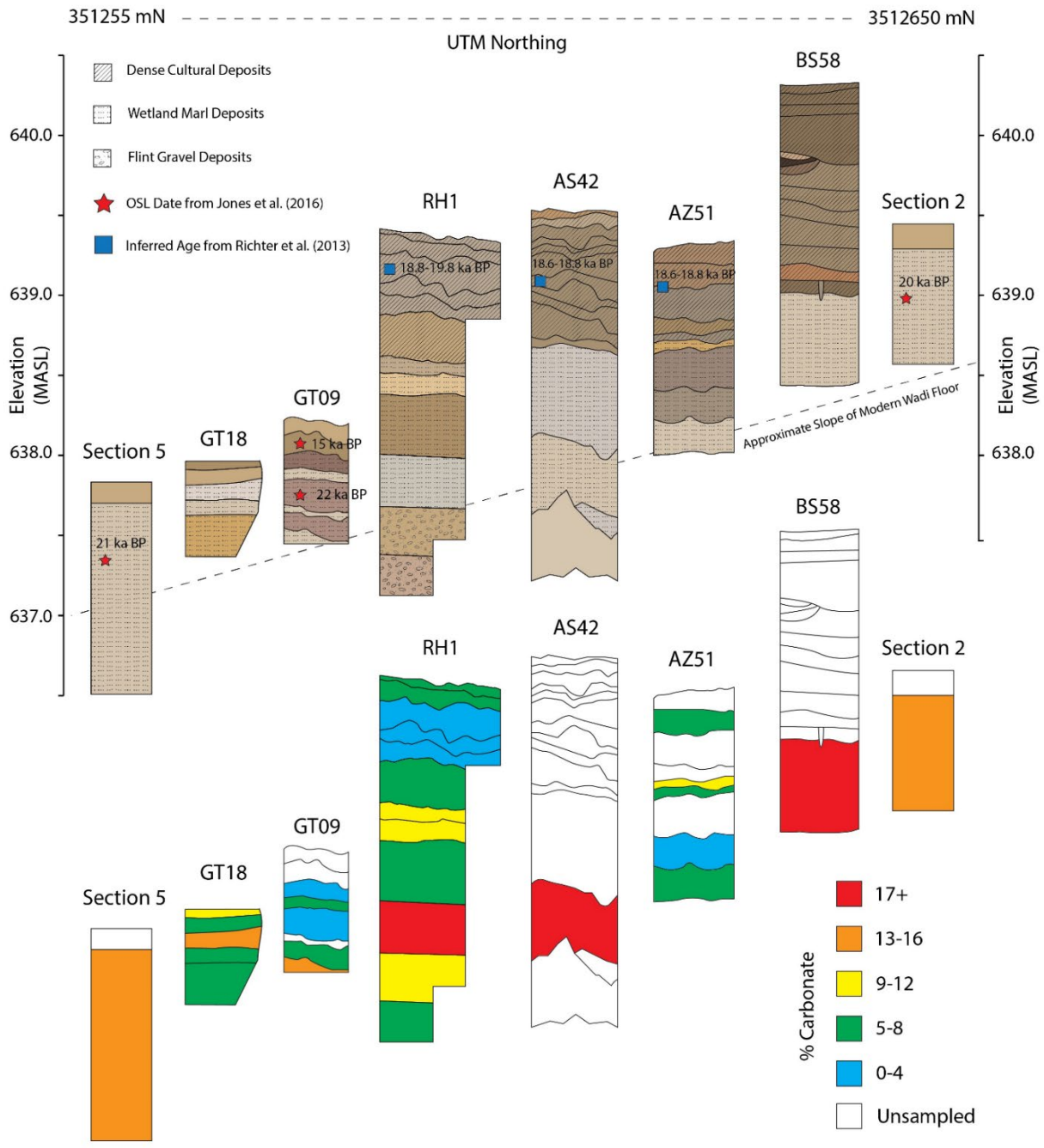

Figure 4.17. Top: stratigraphy of select Kharaneh excavations, arranged from south (left) to north (right), with OSL dated samples (red stars; Jones et al., 2016) and inferred age of cultural deposits from Richter et al. (2013) (blue squares). Bottom: carbonate LOI data across Kharaneh IV excavation units.

Geological Survey

During the geological survey, we found no evidence of a significant fault in the Kharaneh IV region that would offset bedrock and constrain groundwater flow necessary to form groundwater-derived deposits. The bedrock forming slopes north and east of Kharaneh IV shows minor joining but is structurally intact. We observed that the chalk bedrock that forms the wadi slopes appears to have two units observable at the surface: a homogenous and friable upper layer and a concrete lower layer containing many pebble and cobble-sized chert nodules (Figure 4.18). The upper chalk occurs in eroded, low-lying hills while the lower chalk forms steep slopes along the wadi floor, indicating that the lower chalk is stronger and more resistant to erosion.

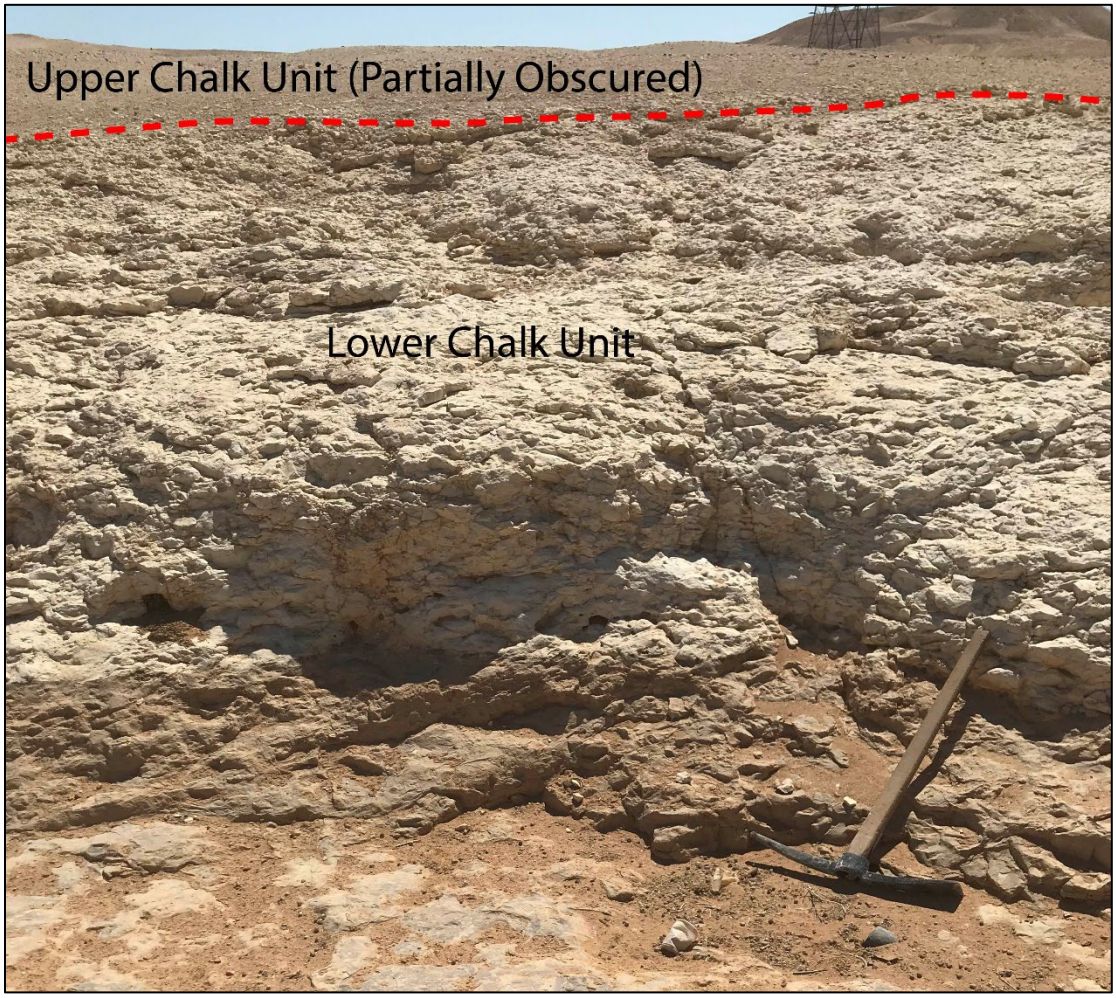

Figure 4.18. Upper chalk unit (partially exposed by colluvium/desert pavement) above lower chalk unit. Note that the lower unit forms steep and clear exposures while the upper unit forms low-angle slopes, showing their relative strength. Photo credit: Jordan Brown.

We observed the lower chalk bedrock outcropping in several locations in the wadi floor (Figures 4.19 and 4.20). The bedrock is nearly continuous for several hundred meters east of Kharaneh IV and outcrops in smaller segments north of the site. Between these locations we

encountered three previously excavated holes in the wadi floor pavement, approximately 1 m across and ranging in depth from approximately 1.5 to 4 m, dug for unknown purposes (Figure 4.21). The holes show that the subsurface in this region is dominated by gravel to cobble-sized alluvium. As previously mentioned, the flint gravel of Loci 11 and 12 in RH1 is similar in elevation and composition to the surface and subsurface gravels documented during this survey, by previous characterizations of Kharaneh geomorphology (Besançon et al., 1989) and possibly the flints noted by Jones et al. (2016) at the base of Section 5. Taken together, the gravels underlying wetland marls at Kharaneh IV and possibly the marls offsite at Section 5 were likely once linked as a paleosurface to gravels that form the wadi floor pavement east of Kharaneh today before the formation of the Kharaneh wetland.

Figure 4.19. Left: Buried cobble and gravel alluvium in wadi profile. Right: chalk bedrock exposed at wadi surface.

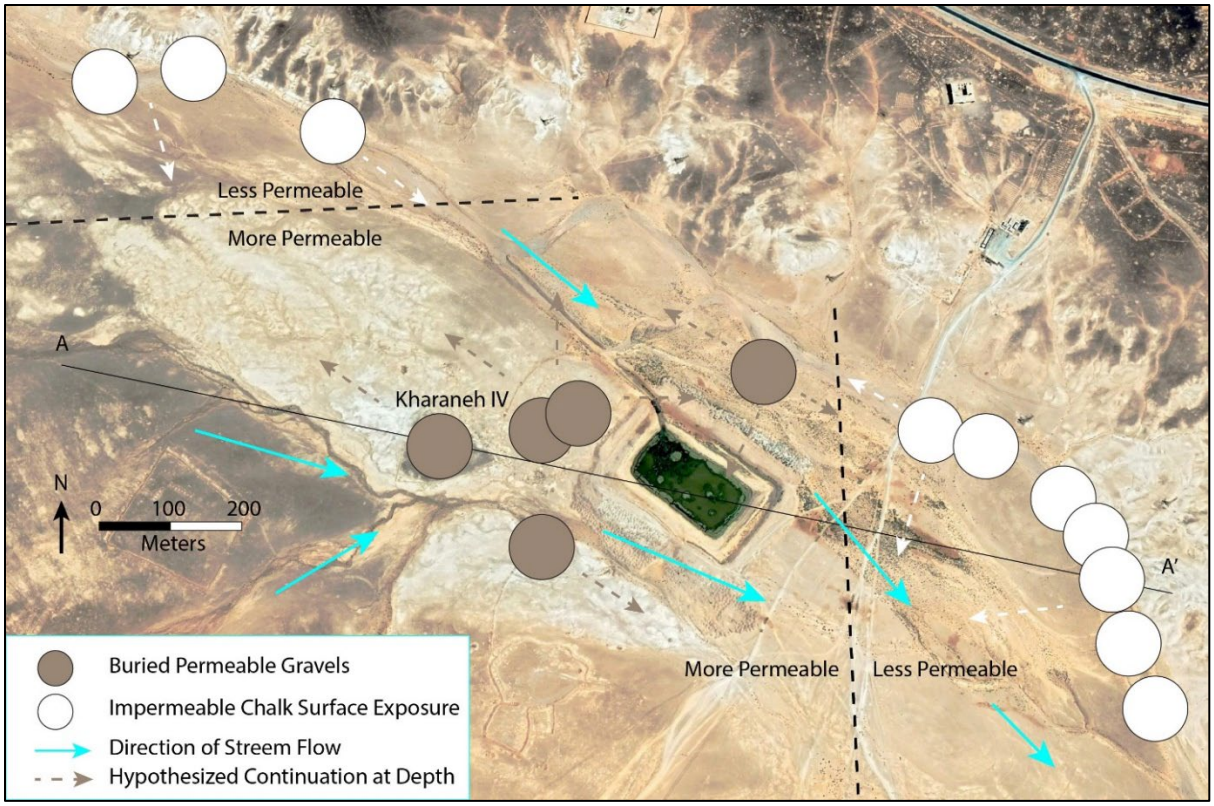

Figure 4.20. Areas where we observed impermeable chalk (white circles) and holes and excavations showing gravel and cobble alluvium at depth (brown circles) with arrows indicated a hypothesized lateral continuation at depth. The dashed black lines divide the map into more and less permeable areas based on field observations. Section A-A' is shown in Figure 4.22.

Figure 4.21. The deepest (4 m) of the three previously excavated holes east of Kharaneh IV identified during the geological survey.

The spatial extents of bedrock marls and wadi gravels in Wadi Kharaneh mark a gradient in permeability across the wadi floor. The gravel alluvium found at depth within holes east of Kharaneh IV is much more permeable than the strongly cemented chalk bedrock to the north and east. The transition from impermeable chalk northwest of Kharaneh IV to permeable gravels beneath and surrounding the site, followed by a shift back to impermeable chalk southeast of Kharaneh IV creates a sink for water to slow down, collect, and reemerge at the contact with concrete chalk in the east (Figure 4.22). While an excavated watering hole and strands of vegetation (see Figure 4.20) show that water is more available at this location than the surrounding landscape today, increased groundwater flow and lower evapotranspiration during wetter periods of the Pleistocene combined with the subsurface permeability gradient described above would have provided the necessary conditions to create the Kharaneh wetland.

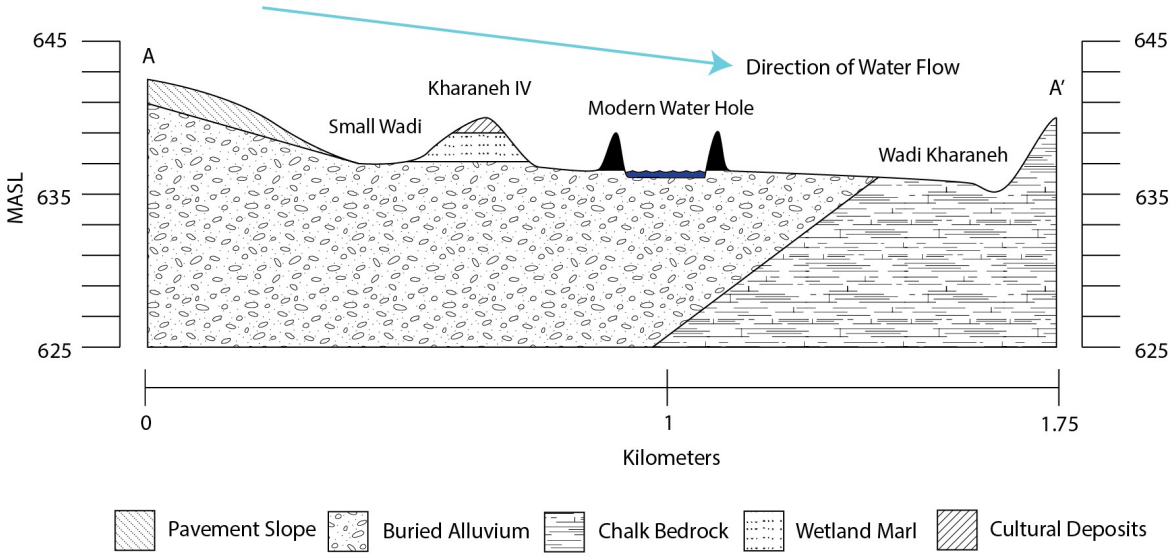

0

Figure 4.22. Cross section A-A' interpreted from field observations, showing hypothesized subsurface relationships.

During the geological survey, we noted that alluvium sediments in the upper levels of the wadi bank north and east of Kharaneh IV are consolidated into a calcrete that resembles conglomerate rock (Figures 4.23 and 4.24). Calcrete forms in semiarid and arid soils around the world through the calcium carbonate cementation of surface and near-surface sediments (Alonso-Zarza and Wright, 2010; Netterberg, 1969). While there are multiple pathways to calcrete formation and the process is complex, it typically involves the gradual downward leaching of carbonate from surficial A horizons and precipitation in a K horizon (pedogenic calcrete, commonly referred to as a hardpan) or the highwater mark of a receding aquifer (groundwater calcrete; similar to groundwater marls *sensu* Pigati et al., 2014) (Alonso-Zarza and Wright, 2010). Calcrete forms slowly, often over the course of thousands to tens of thousands of years (Candy et al., 2004; Elidrissi et al., 2017), so the thick, mature calcretes at the edge of Wadi Kharaneh to the north and east of Kharaneh IV are likely much older than the site. However, we noticed a concentration of small, highly weathered nodules and fragments of what appear to be calcrete on the surface of Kharaneh IV's Area B region (Figure 4.23). These fragments contain many small flint and bone artifacts and ecofacts like the surrounding surface palimpsest but are concreted into nodules that are much more compact than the upper cultural deposits found throughout the rest of the site. These nodules likely represent calcrete formation at the incipient stage, whereby calcite is precipitated within the matrix pores of the parent sediment that gradually displaces and replaces the original matrix (Khalaf, 2007). Because calcretes most often form during warmer interglacials (Candy and Black, 2009), the incipient calcrete at Kharaneh IV is likely a product of Holocene conditions and it may eventually extend throughout Kharaneh IV if similar climatic conditions hold into the future.

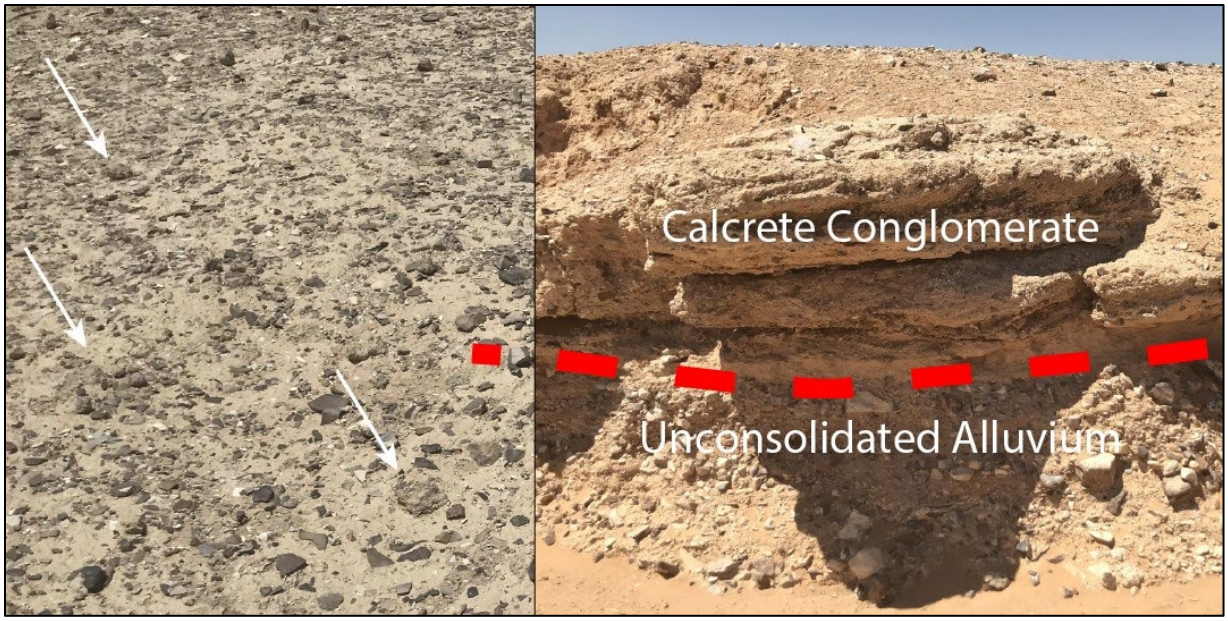

Figure 4.23. Left: weathered calcrete fragments (white arrows) at Kharaneh IV Area B among surface palimpsest. Right: calcrete outcrop in Wadi Kharaneh above loose gravels.

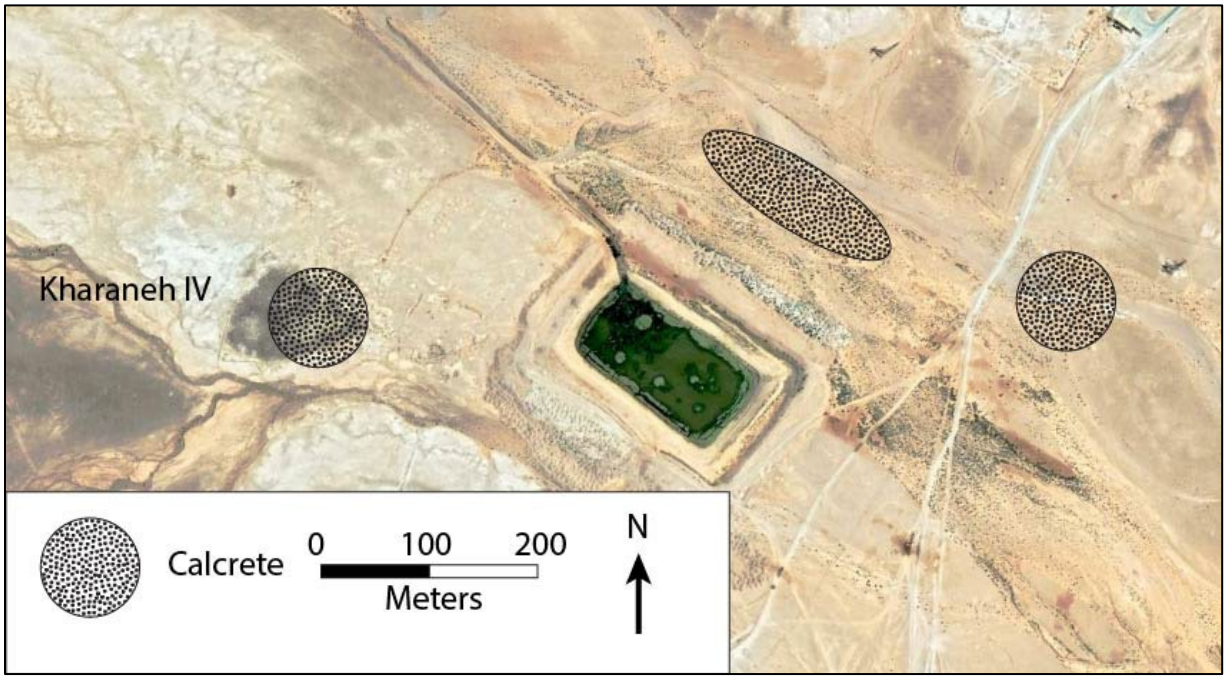

Figure 4.24. Map of calcrete outcrops observed in the field.

A Narrative of Environmental Change at Kharaneh IV

The excavation and survey data presented here in conjunction with previous work at the site allow us to form an environmental history of the Kharaneh wetland, beginning with its formation over 22,000 years ago (Figure 4.25). The 22 ± 1 ka BP OSL date of wetland marl from Geotrench2009 (Jones et al., 2016) serves as a *terminus post quem* for wetland formation, which may have initially occurred during a period of lower regional speleothem $\delta^{18}O$ values (Bar-

Matthews et al., 2003; Grant et al., 2012) and higher Lake Lisan reconstructions (Bartov et al. 2003; Torfstein et al. 2013) that indicate wetter conditions around 27,000 BP (Figure 4.26). Rising groundwater met the surface and saturated the preexisting surface gravels, initiating a facies change to wetland marl formation and deposition (Figure 4.25 Steps 1-3). Thick, white carbonate-rich layers Locus 34 in BS58, Layer 10 in RH1, Locus 115 in AS42, and offsite Sections 2 and 5 likely correspond to this sequence.

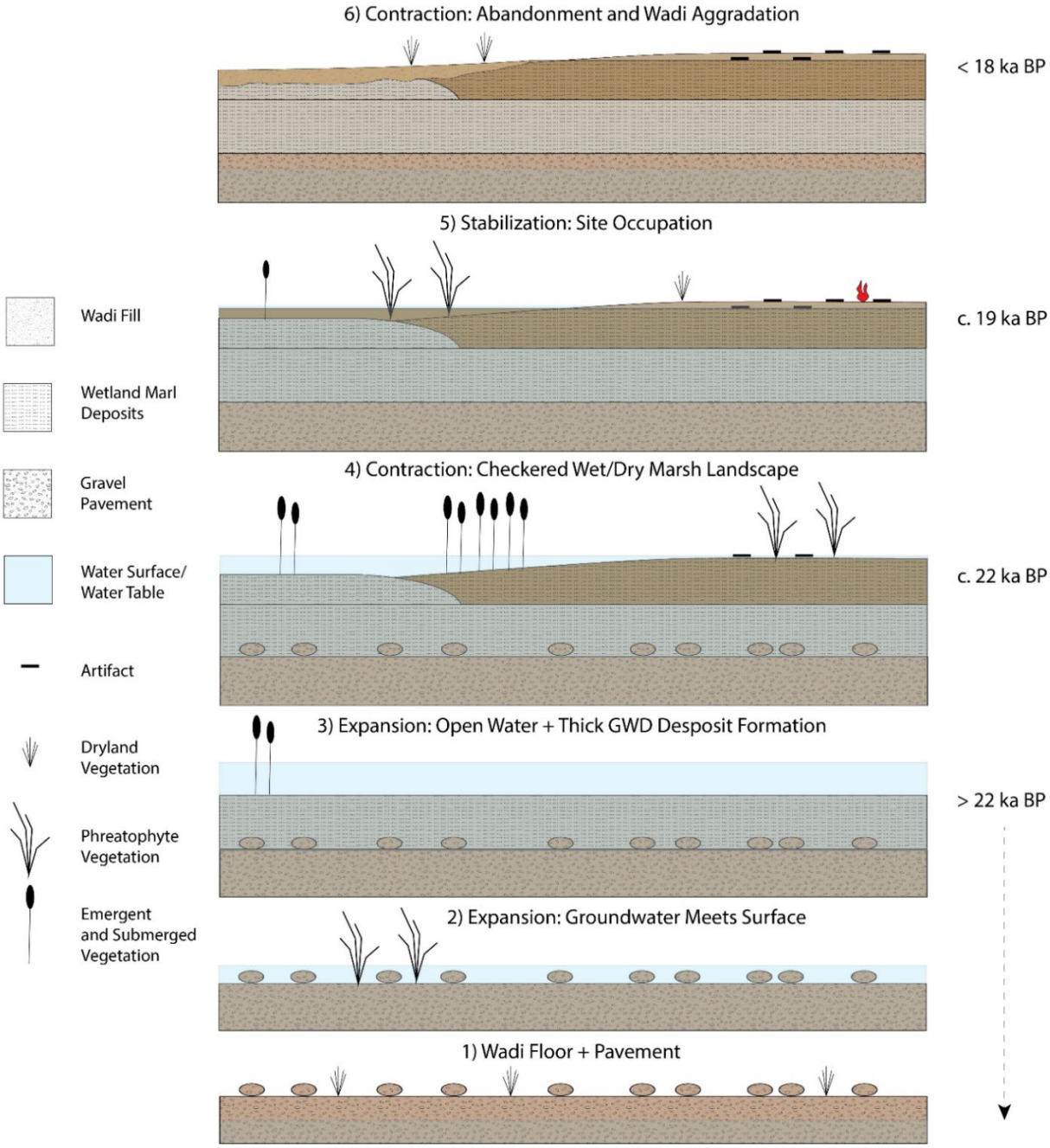

Figure 4.25. Sequential schematic of Kharaneh wetland formation and contraction.

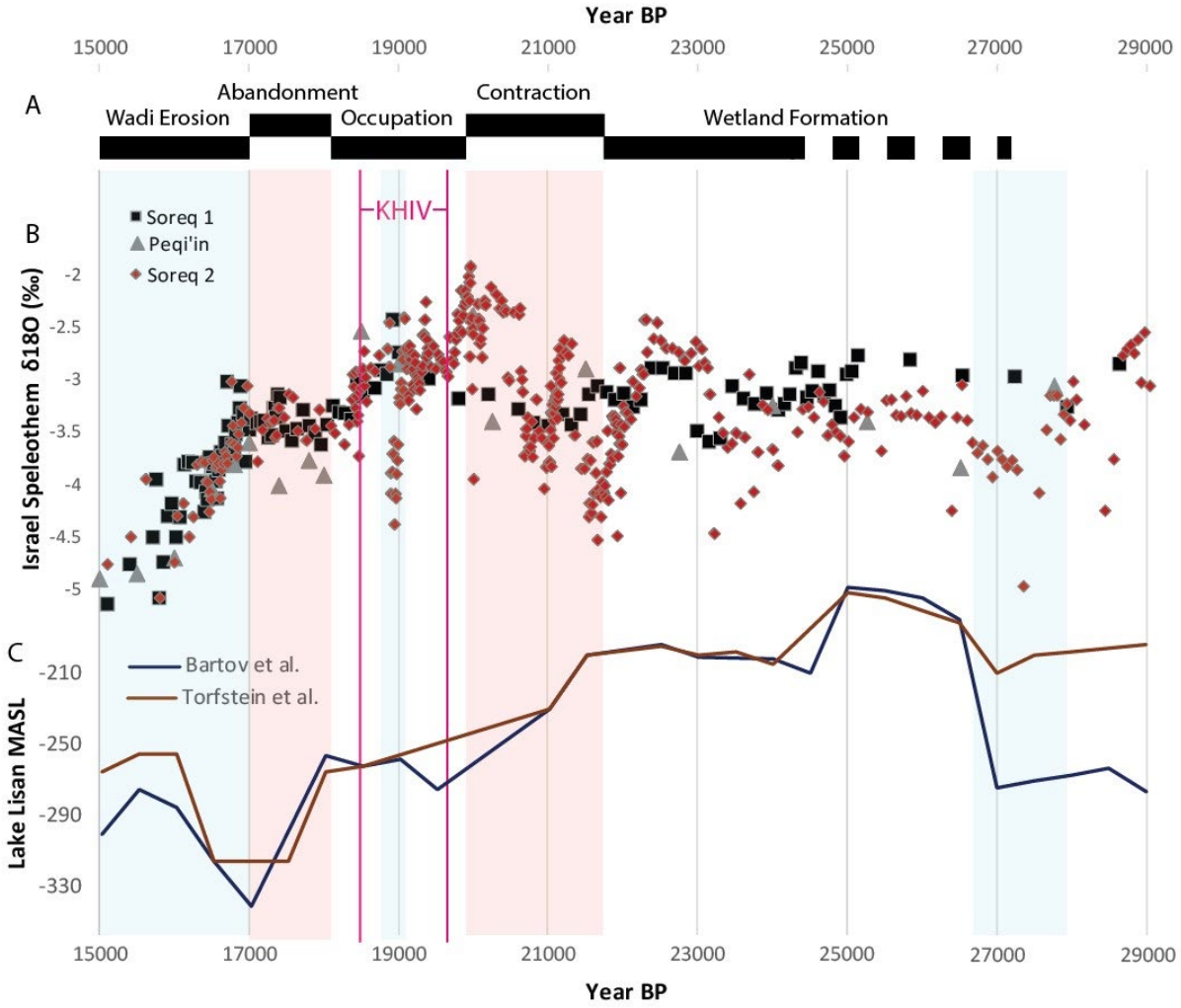

Figure 4.26. A) Interpretation of Kharaneh wetland history compared to B) speleothem $\delta^{18}O$ values from Soreq Cave (Bar-Matthews et al., 2003 = Soreq 1; Grant et al., 2012 = Soreq 2), and Peqi'in Cave (Bar-Matthews et al., 2003), Israel and C) lake level reconstructions for Lake Lisan from Bartov et al. (2003) and Torfstein et al. (2013). Blue and red vertical bars correspond to wetter and drier periods, respectively, in both sets of data.

A shift to a checkered landscape of wet and dry patches due to the contraction of the wetland is marked by alternating brown and white wetland marl layers in Geotrench2009, Geotrench2018, RH1, AS42 that begin to display signs of desiccation, including evaporite minerals and oxidization stains (Figure 4.25 Step 4). The 22 ± 1 ka BP OSL date of Geotrench2009 Locus 5 (Jones et al., 2016) indicates that the shift to a receding wetland began by that time. Wetland contraction by 22 ± 1 ka BP is further supported by a +2‰ excursion in $\delta^{18}O$ values from Soreq Cave (Grant et al., 2012) and a decline in Lake Lisan elevation (Bartov et al. 2003; Torfstein et al. 2013) that began near 22,000 BP and continued to approximately 20,000 BP (Figure 4.26). This change corresponds in time with the Last Glacial Maximum, centered on 21,000 BP (Otto-Bliesner et al., 2006), linking local and regional environmental shifts with global climate change. Basal artifacts within wetland marl deposits from

Geotrench2009, Geotrench2018, RH1, and AS42 indicate that human activities occurred, at least infrequently, at the Kharaneh wetland over several thousand years before the site was heavily occupied.

Although traditional paleoenvironmental archives are unavailable during Kharaneh IV's dense occupation from 19,800 to 18,600 BP due to the erosion of contemporary sedimentary features (Jones et al., 2016), stable isotope data presented in Chapter 3 and phytolith data from Ramsey et al. (2016) suggest that the wetland reached a stable, but reduced size following the preceding drying trend (Figure 4.25 Step 5). A stable local environment is supported by regional speleothem stable isotope values (Bar-Matthews et al., 2003; Grant et al., 2012) and Lake Lisan elevation reconstructions (Bartov et al. 2003; Torfstein et al. 2013) that show less variation than the preceding and following times. An exception to this stability was a possible increase in local precipitation marked by a concurrent decline in gazelle tooth enamel $\delta^{18}O$ values and Soreq Cave speleothem $\delta^{18}O$ values (Grant et al., 2012) centered on c. 18.8 ka BP (Figure 4.26).

While the erosion of contemporary sedimentary features is also a problem for understanding Kharaneh IV's post-occupational history, the excavation and survey data presented here provide at least a partial paleoenvironment context. A facies change from groundwater-derived wetland deposits to surface water-dominated alluvial erosion, aggradation, and deposition occurred by the 15 ± 1 ka BP OSL date of Geotrench2009 Locus 2 (Jones et al., 2016) (Figure 4.25 Step 6). Geotrench2009 Locus 2 and Geotrench2018 Layer B are wadi silts deposited by alluvial processes, possibly related to a small wadi approximately 25 m south of Kharaneh IV before it was downcut to its current position. The transition from wetland and cultural-related deposition to alluvial deposition first brought erosion, as alluvial activity cut into and formed the contact between Geotrench2018 wetland marl Layer C and wadi silt Layer B, creating an unconformity. Sedimentary aggradation then deposited the silt that forms Geotrench2009 Layer B and Geotrench2018 Locus 2 by approximately 15 ka BP.

The period from the end of Kharaneh IV's occupation to the timing of wadi silt deposition roughly corresponds with Heinrich Stadial 1 (18,000-16,000 BP; Bard et al., 2000; Heinrich, 1988; Stager et al., 2011). Researchers have associated Heinrich Stadial 1 and its regional equivalent the Oldest Dryas to substantial cooling (Clark et al., 2012, 2001; Keigwin and Lehman, 1994; Lischke et al., 2013) and regional archives point to a drier period between 18,000 and 17,000 BP, followed by relatively wetter conditions from 17,000 to 15,000 BP (Bar-Matthews et al., 2003; Bartov et al., 2003; Grant et al., 2012; Torfstein et al., 2013) (Figure 4.26). It is during this dynamic period that deposition at the Kharaneh wetland transitioned to alluvial-dominated processes, which continue to shape Wadi Kharaneh to this day. The occurrence of incipient calcrete nodules on the surface of Kharaneh IV suggests that calcrete may slowly envelop the site if current climatic conditions persist, a process known to have occurred at other archaeological sites (Carson and Peterson, 2011; Netterberg, 1974). However, surface disturbances at the site from excavation, looting, and offroad vehicles limit calcrete growth.

The narrative of climatic changes at Kharaneh IV presented here contributes to a larger understanding of the environmental history of the Azraq Basin. A common thread of research within the basin is the identification of alternating wet and dry periods and corresponding implications for human habitation. Research by Ames et al. (2022) and Cordova et al. (2013) used stratigraphic, sedimentological, and micropaleontological analyses to document three cycles

of expanding and contracting wetlands in the Azraq Basin since c. 350,000 BP and noted the importance of the basin as a refugia for hominin migrations throughout the Eurasian-African juncture. Working on a similar timescale, Ahmad and Davies (2017, 2021) interpreted variations in carbonate oxygen and carbon and organic matter carbon and nitrogen isotope ratios from Azraq Basin lacustrine sediments as reflecting alternating wet and dry periods. Jones and Richter (2011) presented a c. 60,000 year paleoenvironmental record from 'Ayn Qasiyya at the edge of the Azraq Wetland to show that wet conditions prevailed before the Last Glacial Maximum, but the wetland desiccated in the leadup to the Holocene from approximately 16,000 to 10,500 BP.

This chapter contributes to previous work in the Azraq Basin by operating on a smaller timescale to focus on human activity between significant wet and dry periods. As discussed, Kharaneh IV's occupation is bounded by drying episodes, but these events are not pertinent to the bulk of archaeological remains that were deposited between them. Rather, Kharaneh IV's site history occurred against the backdrop of a relatively stable and reliable local environment, which may have been temporarily disrupted by an increase in local precipitation during its Middle Epipaleolithic occupation (Chapter 3). The site-scale information presented here and in previous chapters, combined with local (Besançon et al., 1989; Garrard et al., 1985; Jones et al., 2016) and regional studies (Bar-Matthews et al., 2003; Bartov et al., 2003; Grant et al., 2012; Torfstein et al., 2013) highlight the importance of using a multiscale approach in environmental archaeology and allow us to further refine our understanding of environmental change within the Azraq Basin (Figure 4.27).

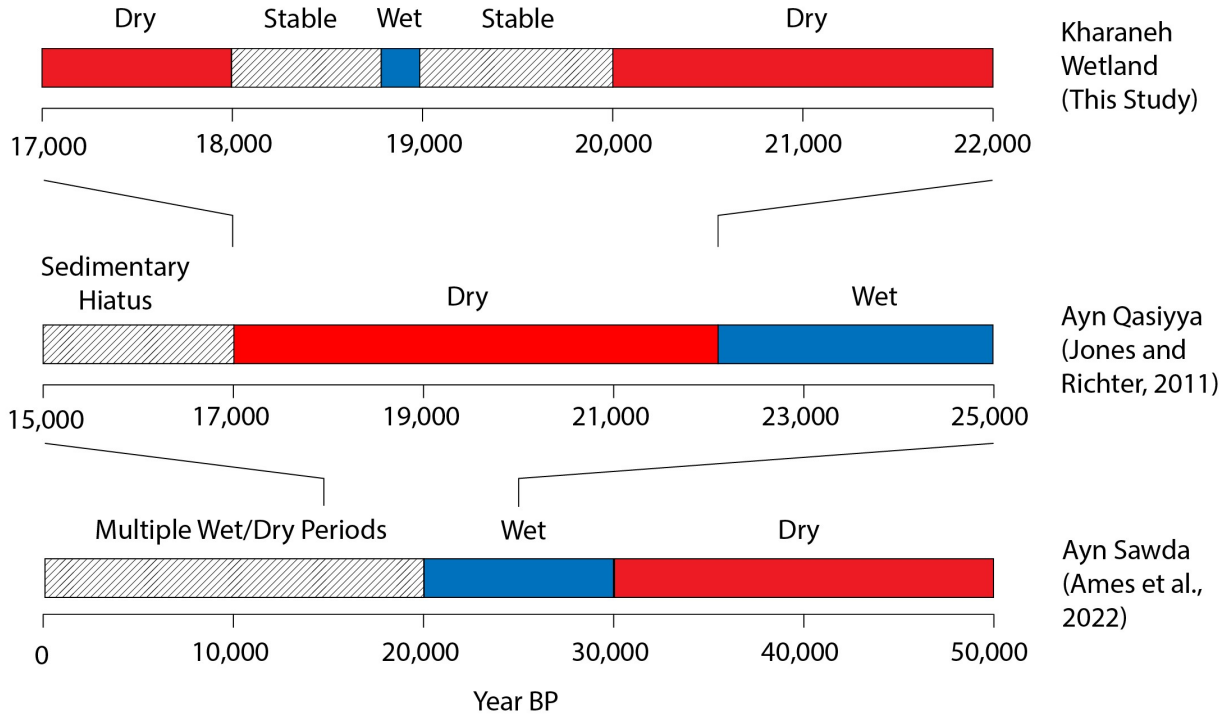

Figure 4.27. Dry/wet cycles interpreted from multiple environmental archives within the Azraq Basin conducted by studies at long (Ames et al., 2022), medium (Jones and Richter, 2011), and short (this study) timescales.

The Paleoenvironment and Persistent Places Interwoven at Kharaneh IV

There is a clear association between water availability and occupation intensity at Kharaneh IV, with artifact density peaking following a drying trend from approximately 20-22 ka BP, and abandonment of the site during a second drying trend near 18 ka BP. But water availability is only a partial explanation for why the Kharaneh wetland was so densely occupied by Epipaleolithic people. To return to the concept of Schlanger's (1992) 'unique properties' that make up persistent places, the wetland does not appear to have had a particularly unique hydrological setting, such as a fault-controlled spring, that set it apart from the surrounding landscape. It would seem that the Kharaneh Wetland was *a* water source, not *the* water source for the region. Research by Jones and Richter (2011) shows that the Azraq oasis approximately 40 km northeast of Kharaneh IV contained water at the time of the site's occupation, and similar permeability gradients may occur in wadis throughout the region. In studying the creation of persistent places, their unique qualities that are conducive to certain activities (Schlanger 1992) are best understood as a gradient – water availability at Kharaneh IV was unique enough to provide resources for Epipaleolithic groups, plants, and prey, but not unique in the singular or unparalleled sense of the word.

The reliability of the wetland over a thousand-year period, as demonstrated by a mostly stable paleoenvironment (Chapter 3; Figure 4.26) and reliable wetland plant community (Ramsey et al., 2016) encouraged continued reoccupations of the site, and thereby demonstrates Schlanger's (1992) second attribute of persistent places. This in turn relates to Schlanger's third attribute of persistent places by the gradual accumulation of cultural material over a thousand years that formed a modest tell above the surrounding wetland, which itself encouraged further revisitation by creating an occupation surface above the wetland muds. The results of place-making at Kharaneh IV are evident in the temporary period of increased precipitation during Kharaneh IV's Middle Epipaleolithic occupation. Instead of leaving to pursue expanded resource opportunities away from Kharaneh IV, the site's inhabitants chose to continue their close connection to the Kharaneh wetland. While this study has hoped to the quantifiably demonstrate the connections between paleoclimatic and paleoenvironmental conditions and persistent places, it is important to state that Kharaneh IV's environmental setting was just one factor among a constellation of cultural considerations, including exchange networks ranging from the Mediterranean to the Red Sea, connections to Epipaleolithic groups throughout the Levant, symbolic ties to the past through ritual burials, and place-making through hut structures, food processing stations, and the accumulation of millions of artifacts that literally raised the site above the landscape, that combined to form a persistent place (Macdonald et al., 2018b; Macdonald and Maher, 2022; Maher, 2021, 2019; Maher et al., 2021a, 2012; Maher and Macdonald, 2020; Spyrou et al., 2019; Whitehurse, 2021).

Although the main occupation of Kharaneh IV ceased approximately 18,000 years ago, the Kharaneh landscape was never truly abandoned. We identified multiple hearths in Geotrench2018 sediments that postdate the site. Several later Epipaleolithic and Neolithic sites are present in Wadi Kharaneh (Garrard and Byrd, 2013; Garrard et al., 1977) and a large Ummayad structure, Qasr Kharaneh, is located less than a kilometer northeast of Kharaneh IV (Arce, 2014). Bedouin-style burials can be found in Wadi Kharaneh and a recently excavated

watering hole approximately 250 meters east of Kharaneh IV serves modern Bedouin herders. Additionally, the Kharaneh landscape was inhabited before the site's main occupation, as evidenced by Epipaleolithic artifacts that extend with depth through the site's basal marls and Lower to Middle Paleolithic tools that are commonly found on pavement surfaces and in wadi gravels surrounding Wadi Kharaneh (Besancon et al., 1989). While each iteration of human activity was situated within a unique cultural context, from congregations of Epipaleolithic groups at Kharaneh IV to a node in the administration of the Umayyad Caliphate (Urice, 1987), their presence was anchored by the ability of the Kharaneh landscape to provide water (Figure 4.28). We note that these occupations through time mirror each other, with similar pathways between Kharaneh IV and other notable places on the landscape during the Epipaleolithic, Umayyad, and modern periods (Figure 4.29). While cultural activity on the Kharaneh landscape ebbs and flows, so too does the strength of its wetland due to dramatic environmental changes through the Pleistocene and Holocene. Despite this, the permeability gradient of Wadi Kharaneh played a role in the development of Kharaneh IV as a persistent place and it in turn has formed a persistent landscape that supports human activity when cultural and environmental needs coincide.

Figure 4.28. Episodes of human activity on the Kharaneh landscape through time: from left, an Acheulean handaxe, the Epipaleolithic aggregation site Kharaneh IV, and the Umayyad structure Qasr Kharaneh.

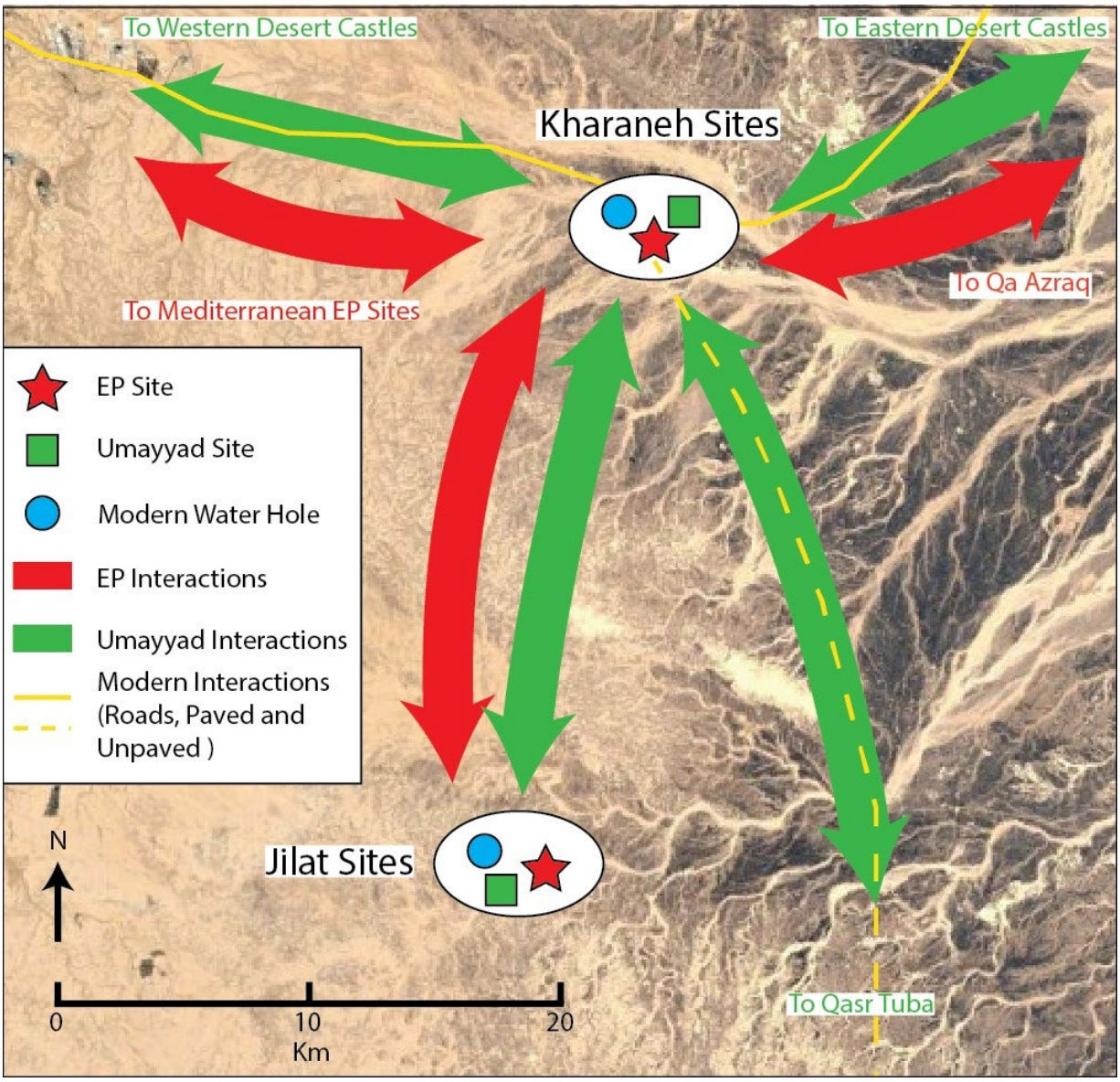

Figure 4.29. Cultural connections beyond the immediate Kharaneh landscape, showing: hypothesized Epipaleolithic connections to Jilat 6 in Wadi Jilat (Garrard and Byrd, 1992), Qa Azraq (Jones and Richter, 2011), and sites further away toward the Mediterranean (Macdonald et al., 2018b; Maher, 2019); historic Umayyad connections to the western and eastern Desert Castles (Grabar, 2005) and a Wadi Jilat dam utilized throughout the historic period (Politis, 1993); and modern connections to watering holes at Wadi Jilat and modern paved (solid yellow line) and unpaved (dashed yellow line) roads.

Chapter 5

Conclusion

This dissertation demonstrates the benefits of integrating paleoenvironmental analysis with archaeological theory. Persistent place theory helps us understand why Kharaneh IV was occupied over a thousand-year period. The site was the product of countless activities, including hunting, gathering, cooking, manufacturing, building, feasting, and playing, that took on larger importance through memory, tradition, and landscape knowledge that encouraged further activities, each one incrementally raising the site above the wetland into an even more prominent space on the Kharaneh landscape.

But persistent place theory alone does not tell us why Kharaneh IV was occupied in the first place. Of course, we cannot say with certainty what motivated Epipaleolithic hunter-gatherers to settle at and develop the site, but geoarchaeological tools help us to define and quantify the "unique qualities" (Schlanger, 1992:92) of persistent places that may have played a role in the site's foundation. Chapter 4 noted that the hydrological setting of Kharaneh IV does not appear to be unique in the sense of a fault-controlled spring nor was it the only source of water for the region. However, the permeability gradient identified by this dissertation between wadi gravels and shallow limestone bedrock surrounding Kharaneh IV was unique enough to provide water, plants, and prey for Epipaleolithic groups and set the stage for place-making events to begin and imbue the wetland with cultural meaning, if such importance did not exist already.

A second unique property of the Kharaneh wetland was its reliability and stability. As demonstrated through isotopic analysis of gazelle tooth enamel in Chapter 3, the local hydroclimate was similar during the occupations of Area A and Area B. This finding is further supported by phytolith data (Ramsey et al., 2016), regional speleothem stable isotope values (Bar-Matthews et al., 2003; Grant et al., 2012), and Lake Lisan elevation reconstructions (Bartov et al. 2003; Torfstein et al. 2013) that show less variation in their respective proxies during Kharaneh IV's occupation. Chapter 3 identified one exception to the wetland's stability during the site's Area A habitation through a decline in gazelle tooth enamel $\delta^{18}O$ values and Soreq Cave speleothem $\delta^{18}O$ values (Grant et al., 2012) centered on c. 18.8 ka BP. This suggests that the wetland and surrounding region temporarily experienced greater local precipitation before reverting to a drier state. Kharaneh IV's archaeological deposits do not indicate any significant cultural changes that accompanied this environmental change, showing the strong connection of Epipaleolithic groups to this place and demonstrating the complexities of human-environment relationships. While much attention is focused on identifying climatic events and corresponding changes in ancient cultures (Benson et al., 2007; Bird et al., 2017; Cook et al., 2007; Diamond, 2006; Hodell et al., 2001; Jones and Schwitalla, 2008; Patterson et al., 2010), far fewer attention is placed on resilience, stability, and the often subtle and indirect relationship between humans and the environment through time (Fitzhugh et al., 2016; Habu and Hall, 2013).

Multiple site-scale analyses and paleoclimatic proxies were necessary to create the narrative of environmental change at Kharaneh IV presented in this dissertation. Chapter 4 incorporated LOI data, sedimentological descriptions, micro- and macrofossil counts, and geologic survey data to characterize the paleoenvironment leading up to and following the site's

main occupation. Chapter 3 used gazelle tooth enamel isotopic data to understand the paleoenvironment during the site's Early and Middle Epipaleolithic phases. Chapter 2 documented an effort to use fecal stanol molecules as a proxy of human population change at the site. Although the technique does not appear to be viable at Kharaneh IV, the effort produced important data for method development by demonstrating the limitations of fecal stanol analysis in archaeology and presenting an opportunity to evaluate the additional work that needs to be done to improve the method.

Chapter 2 recommended that future studies investigate the relationship between diet and stanol production, expand testing on animal feces to determine which other animals produce coprostanol in amounts that could interfere with the human signal, and design experiments to better understand the movement of fecal stanol molecules through sediments and across the landscape. A Kharaneh IV, this dissertation brings us closer to understanding human-environmental dynamics at the site, but additional work will provide further confidence to these findings. Such work could include conducting isotopic analyses of carbonate nodules within the site's wetland deposits, its upper cultural deposits, and the thin layer of aeolian dust at the site's surface (Layer A) to have additional data that gauge the difference between the ancient and present landscape. Studying the isotopic composition of modern gazelle teeth from Jordan, such gazelle populations maintained within nature reserves, would show the magnitude of change from the Azraq paleoenvironment to the present.

In conclusion, multiproxy, site-scale paleoenvironmental analyses can be integrated with archaeological theory to produce clearer and more comprehensive evaluations of human-environmental dynamics. At Kharaneh IV, LOI, sedimentological descriptions, micro- and macrofossil counts, geologic survey, and gazelle tooth enamel isotopic data indicate a mostly reliable and stable wetland that encouraged place-making activities to occur. These activities later continued uninterrupted when the environment temporarily shifted during the site's Middle Epipaleolithic occupation, showing the importance of place to Kharaneh IV's inhabitants despite climatic perturbations. Although the wetland eventually contracted further and Epipaleolithic occupation activities were greatly diminished, the importance of the Kharaneh landscape to various groups through time has continued, as demonstrated by the Umayyad Qasr Kharaneh complex and Bedouin herders who stop for water to this day.

References

Ahmad, K., Davies, C., 2017. Stable isotope (δ13C and δ15N) based interpretation of organic matter source and paleoenvironmental conditions in Al-Azraq basin, Jordan. Applied Geochemistry 78, 49–60.

Ahmad, K., Davies, C.P., 2021. Stable isotopic and geochemical analysis of lacustrine carbonates from the Al-Azraq basin, Jordan: implications for paleoenvironment and paleohydrology. Arab J Geosci 14, 470. https://doi.org/10.1007/s12517-021-06650-1

Al-Hunjul, N., 2001. The Geology of Qasr Al Harrana Map sheet No. 3253-II (No. 49). Geology Directorate, Natural Resources Authority, Amman.

Alonso-Zarza, A.M., Wright, V.P., 2010. Chapter 5 Calcretes, in: Alonso-Zarza, A.M., Tanner, L.H. (Eds.), Developments in Sedimentology, Carbonates in Continental Settings: Facies, Environments, and Processes. Elsevier, pp. 225–267. https://doi.org/10.1016/S0070-4571(09)06105-6

Al-Tamimi, M.H., Alqudah, M., Al-Atawneh, M.S., Nazzal, J., AlShraideh, S., 2021. Depositional environment of Eocene oil shales of Wadi Shallala Formation from northern Jordan. Arab J Geosci 14, 209. https://doi.org/10.1007/s12517-021-06565-x

Ames, C.J.H., Cordova, C.E., Boyd, K., Schmidt, C., Degering, D., Kalbe, J., Jones, B.G., Dosseto, A., Pokines, J.T., Alsouliman, A.S., Beller, J.A., Nowell, A., 2022. Middle to Late Quaternary palaeolandscapes of the central Azraq Basin, Jordan: Deciphering discontinuous records of human-environment dynamics at the arid margin of the Levant. Quaternary International, Geoarchaeology from Mediterranean Areas to Arid Margins 635, 31–52. https://doi.org/10.1016/j.quaint.2021.10.007

Amr, Z.S., Baker, M.A., 2004. Freshwater snails of Jordan. Denisia 14, 221–227.

Arce, I., 2014. Qasr Kharana Revisited, in: Proceedings of the 9th International Congress on the Archaeology of the Ancient Near East. pp. 335–355.

Arnold, T.E., Hillman, A.L., McGrath, S.J., Abbott, M.B., Werne, J.P., Hutchings, J., Arkush, E.N., 2021. Fecal stanol ratios indicate shifts in camelid pastoralism in the highlands of Peru across a 4,000-year lacustrine sequence. Quaternary Science Reviews 270, 107193. https://doi.org/10.1016/j.quascirev.2021.107193

Balée, W., 2006. The Research Program of Historical Ecology. Annual Review of Anthropology 35, 75–98.

Ball, D.F., 1964. Loss-on-Ignition as an Estimate of Organic Matter and Organic Carbon in Non-Calcareous Soils. Journal of Soil Science 15, 84–92. https://doi.org/10.1111/j.1365-2389.1964.tb00247.x

Bard, E., Rostek, F., Turon, J.-L., Gendreau, S., 2000. Hydrological Impact of Heinrich Events in the Subtropical Northeast Atlantic. Science 289, 1321–1324. https://doi.org/10.1126/science.289.5483.1321

Bar-Matthews, M., Ayalon, A., Gilmour, M., Matthews, A., Hawkesworth, C.J., 2003. Sea–land oxygen isotopic relationships from planktonic foraminifera and speleothems in the Eastern Mediterranean region and their implication for paleorainfall during interglacial intervals. Geochimica et Cosmochimica Acta 67, 3181–3199.

Bartov, Y., Goldstein, S.L., Stein, M., Enzel, Y., 2003. Catastrophic arid episodes in the Eastern Mediterranean linked with the North Atlantic Heinrich events. Geology 31, 439–442.

Bar-Yosef, O., Tchernov, E., 1970. The Natufian bone industry of ha-Yonim Cave. Israel Exploration Journal 20, 141–150.

Battistel, D., Argiriadis, E., Kehrwald, N., Spigariol, M., Russell, J.M., Barbante, C., 2017. Fire and human record at Lake Victoria, East Africa, during the Early Iron Age: Did humans or climate cause massive ecosystem changes? The Holocene 27, 997–1007. https://doi.org/10.1177/0959683616678466

Benson, L., Berry, M.S., Jolie, E.A., Spangler, J.D., Stahle, D.W., Hattori, E.M., 2007. Possible impacts of early-11th-, middle-12th-, and late-13th-century droughts on western Native Americans and the Mississippian Cahokians. Quaternary Science Reviews 26, 15. https://doi.org/10.1016/j.quascirev.2006.08.001

Besancon, J., Geyer, B., Sanlaville, P., 1989. Contribution to the study of the geomorphology of the Azraq Basin, Jordan, in: Copeland, L., Hours, F. (Eds.), The Hammer on the Rock: Studies in the Early Palaeolithic of Azraq, Jordan. B.A.R., pp. 7–63.

Bethell, P.H., Goad, L.J., Evershed, R.P., Ottaway, J., 1994. The Study of Molecular Markers of Human Activity: The Use of Coprostanol in the Soil as an Indicator of Human Faecal Material. Journal of Archaeological Science 21, 619–632. https://doi.org/10.1006/jasc.1994.1061

Bird, B.W., Wilson, J.J., Gilhooly Iii, W.P., Steinman, B.A., Stamps, L., 2017. Midcontinental Native American population dynamics and late Holocene hydroclimate extremes. Scientific Reports 7, 41628. https://doi.org/10.1038/srep41628

Bode, L.J.K., Livarda, A., Jones, M.D., 2022. Plant gathering and people-environment interactions at Epipalaeolithic Kharaneh IV, Jordan. Veget Hist Archaeobot 31, 85–96. https://doi.org/10.1007/s00334-021-00839-w

Briles, C., Serenchenko, O., Stevens, L., White, A.J., Huong, N.T.M., 2019. Late Holocene Anthropogenic and Climatic Impact on a Tropical Island Ecosystem of Northern Vietnam. Front. Ecol. Evol. 7. https://doi.org/10.3389/fevo.2019.00121

Buckner, P.H., 2020. There and back again in the Rawah wilderness: Reoccupation at high elevations in the Medicine Bow Mountains, Colorado. Colorado State University.

Bull, I.D., Elhmmali, M.M., Perret, V., Matthews, W., Roberts, D.J., Evershed, R.P., 2005. Biomarker evidence of faecal deposition in archaeological sediments at Çatalhöyük. Inhabiting Çatalhöyük: Reports from the 1995e99 Seasons. McDonald Institute Monographs, Cambridge 415–420.

Bull, I.D., Lockheart, M.J., Elhmmali, M.M., Roberts, D.J., Evershed, R.P., 2002. The origin of faeces by means of biomarker detection. Environment International 27, 647–654. https://doi.org/10.1016/S0160-4120(01)00124-6

Bull, I.D., Simpson, I.A., Bergen, P.F. van, Evershed, R.P., 1999. Muck 'n' molecules: organic geochemical methods for detecting ancient manuring. Antiquity 73, 86–96. https://doi.org/10.1017/S0003598X0008786X

Candy, I., Black, S., 2009. The timing of Quaternary calcrete development in semi-arid southeast Spain: Investigating the role of climate on calcrete genesis. Sedimentary Geology 218, 6–15. https://doi.org/10.1016/j.sedgeo.2009.03.005

Candy, I., Black, S., Sellwood, B.W., 2004. Quantifying time scales of pedogenic calcrete formation using U-series disequilibria. Sedimentary Geology 170, 177–187. https://doi.org/10.1016/j.sedgeo.2004.07.003

Carson, M.T., Peterson, J.A., 2011. Calcrete formation and implications for buried archaeological deposits in the Mariana Islands, western Pacific. Geoarchaeology 26, 501–513.

Casby-Horton, S., Herrero, J., Rolong, N.A., 2015. Chapter Four - Gypsum Soils—Their Morphology, Classification, Function, and Landscapes, in: Sparks, D.L. (Ed.), Advances in Agronomy. Academic Press, pp. 231–290. https://doi.org/10.1016/bs.agron.2014.10.002

Cheng, W., Kimpe, L.E., Mallory, M.L., Smol, J.P., Blais, J.M., 2021. An~ 1100 yr record of human and seabird occupation in the High Arctic inferred from pond sediments. Geology 49, 510–514.

Childe, V.G., 1928. The most ancient East. K. Paul, Trench, Trubner & co., ltd, England.

Christie-Blick, N., 1991. Onlap, offlap, and the origin of unconformity-bounded depositional sequences. Marine Geology 97, 35–56. https://doi.org/10.1016/0025-3227(91)90018-Y

Clark, P.U., Marshall, S.J., Clarke, G.K.C., Hostetler, S.W., Licciardi, J.M., Teller, J.T., 2001. Freshwater Forcing of Abrupt Climate Change During the Last Glaciation. Science 293, 283–287. https://doi.org/10.1126/science.1062517

Clark, P.U., Shakun, J.D., Baker, P.A., Bartlein, P.J., Brewer, S., Brook, E., Carlson, A.E., Cheng, H., Kaufman, D.S., Liu, Z., 2012. Global climate evolution during the last deglaciation. Proceedings of the National Academy of Sciences 109, E1134–E1142.

Cook, E.R., Seager, R., Cane, M.A., Stahle, D.W., 2007. North American drought: Reconstructions, causes, and consequences. Earth-Science Reviews 81, 93–134. https://doi.org/10.1016/j.earscirev.2006.12.002

Cordova, C.E., Nowell, A., Bisson, M., Ames, C.J., Pokines, J., Chang, M., al-Nahar, M., 2013. Interglacial and glacial desert refugia and the Middle Paleolithic of the Azraq Oasis, Jordan. Quaternary International 300, 94–110.

Cosgrove, D., Daniels, S., 1988. The Iconography of Landscape: Essays on the Symbolic Representation, Design and Use of Past Environments. Cambridge University Press.

Curtin, L., D'Andrea, W.J., Balascio, N.L., Shirazi, S., Shapiro, B., de Wet, G.A., Bradley, R.S., Bakke, J., 2021. Sedimentary DNA and molecular evidence for early human occupation of the Faroe Islands. Commun Earth Environ 2, 1–7. https://doi.org/10.1038/s43247-021-00318-0

D'Anjou, R.M., Bradley, R.S., Balascio, N.L., Finkelstein, D.B., 2012. Climate impacts on human settlement and agricultural activities in northern Norway revealed through sediment biogeochemistry. PNAS 109, 20332–20337. https://doi.org/10.1073/pnas.1212730109

Dansgaard, W., 1964. Stable isotopes in precipitation. Tellus 16, 436–468. https://doi.org/10.3402/tellusa.v16i4.8993

Davies, B.E., 1974. Loss-on-Ignition as an Estimate of Soil Organic Matter 1. Soil Science Society of America Journal 38, 150–151. https://doi.org/10.2136/sssaj1974.03615995003800010046x

Davis, S.J., 1980. A note on the dental and skeletal ontogeny of Gazella. Israel Journal of Ecology and Evolution 29, 129–134.

de La Torre, M.S., Gratuze, B., Mangado, X., Delage, C., 2019. The lithic landscape around Kharaneh IV (Azraq Basin, Jordan): Petrographical and geochemical characterization of geological cherts. Journal of Archaeological Science: Reports 26, 101857.

DeNiro, M.J., Epstein, S., 1978. Influence of diet on the distribution of carbon isotopes in animals. Geochimica et cosmochimica acta 42, 495–506.

De Peña, F.V., 2022. Breaking the Learning Curve: Assessing Flintknapper Skill at the Epipalaeolithic Site of Kharaneh IV, Jordan. UC Berkeley.

Diamond, J.M., 2006. Collapse: How Societies Choose to Fail Or Succeed. Penguin.
Durn, G., 2003. Terra rossa in the Mediterranean region: parent materials, composition and origin. Geologia Croatica 56, 83–100.
Elidrissi, S., Daoudi, L., Arabi, B., Fagel, N., 2017. Development of quaternary calcrete in the Tensift Al Haouz area, Central Morocco: Characterization and environmental significance. CATENA 149, 331–340. https://doi.org/10.1016/j.catena.2016.10.009
Ellen, R., 1982. Environment, Subsistence and System by Roy Ellen. https://doi.org/10.1017/CBO9780511607738
Enzel, Y., Amit, R., Dayan, U., Crouvi, O., Kahana, R., Ziv, B., Sharon, D., 2008. The climatic and physiographic controls of the eastern Mediterranean over the late Pleistocene climates in the southern Levant and its neighboring deserts. Global and Planetary Change 60, 165–192.
Erickson, C.L., 1999. Neo-environmental determinism and agrarian 'collapse' in Andean prehistory. Antiquity 73, 634–642. https://doi.org/10.1017/S0003598X00065236
Evershed, R.P., Bethell, P.H., 1996. Application of multimolecular biomarker techniques to the identification of fecal material in archaeological soils and sediments. ACS Publications.
Fadda, E., 1998. The Geology of Wadi Ed Dab'i Area Map Sheet No. 3353-III (No. 42). Geology Directorate, Natural Resources Authority, Amman.
Finstad, K., Pfeiffer, M., McNicol, G., Barnes, J., Demergasso, C., Chong, G., Amundson, R., 2016. Rates and geochemical processes of soil and salt crust formation in Salars of the Atacama Desert, Chile. Geoderma 284, 57–72. https://doi.org/10.1016/j.geoderma.2016.08.020
Fish, P.R., Fish, S.K., DeBlasis, P., Gaspar, M.D., Thompson, V.D., Waggoner, J.C., 2013. Monumental shell mounds as persistent places in southern coastal Brazil. The archaeology and historical ecology of small scale economies 120–140.
Fitzhugh, B., Gjesfjeld, E.W., Brown, W.A., Hudson, M.J., Shaw, J.D., 2016. Resilience and the population history of the Kuril Islands, Northwest Pacific: A study in complex human ecodynamics. Quaternary International 419, 165–193. https://doi.org/10.1016/j.quaint.2016.02.003
Fleitmann, D., Cheng, H., Badertscher, S., Edwards, R.L., Mudelsee, M., Göktürk, O.M., Fankhauser, A., Pickering, R., Raible, C.C., Matter, A., 2009. Timing and climatic impact of Greenland interstadials recorded in stalagmites from northern Turkey. Geophysical Research Letters 36.
Friedman, I., O'Neil, J.R., 1977. Data of Geochemistry: Compilation of stable isotope fractionation factors of geochemical interest. US Government Printing Office.
Garbrecht, G., Peleg, Y., 1994. The water supply of the desert fortresses in the Jordan Valley. The Biblical Archaeologist 57, 161–170.
Garrard, A., Byrd, B., 2013. Beyond the Fertile Crescent: Late Palaeolithic and Neolithic Communities of the Jordanian Steppe. The Azraq Basin Project Volume 1: Project Background and the Late Palaeolithic (Geological Context and Technology). Oxbow Books.
Garrard, A., Byrd, B., Harvey, P., Hivernel, F., 1985. Prehistoric environment and settlement in the Azraq Basin. A report on the 1982 survey season. Levant 17, 1–28.
Garrard, A.N., Byrd, B.F., 1992. New dimensions to the Epipalaeolithic of the Wadi el-Jilat in central Jordan. Paléorient 47–62.

Garrard, A.N., Stanley Price, N.P., Copeland, L., 1977. A Survey of Prehistoric sites in the Azraq Basin, Eastern Jordan. Paléorient 3, 109–126. https://doi.org/10.3406/paleo.1975.4192
Goring-Morris, A.N., 1987. At the edge. Bar Oxford.
Grabar, O., 2005. Umayyad palaces reconsidered, in: Early Islamic Art, 650–1100. Routledge, pp. 187–212.
Grant, K.M., Rohling, E.J., Bar-Matthews, M., Ayalon, A., Medina-Elizalde, M., Ramsey, C.B., Satow, C., Roberts, A.P., 2012. Rapid coupling between ice volume and polar temperature over the past 150,000 years. Nature 491, 744–747. https://doi.org/10.1038/nature11593
Habinger, S.G., De Cupere, B., Dövener, F., Pucher, E., Bocherens, H., 2020. Mobility and origin of camels in the Roman Empire through serial stable carbon and oxygen isotope variations in tooth enamel. Quaternary International, High resolution analyses of large mammals dental remains: broadening horizons 557, 80–91. https://doi.org/10.1016/j.quaint.2020.05.029
Habu, J., Hall, M.E., 2013. Climate Change, Human Impacts on the Landscape, and Subsistence Specialization: Historical Ecology and Changes in Jomon Hunter-Gatherer Lifeways. University Press of Florida.
Heaton, T.H., Vogel, J.C., von La Chevallerie, G., Collett, G., 1986. Climatic influence on the isotopic composition of bone nitrogen. Nature 322, 822–823.
Hedges, R.E., Stevens, R.E., Richards, M.P., 2004. Bone as a stable isotope archive for local climatic information. Quaternary Science Reviews 23, 959–965.
Heinrich, H., 1988. Origin and Consequences of Cyclic Ice Rafting in the Northeast Atlantic Ocean During the Past 130,000 Years. Quaternary Research 29, 142–152. https://doi.org/10.1016/0033-5894(88)90057-9
Heiri, O., Lotter, A.F., Lemcke, G., 2001. Loss on ignition as a method for estimating organic and carbonate content in sediments: reproducibility and comparability of results. Journal of Paleolimnology 25, 101–110. https://doi.org/10.1023/A:1008119611481
Henton, E., Martin, L., Garrard, A., Jourdan, A.-L., Thirlwall, M., Boles, O., 2017. Gazelle seasonal mobility in the Jordanian steppe: The use of dental isotopes and microwear as environmental markers, applied to Epipalaeolithic Kharaneh IV. Journal of Archaeological Science: Reports 11, 147–158. https://doi.org/10.1016/j.jasrep.2016.11.031
Hodell, D.A., Brenner, M., Curtis, J.H., Guilderson, T., 2001. Solar Forcing of Drought Frequency in the Maya Lowlands. Science 292, 1367–1370. https://doi.org/10.1126/science.1057759
Hoppe, K.A., Paytan, A., Chamberlain, P., 2006. Reconstructing grassland vegetation and paleotemperatures using carbon isotope ratios of bison tooth enamel. Geology 34, 649–652.
Iacumin, P., Longinelli, A., 2002. Relationship between δ18O values for skeletal apatite from reindeer and foxes and yearly mean δ18O values of environmental water. Earth and Planetary Science Letters 201, 213–219. https://doi.org/10.1016/S0012-821X(02)00635-0
IAEA/WMO, 2022. Global Network of Isotopes in Precipitation. The GNIP Database. [WWW Document]. URL https://nucleus.iaea.org/wiser (accessed 10.20.22).
Ingold, T., 1993. The Temporality of the Landscape. World Archaeology 25, 152–174.

Johnson, M.H., 2012. Phenomenological approaches in landscape archaeology. Annual Review of Anthropology 41, 269–284.
Johnson, M.H., 2006. On the nature of theoretical archaeology and archaeological theory. Archaeological Dialogues 13, 117–132. https://doi.org/10.1017/S138020380621208X
Jones, J.R., 2012. Using gazelle dental cementum studies to explore seasonality and mobility patterns of the Early-Middle Epipalaeolithic Azraq Basin, Jordan. Quaternary International 252, 195–201.
Jones, M.D., Maher, L.A., Macdonald, D.A., Ryan, C., Rambeau, C., Black, S., Richter, T., 2016. The environmental setting of Epipalaeolithic aggregation site Kharaneh IV. Quaternary International, Late Pleistocene Eastern Levant: Landscape Strategies in Open Spaces 396, 95–104. https://doi.org/10.1016/j.quaint.2015.08.092
Jones, M.D., Richter, T., 2011. Paleoclimatic and archeological implications of Pleistocene and Holocene environments in Azraq, Jordan. Quaternary Research 76, 363–372.
Jones, N.B., 2016. Demography and evolutionary ecology of Hadza hunter-gatherers. Cambridge University Press.
Jones, T.L., Schwitalla, A., 2008. Archaeological perspectives on the effects of medieval drought in prehistoric California. Quaternary International, The 22nd Pacific Climate Workshop 188, 41–58. https://doi.org/10.1016/j.quaint.2007.07.007
Juste, C., Gérard, P., 2021. Cholesterol-to-coprostanol conversion by the gut microbiota: what we know, suspect, and ignore. Microorganisms 9, 1881.
Kaiser, J., Lerch, M., 2022. Sedimentary faecal lipids as indicators of Baltic Sea sewage pollution and population growth since 1860 AD. Environmental Research 204, 112305. https://doi.org/10.1016/j.envres.2021.112305
Keenan, B., Douglas, P., Breckenridge, A.J., Johnston, K., 2018. Using faecal stanols from a tropical lake core to reconstruct human population dynamics in the southwestern Maya Lowlands. AGUFM 2018, PP24B-08.
Keenan, B., Imfeld, A., Gélinas, Y., Douglas, P.M., 2022. Understanding controls on stanols in lake sediments as proxies for palaeopopulations in Mesoamerica. Journal of Paleolimnology 67, 375–390.
Keenan, B., Imfeld, A., Johnston, K., Breckenridge, A., Gélinas, Y., Douglas, P.M., 2021. Molecular evidence for human population change associated with climate events in the Maya lowlands. Quaternary Science Reviews 258, 106904.
Keigwin, L.D., Lehman, S.J., 1994. Deep circulation change linked to HEINRICH Event 1 and Younger Dryas in a middepth North Atlantic Core. Paleoceanography 9, 185–194. https://doi.org/10.1029/94PA00032
Khalaf, F.I., 2007. Occurrences and genesis of calcrete and dolocrete in the Mio-Pleistocene fluviatile sequence in Kuwait, northeast Arabian Peninsula. Sedimentary Geology 199, 129–139. https://doi.org/10.1016/j.sedgeo.2007.01.021
Kohn, M.J., Schoeninger, M.J., Valley, J.W., 1996. Herbivore Tooth Oxygen Isotope Compositions: Effects of Diet and Physiology. Geochimica et Cosmochimica Acta 60, 3889–96. https://doi.org/10.1016/0016-7037(96)00248-7.
Kohn, M.J., Schoeninger, M.J., Valley, J.W., 1998. Variability in oxygen isotope compositions of herbivore teeth: reflections of seasonality or developmental physiology? Chemical Geology 152, 97–112. https://doi.org/10.1016/S0009-2541(98)00099-0
Lane, P.J., 2014. Hunter-gatherer-fishers, ethnoarchaeology, and analogical reasoning. The Oxford handbook of the archaeology and anthropology of hunter-gatherers pp. 104–150.

Langgut, D., Shahack-Gross, R., Arie, E., Namdar, D., Amrani, A., Le Bailly, M., Finkelstein, I., 2016. Micro-archaeological indicators for identifying ancient cess deposits: An example from Late Bronze Age Megiddo, Israel. Journal of Archaeological Science: Reports 9, 375–385. https://doi.org/10.1016/j.jasrep.2016.08.013

Leeming, R., Ball, A., Ashbolt, N., Nichols, P., 1996. Using faecal sterols from humans and animals to distinguish faecal pollution in receiving waters. Water Research 30, 2893–2900. https://doi.org/10.1016/S0043-1354(96)00011-5

Leng, M.J., Melanie, J., 2006. Isotopes in palaeoenvironmental research. Springer.

Lightfoot, K.G., Cuthrell, R., Hylkema, M.G., Lopez, V., Gifford-Gonzalez, D., Jewett, R.A., Grone, M.A., Sanchez, G.M., Nelson, P.A., Apodaca, A.J., 2021. The Eco-Archaeological Investigation of Indigenous Stewardship Practices on the Santa Cruz Coast. Journal of California and Great Basin Anthropology 41, 187–205.

Lischke, H., von Grafenstein, U., Ammann, B., 2013. Forest dynamics during the transition from the Oldest Dryas to the Bølling–Allerød at Gerzensee—a simulation study. Palaeogeography, Palaeoclimatology, Palaeoecology, Early Rapid Warning 391, 60–73. https://doi.org/10.1016/j.palaeo.2012.12.001

Littleton, J., Allen, H., 2007. Hunter-gatherer burials and the creation of persistent places in southeastern Australia. Journal of Anthropological Archaeology 26, 283–298. https://doi.org/10.1016/j.jaa.2006.11.004

Livingstone, D.N., 2012. Changing Climate, Human Evolution, and the Revival of Environmental Determinism. Bulletin of the History of Medicine 86, 564–595. https://doi.org/10.1353/bhm.2012.0071

Lucke, B., Kemnitz, H., Bäumler, R., Schmidt, M., 2014. Red Mediterranean Soils in Jordan: New insights in their origin, genesis, and role as environmental archives. CATENA, Landscapes and Soils through Time 112, 4–24. https://doi.org/10.1016/j.catena.2013.04.006

Macdonald, D.A., Allentuck, A., Maher, L.A., 2018a. Technological Change and Economy in the Epipalaeolithic: Assessing the Shift from Early to Middle Epipalaeolithic at Kharaneh IV. Journal of Field Archaeology 43, 437–456. https://doi.org/10.1080/00934690.2018.1504542

Macdonald, D.A., Allentuck, A., Maher, L.A., 2018b. Technological Change and Economy in the Epipalaeolithic: Assessing the Shift from Early to Middle Epipalaeolithic at Kharaneh IV. J. Field Archaeol. 43, 437–456. https://doi.org/10.1080/00934690.2018.1504542

Macdonald, D.A., Maher, L.A., 2022. Leaving home: Technological and landscape knowledge as resilience at pre-Holocene Kharaneh IV, Azraq Basin, Jordan. The Holocene 09596836221121784.

Maher, L.A., 2021. Landscapes of the past: Creation of persistent places in hunter-gatherer landscapes of Southwest Asia and Japan. Japanese journal of archaeology 8.

Maher, L.A., 2019. Persistent Place-Making in Prehistory: the Creation, Maintenance, and Transformation of an Epipalaeolithic Landscape. Journal of Archaeological Method and Theory 26, 998–1083.

Maher, L.A., Macdonald, D.A., 2020. Communities of Interaction: Tradition and Learning in Stone Tool Production Through the Lens of the Epipaleolithic of Kharaneh IV, Jordan, in: Culture History and Convergent Evolution. Springer, pp. 213–243.

Maher, L.A., Macdonald, D.A., Pomeroy, E., Stock, J.T., 2021a. Life, death, and the destruction of architecture: Hunter-gatherer mortuary behaviors in prehistoric Jordan. Journal of Anthropological Archaeology 61, 101262.
Maher, L.A., Richter, T., Macdonald, D., Jones, M.D., Martin, L., Stock, J.T., 2012. Twenty Thousand-Year-Old Huts at a Hunter-Gatherer Settlement in Eastern Jordan. PLOS ONE 7, e31447. https://doi.org/10.1371/journal.pone.0031447
Maher, L.A., Macdonald, D.A., 2013. Assessing typo-technological variability in Epipalaeolithic assemblages: Preliminary results from two case studies from the Southern Levant. In: Borrell, F., Molist, M. & Ibanez, J. J. (eds.) The State of Stone: Terminologies, Continuities and Contexts in Near Eastern Lithics. Studies in Early Near Eastern Production, Subsistence and Environment 14. Berlin: ex oriente.
Maher, L.A., White, A.J., Brown, J., De Peña, F., Ames, C.J., 2021b. From wetlands to deserts: The role of water in the prehistoric occupation of eastern Jordan, in: Palaeolandscapes in Archaeology. Routledge, pp. 82–129.
Mariani, M., Connor, S.E., Theuerkauf, M., Herbert, A., Kuneš, P., Bowman, D., Fletcher, M.-S., Head, L., Kershaw, A.P., Haberle, S.G., 2022. Disruption of cultural burning promotes shrub encroachment and unprecedented wildfires. Frontiers in Ecology and the Environment 20, 292–300.
Mariotti Lippi, M., Bellini, C., Mori Secci, M., 2010. Palaeovegetational reconstruction based on pollen and seeds/fruits from a Bronze Age archaeological site in Tuscany (Italy). Plant Biosystems 144, 902–908.
Martin, L., Edwards, Y., Garrard, A., 2010. Hunting practices at an eastern Jordanian Epipalaeolithic aggregation site: the case of Kharaneh IV. Levant 42, 107–135.
McFadden, L.D., Wells, S.G., Jercinovich, M.J., 1987. Influences of eolian and pedogenic processes on the origin and evolution of desert pavements. Geology 15, 504–508.
McGlade, J., 1995. Archaeology and the ecodynamics of human-modified landscapes. Antiquity 69, 113–132. https://doi.org/10.1017/S0003598X00064346
Mercuri, A.M., Allevato, E., Arobba, D., Mazzanti, M.B., Bosi, G., Caramiello, R., Castiglioni, E., Carra, M.L., Celant, A., Costantini, L., 2015. Pollen and macroremains from Holocene archaeological sites: A dataset for the understanding of the bio-cultural diversity of the Italian landscape. Review of palaeobotany and Palynology 218, 250–266.
Mercuri, A.M., Mazzanti, M., Florenzano, A., Montecchi, M.C., Rattighieri, E., Torri, P., 2013. Anthropogenic Pollen Indicators (API) from archaeological sites as local evidence of human-induced environments in the Italian peninsula. Annali di Botanica 3, 143–153.
Meyer, W.B., Guss, D.M.T., 2017. Environmental Determinism: What Is It?, in: Meyer, W.B., Guss, D.M.T. (Eds.), Neo-Environmental Determinism: Geographical Critiques. Springer International Publishing, Cham, pp. 5–13. https://doi.org/10.1007/978-3-319-54232-4_2
Miller, M.J., 2016. Social Inequality and the body: diet, activity, and health differences in a prehistoric Muisca population (Sabana de Bogotá, Colombia, AD 1000-1400). University of California, Berkeley.
Moore, C.R., Thompson, V.D., 2012. Animism and Green River persistent places: A dwelling perspective of the Shell Mound Archaic. Journal of Social Archaeology 12, 264–284. https://doi.org/10.1177/1469605311431518
Muheisen, M., 1983. La Préhistoire en Jordanie: Recherches sur l'Epi-paléolithique : L'exemple du gisement de Kharaneh IV. Universite de Bordeaux.

Muheisen, M., Wada, H., 1995. An Analysis of the microliths at Kharaneh IV, phase D, Square A20/37. Paléorient 75. https://doi.org/10.3406/paleo.1995.4610
Naito, Y.I., Hirose, M., Belmaker, M., Henry, D.O., Osawa, M., Nakazawa, T., Habinger, S.G., Tung, P., Bocherens, H., Massadeh, S., Kadowaki, S., 2022. Paleoenvironment and human hunting activity during MIS 2 in southern Jordan: Isotope records of prey remains and paleosols. Quaternary Science Reviews 282, 107432. https://doi.org/10.1016/j.quascirev.2022.107432
Netterberg, F., 1974. Observations on calcretes at some archaeological and palaeontological sites in South Africa. Goodwin Series 20–24.
Netterberg, F., 1969. The interpretation of some basic calcrete types. The South African Archaeological Bulletin 24, 117–122.
O'Leary, M.H., 1981. Carbon isotope fractionation in plants. Phytochemistry 20, 553–567. https://doi.org/10.1016/0031-9422(81)85134-5
Otto-Bliesner, B.L., Brady, E.C., Clauzet, G., Tomas, R., Levis, S., Kothavala, Z., 2006. Last glacial maximum and Holocene climate in CCSM3. Journal of Climate 19, 2526–2544.
Parker, J.W., 1994. Dots on a map: using cultural resource management data to reconstruct prehistoric settlement patterns in the Clear Lake Basin, California. University of California, Los Angeles.
Patterson, W.P., Dietrich, K.A., Holmden, C., Andrews, J.T., 2010. Two millennia of North Atlantic seasonality and implications for Norse colonies. PNAS 107, 5306–5310. https://doi.org/10.1073/pnas.0902522107
Peng, X., Zhang, G., Mai, B., Min, Y., Wang, Z., 2002. Spatial and temporal trend of sewage pollution indicated by coprostanol in Macao Estuary, southern China. Marine Pollution Bulletin 45, 295–299. https://doi.org/10.1016/S0025-326X(02)00101-7
Phua, L.C., Koh, P.K., Cheah, P.Y., Ho, H.K., Chan, E.C.Y., 2013. Global gas chromatography/time-of-flight mass spectrometry (GC/TOFMS)-based metabonomic profiling of lyophilized human feces. Journal of Chromatography B 937, 103–113. https://doi.org/10.1016/j.jchromb.2013.08.025
Pickering, M.D., Ghislandi, S., Usai, M.R., Wilson, C., Connelly, P., Brothwell, D.R., Keely, B.J., 2018. Signatures of degraded body tissues and environmental conditions in grave soils from a Roman and an Anglo-Scandinavian age burial from Hungate, York. Journal of archaeological science 99, 87–98.
Pigati, J.S., Rech, J.A., Quade, J., Bright, J., 2014. Desert wetlands in the geologic record. Earth-Science Reviews 132, 67–81.
Politis, K.D., 1993. The stepped dam at Wadi el-Jilat. Palestine exploration quarterly 125, 43–49.
Prost, K., Birk, J.J., Lehndorff, E., Gerlach, R., Amelung, W., 2017. Steroid Biomarkers Revisited – Improved Source Identification of Faecal Remains in Archaeological Soil Material. PLOS ONE 12, e0164882. https://doi.org/10.1371/journal.pone.0164882
Prost, K., Bradel, P.L., Lehndorff, E., Amelung, W., 2018. Steroid dissipation and formation in the course of farmyard manure composting. Organic Geochemistry 118, 47–57. https://doi.org/10.1016/j.orggeochem.2017.12.006
Pumpelly, R., 1908. Explorations in Turkestan; Washington, D. C., Carnegie institution of Washington.
Qudaira, M., 2000. The Geology of Qasr Amra Map Sheet No. 3353-IV (No. 47). Geology Directorate, Natural Resources Authority, Amman.

Queirós, S.S., von der Lühe, B., Silva-Bessa, A., Brito-da-Costa, A.M., Caldas, I.M., Dawson, L., Madureira-Carvalho, Á., 2023. Lipidic compounds found in soils surrounding human decomposing bodies and its use in forensic investigations–a narrative review. Science & Justice 63, 303–312.

Ramsey, M.N., Maher, L.A., Macdonald, D.A., Nadel, D., Rosen, A.M., 2018. Sheltered by reeds and settled on sedges: Construction and use of a twenty thousand-year-old hut according to phytolith analysis from Kharaneh IV, Jordan. Journal of Anthropological Archaeology 50, 85–97. https://doi.org/10.1016/j.jaa.2018.03.003

Ramsey, M.N., Maher, L.A., Macdonald, D.A., Rosen, A., 2016. Risk, Reliability and Resilience: Phytolith Evidence for Alternative 'Neolithization' Pathways at Kharaneh IV in the Azraq Basin, Jordan. PLOS ONE 11, e0164081. https://doi.org/10.1371/journal.pone.0164081

Reddy, S., Sanders, T.A.B., Owen, R.W., Thompson, M.H., 1998. Faecal pH, bile acid and sterol concentrations in premenopausal Indian and white vegetarians compared with white omnivores. British Journal of Nutrition 79, 495–500.

Richter, T., Maher, L.A., Garrard, A.N., Edinborough, K., Jones, M.D., Stock, J.T., 2013. Epipalaeolithic settlement dynamics in southwest Asia: new radiocarbon evidence from the Azraq Basin. Journal of Quaternary Science 28, 467–479. https://doi.org/10.1002/jqs.2629

Rodan, R., 2021. Ancestral Affiliation and the Production of Social Identity: Investigations of Mortuary Practices among Persistent Hunter-Gatherers in Archaic Indian Knoll, Kentucky.

Sarkar, A., Mukherjee, A.D., Bera, M.K., Das, B., Juyal, N., Morthekai, P., Deshpande, R.D., Shinde, V.S., Rao, L.S., 2016. Oxygen isotope in archaeological bioapatites from India: Implications to climate change and decline of Bronze Age Harappan civilization. Scientific Reports 6, 26555.

Schlanger, S.H., 1992. Recognizing Persistent Places in Anasazi Settlement Systems, in: Rossignol, J., Wandsnider, L. (Eds.), Space, Time, and Archaeological Landscapes, Interdisciplinary Contributions to Archaeology. Springer US, Boston, MA, pp. 91–112. https://doi.org/10.1007/978-1-4899-2450-6_5

Schneider, T.D., 2015. Placing refuge and the archaeology of Indigenous hinterlands in colonial California. American Antiquity 80, 695–713.

Schroeter, N., Lauterbach, S., Stebich, M., Kalanke, J., Mingram, J., Yildiz, C., Schouten, S., Gleixner, G., 2020. Biomolecular evidence of early human occupation of a high-altitude site in Western Central Asia during the Holocene. Frontiers in Earth Science 8, 20.

Schwarcz, H.P., White, C.D., Longstaffe, F.J., 2010. Stable and radiogenic isotopes in biological archaeology: some applications. Isoscapes: Understanding movement, pattern, and process on Earth through isotope mapping 335–356.

Shaw, A., Bates, M., Conneller, C., Gamble, C., Julien, M.-A., McNabb, J., Pope, M., Scott, B., 2016. The archaeology of persistent places: the Palaeolithic case of La Cotte de St Brelade, Jersey. Antiquity 90, 1437–1453. https://doi.org/10.15184/aqy.2016.212

Shah, V.G., Dunstan, R.H., Geary, P.M., Coombes, P., Roberts, T.K., Von Nagy-Felsobuki, E., 2007. Evaluating potential applications of faecal sterols in distinguishing sources of faecal contamination from mixed faecal samples. Water research 41, 3691–3700.

Sherblom, P.M., Henry, M.S., Kelly, D., 1997. Questions remain in the use of coprostanol and epicoprostanol as domestic waste markers: examples from coastal Florida. ACS Publications.
Shillito, L.M., Bull, I.D., Matthews, W., Almond, M.J., Williams, J.M., Evershed, R.P., 2011. Biomolecular and micromorphological analysis of suspected faecal deposits at Neolithic Çatalhöyük, Turkey. Journal of Archaeological Science 38, 1869–1877. https://doi.org/10.1016/j.jas.2011.03.031
Shillito, L.M., Matthews, W., Bull, I.D., Williams, J., Matthews, R., 2008. Biomolecular investigations of faecal biomarkers at Sheik-e Abad and Jani. The earliest Neolithic of Iran 105–116.
Shuman, B., 2003. Controls on loss-on-ignition variation in cores from two shallow lakes in the northeastern United States. Journal of Paleolimnology 30, 371–385. https://doi.org/10.1023/B:JOPL.0000007226.68831.e3
Simpson, I.A., van Bergen, P.F., Perret, V., Elhmmali, M.M., Roberts, D.J., Evershed, R.P., 1999. Lipid biomarkers of manuring practice in relict anthropogenic soils. The Holocene 9, 223–229. https://doi.org/10.1191/095968399666898333
Sistiaga, A., Berna, F., Laursen, R., Goldberg, P., 2014. Steroidal biomarker analysis of a 14,000 years old putative human coprolite from Paisley Cave, Oregon. Journal of Archaeological Science 41, 813–817. https://doi.org/10.1016/j.jas.2013.10.016
Smith, B.N., Epstein, S., 1971. Two Categories of 13C/12C Ratios for Higher Plants 1. Plant Physiol 47, 380–384.
Spyrou, A., Maher, L.A., Martin, L.A., Macdonald, D.A., Garrard, A., 2019. Meat outside the freezer: Drying, smoking, salting and sealing meat in fat at an Epipalaeolithic megasite in eastern Jordan. Journal of Anthropological Archaeology 54, 84–101. https://doi.org/10.1016/j.jaa.2019.02.004
Stager, J.C., Ryves, D.B., Chase, B.M., Pausata, F.S.R., 2011. Catastrophic Drought in the Afro-Asian Monsoon Region During Heinrich Event 1. Science 331, 1299–1302. https://doi.org/10.1126/science.1198322
Suleiman, A., Al-Bakri, J., 2011. Estimating actual evapotranspiration using ALARM and the dimensionless temperature. Evapotranspiration. Croatia: InTech Publisher 163–194.
Thienemann, M., Masi, A., Kusch, S., Sadori, L., John, S., Francke, A., Wagner, B., Rethemeyer, J., 2017. Organic geochemical and palynological evidence for Holocene natural and anthropogenic environmental change at Lake Dojran (Macedonia/Greece). The Holocene 27, 1103–1114. https://doi.org/10.1177/0959683616683261
Thompson, V.D., Arnold III, P.J., Pluckhahn, T.J., Vanderwarker, A.M., 2011. Situating remote sensing in anthropological archaeology. Archaeological Prospection 18, 195–213.
Torfstein, A., Goldstein, S.L., Stein, M., Enzel, Y., 2013. Impacts of abrupt climate changes in the Levant from Last Glacial Dead Sea levels. Quaternary Science Reviews 69, 1–7. https://doi.org/10.1016/j.quascirev.2013.02.015
Urice, S.K., 1987. Qasr Kharana in the Transjordan. American Schools of Oriental Research.
Vachula, R.S., Huang, Y., Longo, W.M., Dee, S.G., Daniels, W.C., Russell, J.M., 2019. Evidence of Ice Age humans in eastern Beringia suggests early migration to North America. Quaternary Science Reviews 205, 35–44. https://doi.org/10.1016/j.quascirev.2018.12.003

von der Lühe, B., Dawson, L.A., Mayes, R.W., Forbes, S.L., Fiedler, S., 2013. Investigation of sterols as potential biomarkers for the detection of pig (S. s. domesticus) decomposition fluid in soils. Forensic Science International 230, 68–73.
von der Lühe, B., Prost, K., Birk, J.J., Fiedler, S., 2020. Steroids aid in human decomposition fluid identification in soils of temporary mass graves from World War II. Journal of Archaeological Science: Reports 32, 102431.
Walker, R.W., Wun, C.K., Litsky, W., Dutka, B.J., 1982. Coprostanol as an indicator of fecal pollution. Critical Reviews in Environmental Science and Technology 12, 91–112.
Wang, Q., Li, Y., Wang, Y., 2011. Optimizing the weight loss-on-ignition methodology to quantify organic and carbonate carbon of sediments from diverse sources. Environmental monitoring and assessment 174, 241–257.
Werner, R.A., Brand, W.A., 2001. Referencing strategies and techniques in stable isotope ratio analysis. Rapid Communications in Mass Spectrometry 15, 501–519.
White, A.J., 2017. Fecal Stanols as Indicators of Ancient Population Change. California State University, Long Beach.
White, A.J., Munoz, S.E., Schroeder, S., Stevens, L.R., 2020. After Cahokia: Indigenous Repopulation and Depopulation of the Horseshoe Lake Watershed AD 1400–1900. American Antiquity 1–16.
White, A.J., Stevens, L.R., Lorenzi, V., Munoz, S.E., Lipo, C.P., Schroeder, S., 2018. An evaluation of fecal stanols as indicators of population change at Cahokia, Illinois. Journal of Archaeological Science 93, 129–134. https://doi.org/10.1016/j.jas.2018.03.009
White, A.J., Stevens, L.R., Lorenzi, V., Munoz, S.E., Schroeder, S., Cao, A., Bogdanovich, T., 2019. Fecal stanols show simultaneous flooding and seasonal precipitation change correlate with Cahokia's population decline. PNAS 116, 5461–5466. https://doi.org/10.1073/pnas.1809400116
White, A.J., Munoz, S.E., Schroeder, S., Stevens, L.R., 2021. Reply to Skousen and Aiuvalasit: On the Primacy of Archaeological Data. American Antiquity 86, 203–205.
Whitehurse, A., 2021. From the Seas to the Sands: An Experimental Approach to Dentalium Shell Beads from Kharaneh IV. The University of Tulsa.
Whitridge, P., 2004. Landscapes, Houses, Bodies, Things: "Place" and the Archaeology of Inuit Imaginaries. Journal of Archaeological Method and Theory 11, 213–250.
Wilke, P.J., Quintero, L.A., 1994. Naviform core-and-blade technology: assemblage character as determined by replicative experiments. Neolithic Chipped Stone Industries of the Fertile Crescent 33–60.
Xiong, Li-Yang, Si-Jin Li, Guang-Hui Hu, Ke Wang, Min Chen, A.-Xing Zhu, and Guo-An Tang. "Past Rainfall-Driven Erosion on the Chinese Loess Plateau Inferred from Archaeological Evidence from Wucheng City, Shanxi." Communications Earth & Environment 4, no. 1 (January 3, 2023): 1–8. https://doi.org/10.1038/s43247-022-00663-8.
Yager, T.J., Furlong, E.T., Kolpin, D.W., Kinney, C.A., Zaugg, S.D., Burkhardt, M.R., 2014. Dissipation of contaminants of emerging concern in biosolids applied to nonirrigated farmland in Eastern Colorado. JAWRA Journal of the American Water Resources Association 50, 343–357.
Yang, W., Lowenstein, T.K., Krouse, H.R., Spencer, R.J., Ku, T.-L., 2005. A 200,000-year δ18O record of closed-basin lacustrine calcite, Death Valley, California. Chemical Geology 216, 99–111.

Yellen, J.E., 1977. Archaeological Approaches to the Present: Models for Reconstructing the Past. Academic Press, New York.
Zazzo, A., Balasse, M., Passey, B.H., Moloney, A.P., Monahan, F.J., Schmidt, O., 2010. The isotope record of short-and long-term dietary changes in sheep tooth enamel: implications for quantitative reconstruction of paleodiets. Geochimica et Cosmochimica Acta 74, 3571–3586.
Zhang, Y., Zhang, D., Yang, Y., Wu, X., 2020. Pollen and lipid analysis of coprolites from Yuhuicun and Houtieying, China: Implications for human habitats and diets. Journal of Archaeological Science: Reports 29, 102135.